Tailoring the Properties of PECVD Deposited Terpinen-4ol Thin Films

Thesis submitted by

Avishek Kumar BTech , M.E

on 15th September 2018

for the degree of Doctor of Philosophy

in the College of Science and Engineering

James Cook University

Declaration

I declare that this thesis is my own work and has not been submitted in any form for another degree or diploma at any university or other institute of tertiary education. Information derived from the published and unpublished work of others has been acknowledged in the text, and a list of reference is given.

_____

Avishek Kumar

September, 2018

Statement of access to this thesis

I, the under signed , the author of this work, understand that James Cook University will make this work available for use within the university library , and via the Australian Digital Thesis Network, for use elsewhere.

I understand that as an unpublished work, a thesis has significant protection under the copyright act. I do not wish to place any restriction on access to this thesis. However, any use of its content must be acknowledged and referenced.

_____

Avishek Kumar

September 2018

Acknowledgement

This thesis is an outcome of blessings and contributions bestowed by many people over last four years. It gives me immense pleasure to recall each of them for helping to make this work successful and I express my most profound regards and gratitude towards them.

I express my overwhelming gratitude to my thesis supervisors, Prof. Mohan V Jacob and Dr Kateryna Bazaka., for their guidance, encouragement, support and most importantly consistent involvement and constructive criticism regarding my research problem. I thank them for introducing me to the field of Plasma polymerization and thin films, and for the encouragement to explore various aspects of these topics. I admire their outstanding capabilities of guiding a research problem in a right direction at every stage of my research work.

I thank Dr Scott Mills, Nigel Bajema and Dr Ian Atkinson for valuable inputs in infield biofouling experimental designs. I thank Ass/Prof. Jeffrey Warner, College of Public Health, Medical and Vet Sciences and Dr Peter Mulvey (AITHM) for introducing me to the field of microbiology and providing access to the facilities of the department. My sincere thanks are due to Ms Eva Duck (AITHM) for helping with the microbial experiments

I am fortunate to have wonderful fellow researchers in the laboratory. I deeply acknowledge the contributions of Dr Daniel Grant and Surjith Alanchery for teaching me the thin film characterization techniques. My heartfelt thanks to Ahmed Al Jumali with whom I collaborated at various stages of this work.

Special thanks to John Rehenan, Loyd Baker, Electrical workshop for helping me out with the experimental instrumentation throughout the work. My sincere thanks to Dr Shane Askew, AAC for helping me with AFM and SEM characterizations facilities. I express my gratitude to Mellisa Norton, Academic service officer for her constant help in academic administrative matters. Also, I would like to acknowledge Dr Elizabeth Tynan, Graduate research school for the academic writing courses which improved my writing skills. The help of Dean Brendon, Mechanical workshop in fabricating sample holder for infield biofouling experiments is highly appreciated.

Inspiration provided by my friend Dr Amit Sharma, Dr. Navneet Kumar Singh, Dr Om Prakash and Dr Tarang Mungole, is deeply acknowledged. Discussions with them are always thought-provoking and enriched my fundamental knowledge of material science and thin films techniques.

My stay at the JCU would not be more wonderful without the company of my friends: Justin Nicholas, Mark Bucholtz and David. My heartfelt thanks to them for their support over the past years. Finally, I thank my parents and all family members for their support.

Abstract

Polymer thin films have been of significant research interest in the field of, mechanics, optics, electronics and medicine. Bioactive coatings are extensively used in marine and medical field for the prevention of biofouling which is colonization of any wetted surface by flora and fauna. Fouling of the surfaces has severe implications for the performance of the material and biocide based coating have been used in the prevention of marine fouling. However, these coatings have adverse environmental effects. Natural antifouling products derived from organisms have been found to be an excellent alternative to biocide based strategies. Terpinen-4-ol derived from Australian Tea tree oil has antimicrobial properties.

The Plasma enhanced chemical vapor deposition (PECVD) method has been used to develop environmentally friendly antifouling coating from Terpinen-4-ol. The effect of Process variables such as substrate temperature have been investigated on the PECVD of terpinen-4-ol. The influence of surface functionalization and the deposition mode of terpinen-4-ol plasma polymer on its antibacterial property has been studied. Coating created in the form of bilayer are tested for their marine antifouling behavior.

The substrate temperature was found to influence the deposition mechanism of Terpinen-4-ol plasma polymers. Hydro Stable terpinen-4-ol plasma polymers were found to be formed at higher substrate temperature. Pulse plasma deposited films exhibited enhanced antibacterial performance. Grafting of ZnO nanoparticles onto the surface of the terpinen-4-ol polymer boosted the antibacterial and UV absorbing properties. The deposited bilayer coatings were effective in preventing the primary stage of marine biofouling. The bilayer acted as biocidal self-polishing coating.

Key Words: Terpinen-4-ol, PECVD, Properties Enhancement, Antifouling coatings

Contents

Table of figures

List of tables

Chapter 1

1.1 Introduction

Polymer thin films have received significant interest in recent past because of their full range of physical, chemical, mechanical, electrical and biological properties, which make them well suited for many applications in medical, mechanical, optics, and electronics fields [1-3]. Bioactive surfaces are extensively used in marine and medical areas and there is an ever increasing demand for antifouling surfaces in marine sectors. Fouling of the surfaces has severe implications for the performance of materials and is responsible for vast economic loss. Since the late 1970s, biocidal based coatings have been used extensively to prevent marine fouling. However, such coatings are species-specific and can influence non-target organisms. Due to Ecological concern biocide based coatings are now subjected to stringent legislation which requires non-toxic alternative methods. Environmentally benign based coatings have recently been developed as antifouling strategies. However, they have not demonstrated superior antifouling performance compared with biocide based coatings. Natural antifouling products derived from organism and plants have been found to be an excellent alternative to biocide based strategies. Thus the development of environmentally benign antifouling coating from naturally derived antimicrobial products is novel trends.

Australian Tea Tree Oil (TTO) has shown the antibacterial, antifungal, antiprotozoal and pharmacological behavior [4, 5]. The antimicrobial activity of TTO is attributed mainly to the cumulative effect of the antimicrobial activity of a variety of compounds present of which Terpinen-4-ol is the key component.

Plasma polymerization is a type of Chemical Vapour Deposition method used extensively to synthesize polymer thin films from organic and inorganic precursors, where plasma discharge is used to catalyze the chemical reactions leading to the formation of the polymer structures [6, 7]. Plasma deposition can polymerize monomers which cannot be fabricated by conventional polymerization methods. It has been found that plasma polymers have high elastic moduli, excellent mechanical, thermal and chemical stability, and outstanding adhesion to a variety of substrates [7]. Their chemical composition and thickness can be easily controlled by controlling

the deposition parameters and the nature of the precursor, affording a much higher degree of versatility and control compared to other synthesis methods. Not surprisingly, plasma polymers have found a host of applications [8], from bioactive to chemically inert coatings for medical devices [9-11], to anti-corrosion coatings for metals [12, 13], to dielectric and encapsulating layers in thin film electronics devices [14-16].

1.2 Motivation and Objective

The project builds on the extensive work on plasma polymerization of terpine-4-ol [17-21]. The plasma polymerized terpinen-4-ol films have shown good adhesion, chemical and physical stability by Bazaka et.al.[17, 22]. Terpinen-4-ol thin films were fabricated at various RF power have been investigated for antibacterial properties in previous work in our lab by Bazaka.et.al.[18, 19].

The aim of this thesis is to fabricate plasma polymer thin films from environmentally benign terpinene-4-ol. The fabricated films are intended to be used in a wide variety of applications ranging from dielectrics to antimicrobial surfaces. The scheme of current work consists of:

- The Investigation of the substrate temperature on deposition mechanism and properties of plasma deposited terpinene-4-ol
- The design and development of multilayer terpinene-4ol plasma polymers for marine antifouling applications.
- Pulse plasma deposition of terpinene-4-ol for enhancement in antibacterial activity

The surface modification of plasma polymerized terpinene-4-ol which is achieved by hydrophilic modification and ZnO nanoparticle's incorporations in films.

Overall this thesis focuses on fabricating the terpinen-4-ol plasma polymer under various deposition parameters never used to tailor the material properties. This thesis reports the effect

of power and time as process variables. The effect of substrate temperature as a process variable and development of terpinene-4-ol plasma polymers for marine antifouling applications are investigated and reported in this thesis. Furthermore, surface functionalization of bioactive terpinene-4-ol plasma polymers also been investigated.

1.3 Thesis Organization

This Ph.D. dissertation consists of seven chapters and an abstract

The first chapter introduces the background information, motivation, objective and chapter organisation.

The second chapter provides a comprehensive review of all the major existing knowledge related to antifouling surfaces used in marine aquatic systems. The sections deal with the biofouling growth and development, preventive methods and current research trends.

The third chapter describes the effect of substrate temperature as a process variable on the property of plasma deposited terpinene-4-ol. Influence of substrate temperature on chemical composition, wettability, refractive index, and crosslinking density of plasma polymers is studied. Deposition conditions were found to influence the deposition mechanism and rate. Increase in cross-linking density of films with increasing deposition rate is observed. Plasma polymers fabricated at high substrate temperature and power showed excellent aqueous stability.

Chapter four documents bilayer fabrication of terpinen-4-ol plasma polymer. Coating chemical composition, water affinity properties, surface energy and roughness are investigated. The deposited bilayer films were tested for the marine antifouling applications. The bilayer films acted as biocidal self-polishing coating and were found to effectively reduce primary stage biofouling.

Chapter five describes the pulse plasma deposition of terpinene-4-ol. Plasma deposition via dissociation of –C-O bonds at a low duty cycle (low effective power) was found to be main polymerization mechanism. The films were tested for antibacterial activity against *Pseudomonas aeruginosa*. Effect of surface wettability of the film on bacterial attachment is studied. Films chemical (composition) and physical (surface energy, roughness) properties are investigated. Films deposited at lower duty cycle showed enhanced antibacterial performance.

Chapter six describes the surface modification of terpinene-4-ol plasma polymers. Wettability and ZnO nanoparticle functionalization of deposited terpinen-4-ol plasma polymers was carried out. Hydrophilic and nanoparticle modification of the films led to enhancement in antibacterial properties. The ZnO grafted films also showed excellent UV blocking characteristics.

Chapter seven summarizes the research, conclusions are made, and recommendations for future research are provided.

References

1. Tobushi, H., et al., *Thermomechanical properties in a thin film of shape memory polymer of polyurethane series.* Smart Materials and Structures, 1996. **5**(4): p. 483.

2. Ibn-Elhaj, M. and M. Schadt, Optical polymer thin films with isotropic and anisotropic nano-corrugated surface topologies. Nature, 2001. **410**(6830): p. 796.

3. Fritz, S.E., et al., Structural characterization of a pentacene monolayer on an amorphous SiO2 substrate with grazing incidence X-ray diffraction. Journal of the American Chemical Society, 2004. **126**(13): p. 4084-4085.

4. Mondello, F., et al., In vivo activity of terpinen-4-ol, the main bioactive component of Melaleuca alternifolia Cheel (tea tree) oil against azole-susceptible and-resistant human pathogenic Candida species. BMC infectious diseases, 2006. **6**(1): p. 158.

5. Carson, C., K. Hammer, and T. Riley, Melaleuca alternifolia (tea tree) oil: a review of antimicrobial and other medicinal properties. Clinical microbiology reviews, 2006. **19**(1): p. 50-62.

6. Goodman, J., *The formation of thin polymer films in the gas discharge.* Journal of Polymer Science, 1960. **44**(144): p. 551-552.

7. Biederman, H., *Plasma polymer films*. 2004: World Scientific.

8. Bazaka, K., M.V. Jacob, and K. Ostrikov, *Sustainable life cycles of natural-precursor-derived nanocarbons.* Chemical reviews, 2015. **116**(1): p. 163-214.

9. McInnes, S.J., et al., "Thunderstruck": plasma-polymer-coated porous silicon microparticles as a controlled drug delivery system. ACS applied materials & interfaces, 2016. **8**(7): p. 4467-4476.

10. Vasudev, M.C., et al., Exploration of plasma-enhanced chemical vapor deposition as a method for thin-film fabrication with biological applications. ACS applied materials & interfaces, 2013. **5**(10): p. 3983-3994.

11. Melnichuk, I., et al., Direct covalent coupling of proteins to nanostructured plasma polymers: a route to tunable cell adhesion. Applied Surface Science, 2015. **351**: p. 537-545.

12. Jeong, D.-C., et al., Low-temperature plasma polymerization of dicyclopentadiene for anti-corrosion properties. Polymer, 2016. **92**: p. 133-139.

13. Hu, R.-G., et al., *Recent progress in corrosion protection of magnesium alloys by organic coatings.* Progress in Organic Coatings, 2012. **73**(2-3): p. 129-141.

14. Joy, L.K., et al., Large enhanced dielectric permittivity in polyaniline passivated core-shell nano magnetic iron oxide by plasma polymerization. Applied Physics Letters, 2014. **104**(12): p. 121603.

15. Seo, H.J., et al., Device characteristics and mechanical flexibility simulation of plasma-polymer gate dielectrics based organic thin film transistors. Science of Advanced Materials, 2016. **8**(3): p. 665-668.

16. Seo, S.-W., et al., Extremely bendable thin-film encapsulation of organic light-emitting diodes. Applied Physics Letters, 2013. **102**(16): p. 161908.

17. Bazaka, K. and M.V. Jacob, Nanotribological and nanomechanical properties of plasma-polymerized polyterpenol thin films. Journal of Materials Research, 2011. **26**(23): p. 2952-2961.

18. Bazaka, K., et al., Plasma-assisted surface modification of organic biopolymers to prevent bacterial attachment. Acta biomaterialia, 2011. **7**(5): p. 2015-2028.

19. Bazaka, K., et al., Efficient surface modification of biomaterial to prevent biofilm formation and the attachment of microorganisms. Applied microbiology and biotechnology, 2012. **95**(2): p. 299-311.

20. Bazaka, K. and M.V. Jacob, *Post-deposition ageing reactions of plasma derived polyterpenol thin films.* Polymer Degradation and Stability, 2010. **95**(6): p. 1123-1128.

21. Bazaka, K., et al., The effect of polyterpenol thin film surfaces on bacterial viability and adhesion. Polymers, 2011. **3**(1): p. 388-404.

22. Bazaka, K., M.V. Jacob, and B.F. Bowden, Optical and chemical properties of polyterpenol thin films deposited via plasma-enhanced chemical vapor deposition. Journal of Materials Research, 2011. **26**(08): p. 1018-1025.

Chapter 2

Literature Review

This chapter gives a brief overview of all the major progress within the area of marine antifouling surfaces. Limitations of currently used technologies and demand for environmentally benign antifouling surfaces are discussed. The literature survey is to be submitted for publication as *Avishek kumar, Ahmed AL-Jumaili, Kateryna Bazaka, Mohan V. Jacob .Recent Progress and Future Trends in Marine Antifouling Technology. Coatings*

Recent Progress and Future Trends in Marine Antifouling Technology

Abstract

Marine biofouling causes severe economic penalties to maritime industries. The so-called "biocidal approach" employed to mitigate biofouling so far comes at a potentially significant cost to the environment into which the biocides are released. In this article, biocide-based strategies and their adverse environmental effects are critically reviewed, showing how these environmental concerns together with recent advances in material science, biology and engineering are driving current research towards the use of natural antifouling products and strategies based on physio-chemical properties. Then, recent progress and promising novel developments in the field of environmentally benign marine antifouling technology are discussed and their benefits and potential drawbacks are compared to existing approaches.

Keywords: Marine biofouling, Antifouling surface, Review

As to be submitted in: Avishek kumar, Ahmed AL-Jumaili, Kateryna Bazaka, Mohan V. Jacob .Recent Progress and Future Trends in Marine Antifouling Technology. Coatings

2.1 Introduction

Any surface immersed in an aquatic environment is subject to colonization by marine organisms. Such uncontrolled colonization by microorganisms, i.e. biofouling, is seldom desired since it often adversely affects the ability of the surface to perform its intended function.

The examples of how biofouling leads to an overall deterioration of performance are numerous and significant, spanning shipping vessels, heat exchangers, oceanographic sensors and aquaculture systems [1-3]. For example, an increase in the roughness of the ship hull due to fouling can cause powering penalties of up to 86% at cruising speed [1]. Furthermore, ship fouling can result in bio-invasion, a process by which marine species are transported and unintentionally introduced into a non-native environment.

Biofouling of autonomous environmental monitoring equipment, such as oceanographic sensors used to measure dissolved oxygen, turbidity, conductivity, pH and fluoresce of seawater is another challenge[4, 5]. Here, attachment of microorganisms to optical windows in cameras and optical sensors and resultant degradation of the properties of the interface significantly limit to their deployment time. Formation of the biofilm on the surface can also considerably disrupt the quality of the measurement and the useful operational lifetime of these sensors [6-8]. For example, biofouling of proton selective glass membrane electrodes used for measuring pH inhibits the proper contact between liquid media and electrodes[9]. Hence, there is a significant impetus to develop antifouling techniques that prevent organism settlement without impeding sensor performance. For instance, in turbidity and chlorophyll sensors, the antifouling coating should be transparent to light so as not to interfere with the clarity of optical window [10, 11].

A wide range of antifouling (AF) techniques has been devised to combat the problem of microorganism attachment and biofilm formation. Figure 2.1 shows the antifouling strategies used in past and present. In terms of their action mechanism, these antifouling strategies can be mechanical, physical or chemical in their nature or rely on a combination of these mechanisms. Chemical methods involve the use of a biocidal agent which inhibit or limit the settlement of foulants using chemically active compounds. Although very effective against many organisms, these chemicals are often non-species specific and can, therefore, influence non-target organisms. One of the most well-known examples of this is the use of TBT (tributyltin), a broad spectrum biocide that has been used extensively since the 1960s to control marine biofouling. However, after its high toxicity to non-target marine species became apparent in the 1980s, the use of TBT

was completely banned in 2008[12]. The self-polishing copolymer (SPC) paints loaded with booster biocides, e.g. copper and zinc pyrithione are currently in use. However, Cu and Zn may pose an ecological risk due to their leaching from SPC into the ambient environment, which may over time lead to their built up to concentrations that are toxic to marine life [13]. These and other ecological concerns have led to the use of biocide-based coatings being subjected to stringent legislation, with calls for non-toxic physical methods to eventually replace them entirely. Physical methods rely on the use of a protective antifouling (AF) coating that can either deter the organism from settling on the surface or enhance the release of the settled organism from the surface (i.e. fouling release coating). Although more environmentally-friendly than biocide-based coatings, the stability and durability of such coatings in water and their potential effects on the ambient marine environment remain a matter of concern. Pure mechanical devices such as wipers and scrapers can be used to remove the fouling, however, they are not suited for small-scale devices and can also damage the surface of sensitive devices, such as sensors.

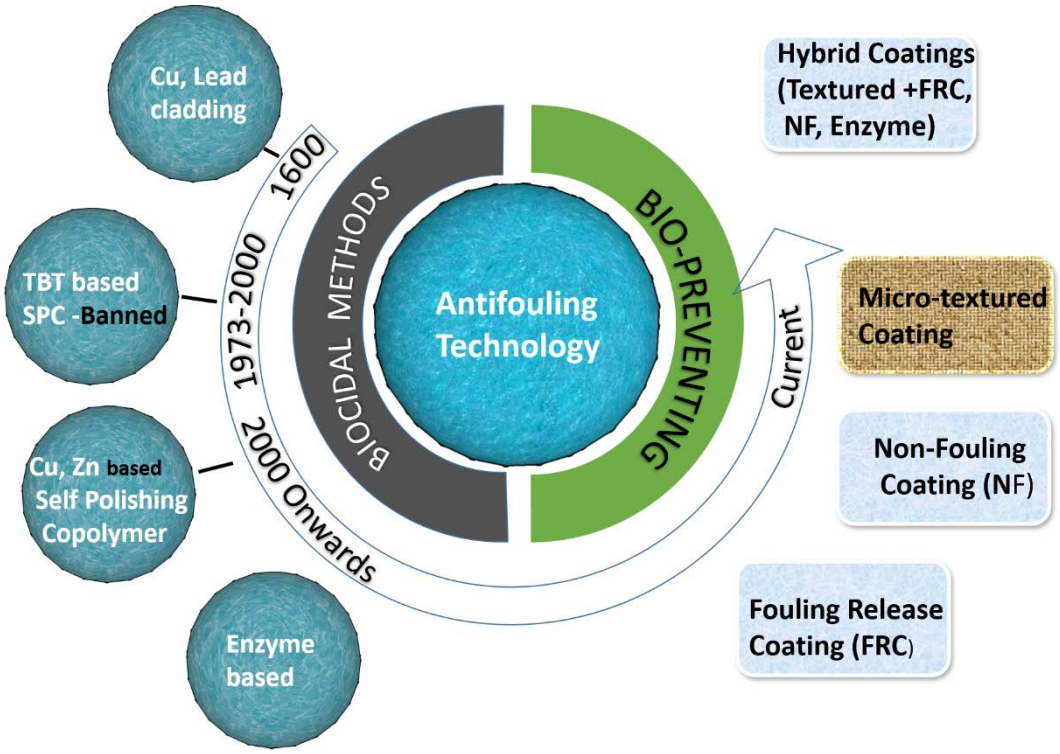

Figure 2. 1 Trends in the development of antifouling coating

2.2 Marine Biofouling

At least 4000 fouling organisms have been identified and are classified on the basis of their size. These organisms can range from unicellular (bacteria) to multicellular (seaweeds & barnacles). Bacteria, algae spores, larvae of invertebrates and diatoms are considered to be primary fouling micro-organisms, while barnacles, algae and mussels are common fouling macro-organisms. Marine biofouling is undesirable colonization of any submerged surface by marine organisms. The process of fouling follows a sequence of events as illustrated in figure 2.2. First, the formation of a conditioning film by physical adsorption of bio-secreted organic molecules (also known as slime) takes place within a few seconds after immersion. The conditioning film changes the surface properties of the immersed surface and sets the scene for primary colonization to occur. Within hours, bacteria colonize this conditioning film, by initially reversibly attaching to the surface via electrostatic interactions and later attaching irreversibly via secretion of extracellular polymeric substances. The microbial film provides sufficient nutrition for the colonization of multicellular species (e.g. colonies of diatoms), increasing the degree of microfouling. The microfouling prompts the settlement of macro-organisms such as macroalgae, barnacles and sponges, is the process referred to as macrofouling. However, this specific sequence of fouling events holds true for only a limited number of organisms. Clare et al. showed that the zoospores of algae *Ulva Linza* could settle on a pristine surface without the presence of a conditioning biofilm[14].

Biofouling is a highly dynamic process, and the fouling community depends on the nature of the substrate [15], geographical location[16], season[17] and organism-related factors such as cross-species competition and predation. Indeed, ecological conditions such as water salinity, temperature, solar radiation and nutrient levels can vary considerably between different locations, directly affecting biofilm growth and development. For example, there is less development of fouling in winter due to the reduction in water temperature and solar radiation intensity[18]. The properties of the substrate also play an important role. For instance, the surface energy of the substrate has been found to influence the settlement of the fouling organism. Spores of green algae *Ulva linza* have been found to settle on the surface with low surface energy preferentially, yet their adherence to high energy surfaces was shown to be weak[19]. However, it should be noted that the adherence behaviour of foulants is species-dependent. Barnacles have been found to prefer hydrophilic surfaces whereas bryozoans adhere strongly to hydrophobic surfaces[20]. Besides surface energy, roughness and porosity of the surface also affect the initial settlement of fouling organisms.

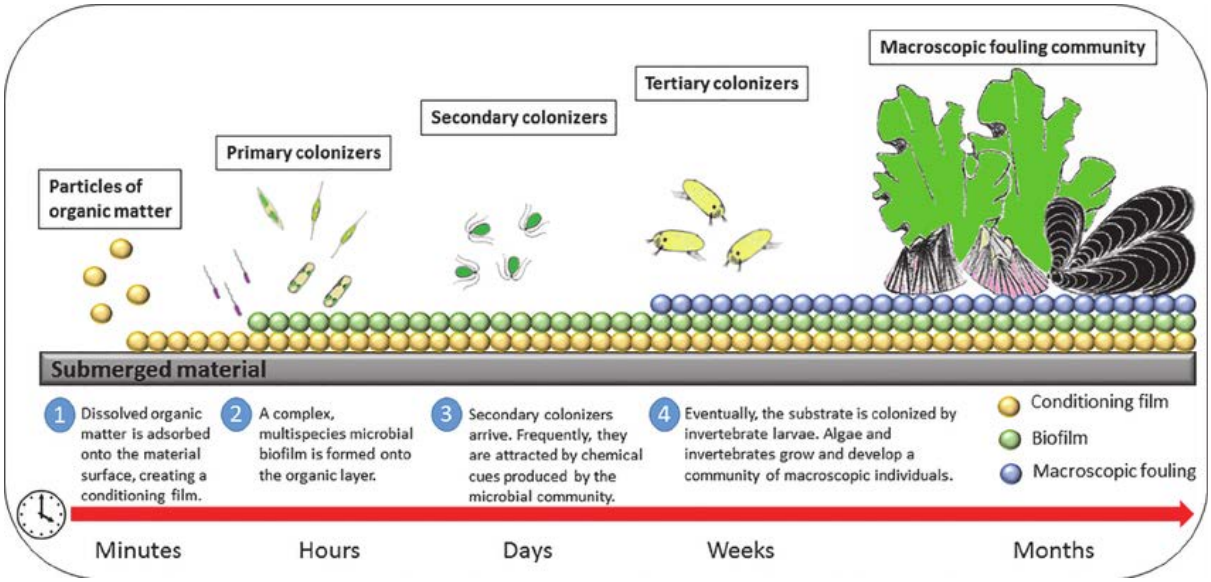

Figure 2.2 Schematic showing different stages of biofouling. Reproduced with permission from [21]

2.3 Progress in antifouling technology

2.3.1 Biocide-based strategy

The development of AF strategies dates back to the 7th century BC [22]. There have been reports of the use of lead and copper sheets to control fouling by ancient Mediterranean civilizations, including Phoenicians and Ancient Greeks (1500-300 BC)[23]. Antifouling strategies employing the use of copper, arsenic, and mercury oxide became prevalent in the late 18th and early 19th century. Nevertheless, these strategies had a short life span, high cost and inefficient performance[22]. A broad spectrum biocide, Tributyltin (TBT) was introduced into commercial AF paints in the late 1950s. TBT- releasing paints were used extensively in the mid-1960s since the TBT-based self-polishing copolymer paint was capable of effectively mitigating marine fouling for up to 5 years when applied onto ship hulls. However, because of the low degradation rate of TBT-bearing compounds, they were found to affect non-target marine species. Once found their way into a biological system, these compounds were shown to disrupt various enzymatic and metabolic functions of an organism, in some instances ultimately leading to its death. The adverse effect of TBT became apparent only during the early 1980s when its negative impact on various marine life was observed[24]. Even low concentrations of TBT were found to cause sexual disorders, such imposex, which is the development of male sex organs in female gastropods[25].

Consequently, the use of TBT was banned completely in 2008. Following the phase-out of TBT in 2008, Cu based biocides have once again gained the importance. Copper-containing AF paints have shown to target specific fouling organism only and their sensitivity towards macroalgae is minimal. Hence booster biocide was added to the copper antifouling coating to overcome the problem of fouling by micro- and macroalgae. Few to mention are Diuron, Irgarol 1051[26, 27], Zinc and Copper pyrithinone[28], dichloro-octyl-isothiazolin (DCOIT, Sea Nine 211)[29]. These are generally herbicides having the negative effect on the growth of the photosynthetic organism. However their use in AF paint has an uncertain future as they may also pose an environmental problem[13, 30]. The estimated overall application cost for a biocidal coating is about 15 $/m^2$/year [31]. Table 2.1 lists the commonly used antifouling biocides along with their action mechanism and half-life in seawater.

Table 2. 1 Commonly used biocides and their action mechanism

Biocide	Chemical name	$T_{1/2}$ seawater (days)	Action mechanism against foulants
Irgarol 1051	2–(Tert–butylamino)–4–cyclopropylamino)–6–(methylthio)–1,3,5–triazine	100-250	Inhibitor of PS II electron transport
Diuron	1–(3,4–Dichlorophenyl)–3,3–dimethylurea	31.4-365	Inhibitor of PS II electron transport
Chlorothalonil	2,4,5,6–Tetrachloroisophthalonitrile	1.8- 8	Mitochondrial electron transport inhibitor
Dichlofluanid	N′-Dimethyl–N–phenylsulphamide	0.12-0.75	Inhibitor of PS II electron transport
Thiram	Tetramethylthioperoxydicarbonic diamide	< 1.6	Multi-site inhibitor
Zn pyrithione	Bis-(1-hydroxy-2(1H)-pyridinethionate-O,S) zinc	< 1	Multi-site inhibitor
Cu pyrithione	Bis(1-hydroxy-1H-pyridine-2-thionato-O,S)copper	12.9-96	Multi-site inhibitor
DCOIT	4,5-Dichloro-2-*n*-octyl-3-(2*H*)–*iso*thiazolin–3–one	0.004-3	Inhibitor of electron transport
TCMTB	2-(Thiocyanomethylthio)benzothiazole	31-36	Mitochondrial electron transport inhibitor
TPBP	Triphenylborane pyridine	1-34	unknown
Tralopyril	4-Bromo-2-(4-chlorophenyl)-5-(trifluoromethyl)-1H-pyrrole-3-carbonitrile	0.67	Mitochondrial electron transport inhibitor
Capsaicin	8-Methyl-N-vanillyl-6-nonenamide	13	Nervous system and metabolic disruptor
Nonivamide	*N*-[(4-Hydroxy-3-methoxyphenyl)methyl]nonanamide	8.8	Nervous system and metabolic disruptor

2.3.1.1 Biocide based coatings

Impregnation of a coating with biocides has been an effective AF method used extensively [18, 32-34]. The biocide-based coating relies on control release of biocides. There are three main categories of the biocide-based coatings: control depletion polymers (CDP), contact leaching coatings, and self–polishing copolymers (SPC). The above classification is based on the mechanism of biocide release from the polymer matrix; the latter commonly referred to as the binder.

(a) Contact leaching coatings (insoluble matrix paints): This coating has a water-insoluble matrix, which is made of high molecular weight binders such as vinyl, epoxy and acrylics. The good mechanical strength of such matrices facilitates incorporation of high amounts of biocides into the coatings. High level of biocide incorporation closely packs active molecules, making them come in contact with each other and resulting in their gradual release. When a coating is immersed in seawater, biocides get released leaving behind a multi-porous structure. As seawater continues to penetrate such coatings deeper with time, the rate of elution of biocides falls and an antifouling action becomes insufficient to prevent colonization (Figure 2.3a). Leaching of biocides from such a coating leads to the formation of a honeycomb structure, its surface becomes rougher and susceptible to retaining of more of seawater pollutants, accumulation of which prevents further release of biocides. A major limitation of this coatings is that the biocide release decreases with the immersion time and so does the antifouling effect. The reported in-service lifetime of this coating is 1-2 years[35, 36].

(b) Soluble matrix paints: Soluble coating matrices were developed to increase a lifespan of an antifouling coating. These coatings have binders based on rosins and their derivatives[37, 38]. The method is based on two processes that occur simultaneously – once submerged - a binder is dissolved, and a biocide is released into seawater (Figure 2.3b). In this type of a coating, the leaching layer is thin, and biocides are directly exposed to water; the combination of these two factors increase a lifespan of the outer layer. However, these coatings have poor mechanical strength and limitations in regards to the quantities of a biocide which can be loaded. Thus, lifespans of early soluble matrix coatings were 12-15 months due to their high erosion and release rate. Henceforth, an advanced variant of a soluble matrix coating, known as a controlled depletion coating (CDP), was developed to address the problem of high erosion. The binder in the CDP coating is reinforced with organic rosins which control the hydration and dissolution of the

soluble binder in the slower manner than rosin-based derivatives. The CDP coating is effective for a period of up to 3 years[31].

(c) Self-polishing copolymer coatings (SPC): These paints are based on biocide blended acrylic or methacrylic copolymers. The copolymer matrices are easily soluble in seawater and their biocide leaching rate can be regulated through controlling of the dissolution of the copolymer matrix (Figure 2.3c). Foulants attaching on the surface of the coating are removed together with the copolymer matrix. First Tributyltin (TBT)- SPC paint was patented by Milne and Hails in 1977 [39]. In these paints, TBT was bonded to the polymer backbone by ester groups. The TBT-SPC coating was widely used before it got banned completely in 2008 because of adverse environmental effects[40, 41]. Tin-free SPC technology has emerged after the complete phase-out of TBT based AF techniques. In this technology, metals such as Cu, Zn are used in place of TBT while keeping the matrix material acrylic based.

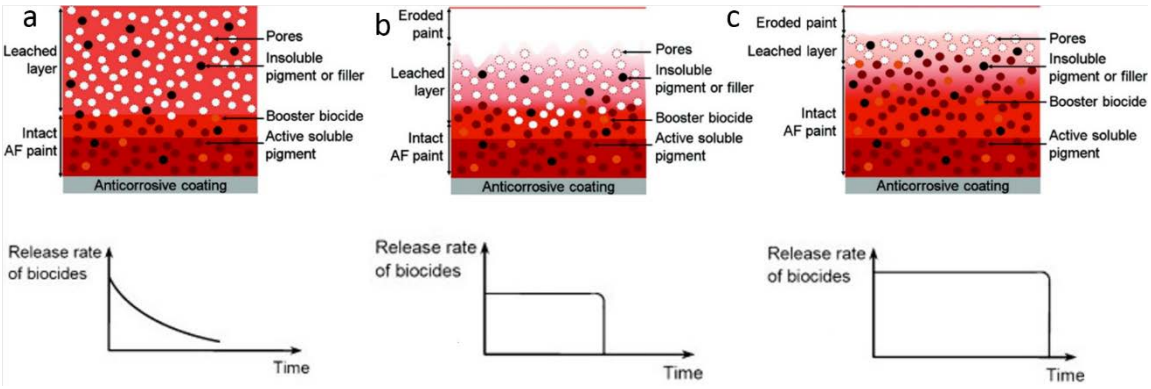

Figure 2.3 Schematic illustrating possible release mechanisms of a biocide-based antifouling coating in seawater. (a) Contact leaching coatings; (b) Soluble matrix or controlled depletion polymer coatings; (c) Self-polishing copolymer coatings. Adapted with permission from [42, 43].

Upon immersion, seawater diffuses into a coating leading to the dissolution of the biocidal particle. The hydrophobic matrix prevents water from penetrating into the film, restricting it to pores created by soluble biocidal particles. As the copolymer matrix is easily hydrolyzable in seawater, controlled and slow hydrolysis of the coating takes place, confined to a few nanometer thick layers from the surface. In time, there is an increase in leached areas with an increase in dissolution of biocides, making the copolymer matrix brittle and easily erodible by seawater. Removal of leached area leaves a new fresh area of coating for further releases of biocidal molecules, a process which is termed a self-polishing effect. After the certain time, the rate of

dissolution of active molecules and ions through the leached layer equals to that of the matrix erosion rate. After this stage, the thickness of a leached layer reaches a steady value of 10-20 μm for the lifetime of the coating [32]. SPC coatings have a polishing rate of 5-20 μm per year which has extended the dry docking intervals for up to a period of 5 years [35]. A degree of polymerization and hydrophilic character of copolymer matrices dictates a release rate of biocides in SPC coatings [44].

2.3.2 Environmentally friendly antifouling coatings

2.3.2.1 Enzyme based coatings

The concept of an enzyme as an AF agent emerged during the 1980s [45], and its applications have been successfully investigated recently [46, 47]. In enzyme-based coatings, the biofouling inhibition is directly related to enzymatic activity [46]. Enzymes can degrade adhesives used by organisms during settlement or generate other biocidal compounds. Enzyme-based AF approaches can be divided into two categories based on their mode of action: indirect enzymatic AF and direct enzymatic AF strategies. The first works via catalytic production of biocides and later by degrading the foulants or their adhesive components. Figure 2.4 shows four mechanisms of enzymatic AF coatings. Essential requirements for enzyme-based coating systems are [46]: (1) retention of enzymatic activity when mixed with other coating components; (2) broad-spectrum AF activity ; (3) long-term stability in dry (docking) and wet (submerged in seawater) conditions; and (4) minimal deterioration in coating performance.

Enzymes that can decompose adhesives, such as protease and glycosylases are widely used in direct enzymatic AF techniques. Proteins and proteoglycans play an important role in macro-fouling processes. Proteases can easily hydrolyze proteins and proteoglycans within the bio-adhesives thus preventing macro-biofouling. Serine proteases (trade name Alcalase) have shown effects in the reduction of adhesion strength of green algae *Ulva Linza*, diatom *Navicula perminuta* and barnacle cyprids [48-50]. It is readily available, biodegradable and nontoxic. Enzymes like trypsin, a-chymotrypsin and dextranase have also been found to be effective in reducing adhesion strength of organisms to the surface. In the case of microfouling, polysaccharides-based bioadhesives are as dominant as the protein ones. Generally, glycosylase is used to degrade polysaccharides-based bioadhesives. However, degradation of polysaccharides based bioadhesives is complex and difficult, which narrows down its effective range [51]. A combination of polysaccharide and proteolytic degrading enzymes can broaden the spectrum of direct enzyme-based techniques [52].

The concept of indirect enzyme-based coatings was first proposed by Kristensen *et al.* [53]. The process is based on the ability of enzymes present in the coating to convert substances present in its environment (i.e. seawater) into compounds with antifouling activity. Examples include coatings containing enzymes such as glucoamylase, hexose oxidase and haloperoxidase. For instance, haloperoxidase catalyzes the generation of hypohalogenic acid which is used as a disinfecting agent in water treatment system [47]. The antifouling effect of enzymes such as glucoamylase and hexose oxidase is associated with the generation of hydrogen peroxide, which induces oxidative damage in cells [53]. However, the critical concentration of hydrogen peroxide generated by such coatings should be greater than MIC for marine bacteria and diatoms in order to achieve the necessary level of inhibition of biofouling. This presents a major challenge.

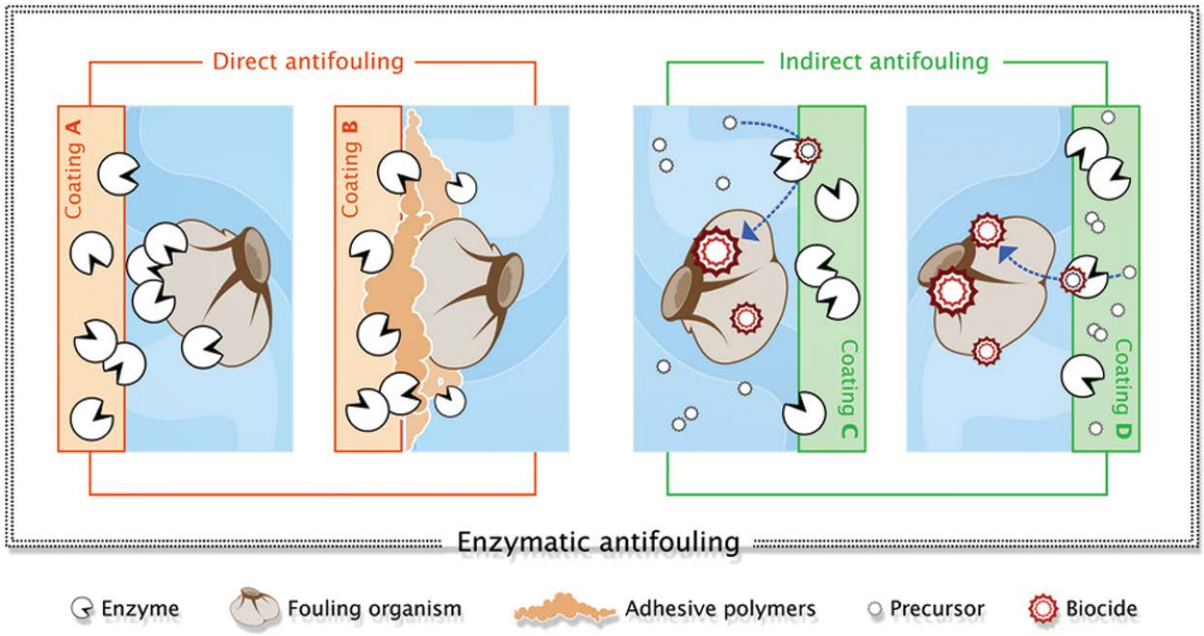

Figure 2.4 Schematic showing antifouling mechanisms of enzyme-based coatings. Reprinted with permission from[46]

Sol-gel and covalent immobilization techniques are the most common methods of incorporating enzymes in an AF coating. Enzyme-based AF coatings fall into fall into a less environmentally dangerous category and as such are considered much more benign to ecosystems. However, stability and self-degradation of enzymes are one of the major challenges for this kind of the coatings [46]. The challenges are due to variations in seawater temperature (-2 to 30 °C) that can affect catalytic activity and lifespan of enzymes Amounts of and distribution of enzymes in coatings, as well as a choice of coating matrices, are also essential factors dictating successful application of these types of coatings.

2.3.2.2 Fouling release coatings:

Fouling release (FR) coatings were first to be commercialized among the biocide free AF coatings. Fouling release coatings are non-toxic coatings based on a dual mode of action: nonstick properties and an FR behavior. An FR coating provides an ultra-smooth topology, which minimizes adhesion strength between a surface and a fouling organism allowing for the fouling to be removed due to shear hydrodynamic stress during navigation [54]. Silicone and fluoropolymers are two main hydrophobic polymers used in the fabrication of the FR coatings.

The Principle of FR coating: The non-stick property can be attributed to the hydrophobic nature and low surface energy of the FR coatings, which significantly reduce the adhesion strength of organisms to a surface. A bond between a foulant and a surface becomes so weak that the former is removed by either shear forces or under their own weight [31]. Surface energy, elastic modulus and coating thickness are parameters that determine the degree of fouling and the ease of foulant removal [55]. Surface wettability, characterized by a surface free energy is considered to be the most important factor in determining the efficacy of fouling release coatings. A relationship between a degree of fouling and a surface energy of any substrate was defined by Baier, where the minimum degree of fouling was found to occur at 22-24 mN/m and not at the lowest critical free energy. The elastic modulus of a surface plays a role in determining the degree of biofouling. Brady reported that a substrate having a low value of elastic modulus shows minimum adhesion [56]. The critical force required to remove the fouling showed a positive relationship with a square root of surface energy (Y_c) and elastic modulus (E) as $P \approx \sqrt{Y_c . E}$ [57]. The dependence of fouling release properties of the coating on surface energy and elastic modulus are shown in figure 2.5. Coating thickness is another factor which affects the removal of foulants from a surface. Singer showed that a force (Pc) required to remove pseudo barnacles from silicones decreases with increasing thickness of the coatings [58].

An inverse relationship between a square root of thickness and pull of force (P_c) was observed :($Pc = k (\sqrt{t})$, where t is the effective thickness. However, pull force Pc becomes independent of thickness for thick coatings. Materials such as silicones (PDMS)[59] and fluorinated polymers [60] have shown antifouling properties because of their low surface energy and hydrophobic nature.

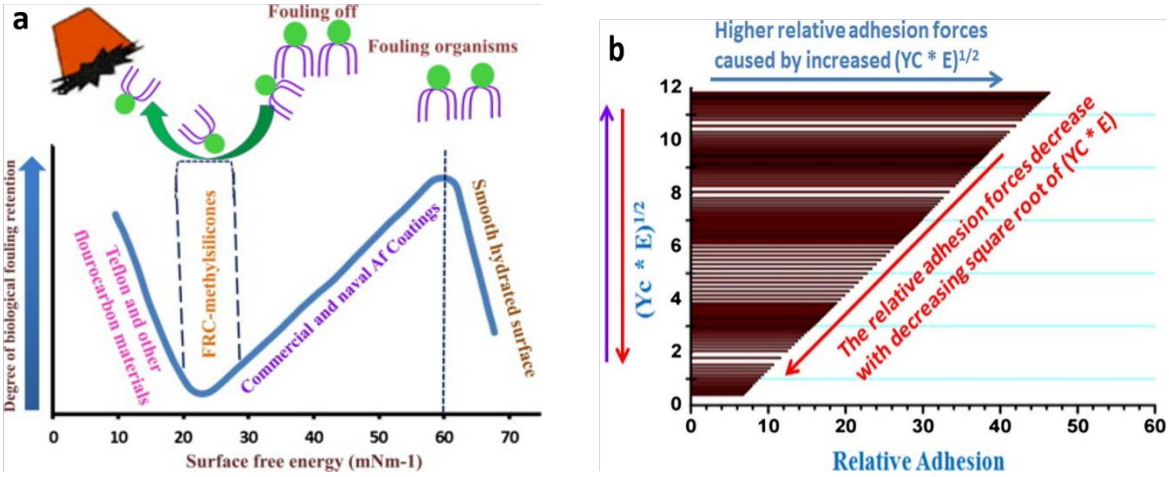

Figure 2.5 (a) The Baier curve demonstrates the relative amount of biofouling versus critical surface tension of the substrate. (b) Dependence of the relative adhesion forces on elastic modulus and surface energy. Reprinted with permission from [61].

(a) Fluoropolymer FR coatings: Fluoropolymers are hydrophobic polymers. Non-polar chemical moieties impart hydrophobic character and low surface energy to these coatings. The surface energy of these coatings fall in 10-20 mN/m range and are lower than that of silicones. These polymers form smooth and non-porous surfaces with good anti-adhesion qualities. These materials are hard and glassy in nature and are applied in thin layers (approx. 75 µm). In the late 1970s, a polytetrafluoroethylene (PTFE) filled fluorinated polyurethane coatings were investigated by Griffiths group [62]. The coatings were UV resistant and could be easily cleaned but could not withstand damages caused by sharp edges of barnacle shells. The damages would result in the roughened surface that enabled strong adherence of barnacles and prevented their easy removal [42]. Research that followed was based on the development of perfluoropolyether polymers, perfluoroalkyl polymers and poly (ethylene glycol) fluoropolymers. Perfluoroalkyl polymers underwent surface reconstruction while immersed under water showing poor antifouling characteristics [63]. Crystalline polymers were blended with perfluoroalkyl polymers to overcome this problem. A semifluorinated ether coating on a block copolymer of poly(styrene) and poly(isoprene) showed best foul release properties and was found to resist surface rearrangement [64]. However, fluoropolymers have high elastic modulus [65] which hinders the easy release of accumulated foulants from the surface. These limitations of fluoropolymers have driven current research towards elastomeric silicon-based coatings.

(b) Silicon-based FR coatings: Silicones (R_2SiO) have the structural resemblance to ketones (R_2CO). Alternating silicon and oxygen atoms form the backbone with two organic groups linked to silicon. These polymers need to be cross-linked in order to form a proper film. Robbart patented the first use of cross-linked silicones as a marine AF coating in 1961 [66] and was later followed by Milne who combined poly(methylphenylsiloxane) with cured silicone rubber to enhance its AF efficiency [67]. These coatings are characterized by the low elastic modulus, low surface energy and low glass transition temperature (T_g). The low T_g enables coatings with high structural mobility. Pure PDMS was the most common silicone polymer used as an AF coating but later got restricted to use as a control material in experiments only. There are three PDMS based commercially available FR coatings: Sylgard 184 (Dow Corning), Silastic T-2 (Dow Corning), and RTV11 (General Electric). Si-O bond length (1.65 A), bond angles (159), partially ionic characteristic of bonds and alternating divalent moieties in the polymer backbone imparts the unique flexibility to PDMS [68]. The low glass transition temperature of PDMS (T_g =-127 C) makes its structure flexible and thus enables it to adopt the lowest surface energy configuration.

Inorganic nanofillers-reinforced PDMS polymers have been investigated for their superior environmental stability. NPs such as SiO_2, TiO_2, ZrO_2, Fe_3O_4 and Al_2O_3 have been added to PDMS coatings to enhance their physical, chemical and mechanical properties [69-71]. Multi-Wall and single wall carbon nanotubes modified PDMS coatings have shown an increased contact angle, decreased roughness and surface energy with improved self-cleaning properties [72, 73]. Photo-reactive silicone functionalized with spherical single crystal TiO_2 particles showed superior FR properties compared to tailored nanocomposites [74]. An increase in hydrophilicity (contact angle of 10°) after UV radiation enhanced the self-cleaning properties of the nanocomposite. Table 2.2 lists some of the presently available FR coatings along with their properties and the fouling release behavior.

Table 2. 2 Fouling Release coating along with their properties and the fouling release behavior

Coating type	Coating	Coating characteristics	Fouling release performance	Ref
Silicone	Silicone + organic modified polysiloxane	Ys = 22 ± 0.4 $mN.m^{-1}$	Reduction in slime adhesion strength with respect to teflon and epoxy coatings	[75]
	Intersleek	Ys = 19.4 ± 1.2 $m.J.m^{-2}$	Reduction in barnacle adhesion strength compared to epoxy coating	[76]
	Pt cured PDMS	θ =118 ± 2°, Ys = 18 ± 2 $m.J.m^{-2}$	Adhesion strength of barnacle decreased with increasing thickness	[55]
Hybrid Silicone	Hempasil X3, (hydrogel functionalized silicone FRC)	θ = 96 ±1°	decrease in settlement of bacteria and barnacles with respect to pure PDMS FRC	[77]
	PDMS + 5 % SiO2-ZnO Nanocomposite	θ = 167 ± 2, Ys = 9.24 mN/m	Reduction in settlement of *Micrococus* sp, *Pseudomonas putida* and fungi	[56]

Although hybrid silicone based FR coatings dominate the present market, they still have limitations. The fouling release property of PDMS is not effective at a low sailing speed and during idle periods [78]. Secondly, they are not effective against colonization by diatoms and bacteria. Moreover, they have poor mechanical properties because of low elastic modulus and are thus quite susceptible to damage that can increase their surface roughness. Also, the biodegradability behavior of PDMS is yet to be thoroughly studied [79, 80]. Biodegradation of PDMS is also of a concern as it gives rise to the formation of carbon dioxide, inorganic silicates and dimethylsilanediol, effects of which on ecological systems should be further investigated. The estimated overall application cost for various fouling release coatings is around $ 12 /m^2/year.

2.3.2.3 Non-fouling (NF) coatings:

The limitations of fouling release coatings (polysiloxane and fluoropolymers) instigated research in the development of anti-adhesion strategies. Fouling starts with the formation of conditioning films which is a process of protein adhesion and adsorption on a surface. Further growth of biofilm depends on the ability of these molecules to adhere to surfaces. Thus the research focused on how to prevent the biofoulants from adhering during primary stages of attachment. Hydrophilic surfaces were used to execute this strategy in both biomedical and marine fields. Hydrophilic PEG moieties on protein drugs have been shown to resist non-specific protein adsorption [81]. Strategies based on PEG, zwitterionic, hydrogel and self-assembled monolayers have been investigated.

The principle of NF coatings: NF coatings are intended to deter attachment of biofoulants during the primary stages of fouling. The hydration layer and the steric repulsion are two main theories which explain the anti-fouling behaviour of these coatings. There is an unfavourable entropy change when there is protein adsorption on the substrate due to compression of a free end of polymer chains [82]. Thus there is an entropically driven repulsion for any non-specific proteins. This theory suits, especially for long chain polymers with one end, fixed to the substrate. However, this theory does not take account of interfacial chemistry and molecular structure which are equally important factors in an aqueous environment. The hydration layer theory is based on molecular chemistry of hydrophilicity where a lower interfacial energy configuration is achieved between a hydrophilic surface and water. There is a formation of a hydration layer between two phases which creates an energy barrier that resists adsorption of any other molecules [83]. Figure 2.6 illustrates the non-fouling mechanism of a PEG-based coating via the formation of hydration layers. The combined effect of both a steric repulsion and a hydration layer provides biofouling resistance and has been universally acknowledged.

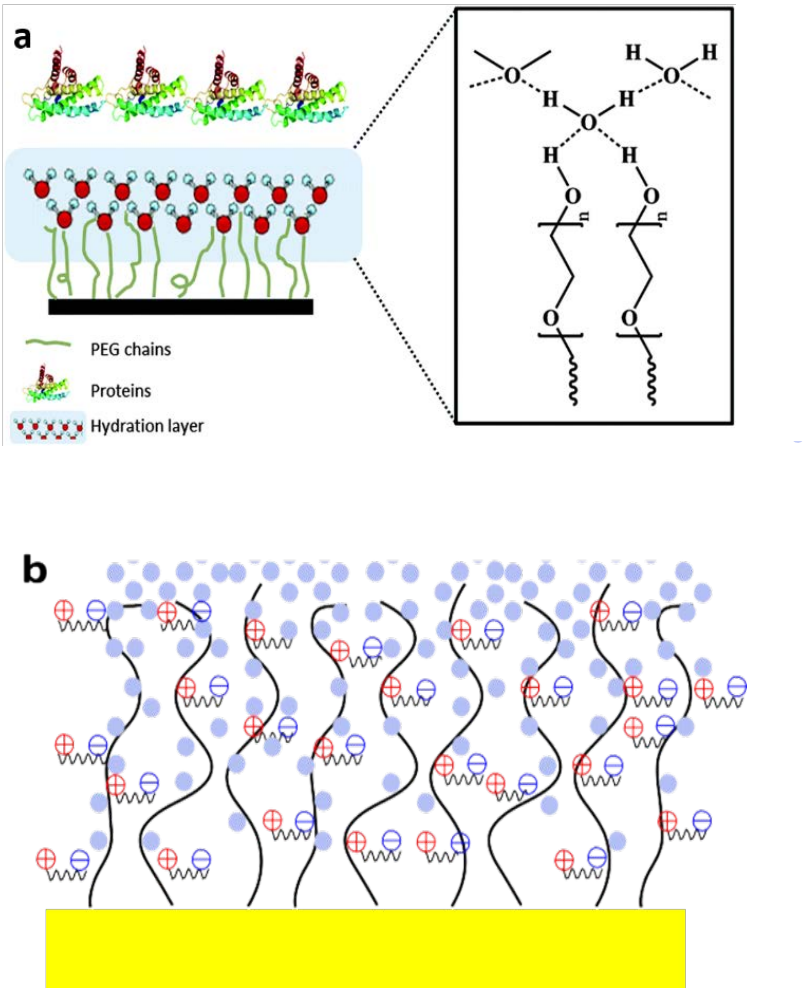

Figure 2.6 Schematic representation of preventing the attachment of proteins via the hydration layer derived on PEG chains. Reprinted with permission from [84]. (b) Schematic of a chain flexibility and hydration in zwitterionic polymers. Adapted with permission from [85].

(a) PEG-based coatings: Poly (ethylene glycol) (PEG) has been the most commonly used material due to its ability to prevent protein adhesion to a surface in a biomedical field because of low thrombogenicity [63, 86]. PEG-coated surfaces show nonspecific protein repellency and their use as marine AF coatings have also been noted [87]. PEG chain length and grafting density have the significant effect on their protein repellency. However, protein attracting state of PEG has also been reported [88, 89]. Physical and chemical adsorption, covalent attachment and block or graft polymerization are used for immobilization of PEG chains on surfaces. PEG surface modification depends strongly on the nature of the substrate and the chemical grafting process.

PEG brush coatings have been extensively used for NF purposes [43, 52]. Although these coatings are effective in resisting protein adsorption, their excessive swelling compromises their mechanical strength and shortens their lifespan. Zhao fabricated the PEG molecular net cloth using a novel ‘‘visible light induced surface controlled graft cross-linking polymerization’’ (VSCGCP) technique. This PEG net cloth showed good resistance to non-specific protein adsorption and ultra-low swelling [90]. Yandi fabricated poly (HEMA-*co*-PEG $_{10}$ MA) copolymer brushes (thickness, 5-100 nm) via surface-initiated atom-transfer radical polymerization which showed most effective AF behavior in the thickness range of 20-40 nm against fouling of all types [91]. Lower hydration potential of thinner films and entanglement and crowding in thicker films seems to be a plausible explanation for this behavior. Schilp demonstrated the effect of PEG chain length on NF properties of the self-assembled monolayer (SAM) of oligo-(ethylene glycol) and PEG [92]. PEG SAM was found to inhibit spore settlement while PEG allowed settlement but with reduced adhesion strength which can be detached by applying minor hydrodynamic force.

Despite good protein repellency, PEG undergoes autoxidation and enzymatic cleaving in presence of oxygen and transition of metal ions which are abundant in seawater [93]. Mechanical robustness of PEG-based coatings is another major limitation. Moreover, PEG surface modification can be a feasible AF strategy for biomedical devices or water membranes, but coating on large marine structures would certainly pose a difficult challenge.

(b) Poly(zwitterion) coatings: The limitations of PEG-based coatings in terms of their stability led to the investigation of different polymer chemistries for antifouling applications. Zwitterionic polymers are ones which have both negative and positive charges. The charges can be on the same monomer (e.g. polybetaines and phosphorylcholines) or on different monomers (polysulfobetaine methacrylate). The principle of action is the same as that of hydrophilic poly(ethylene glycol) based polymers but the hydration is much stronger because of the ionic solvation (Figure 2.6b) [94, 95]. Zwitterionic polymers have shown resistance to protein and cell adsorption [52, 63]. Jiang reported the use of zwitterionic coatings based on poly(sulfobetaine methacrylate) (PSBMA) and poly(carboxybetaine methacrylate) (PCBMA) fabricated via SI-ATRP [93, 96]. These coatings were tested against marine algae *Ulva* and showed a low spore settlement and a lower degree of adhesion.

Interestingly, 2D tracking of the cyprid movement was quite different on these surfaces. pSMBA surface was explored by cyprids but no settlement was observed whereas no exploration by cyprids on the pCMBA surface was observed [96]. These polymers were also found to be non-toxic in solutions. In another work, Ventura *et al.* reported an increase in a non-fouling

performance of the PCBMA-incorporated lauryl methacrylate coatings. The coating showed the enhanced ease of removal of foulant N Incerta [97]. The PCBMA functionalized coating pyridine-based chlorine resistant zwitterionic polymers were found to be effective against the settlement of marine bacteria *V. cyclitrophicus* [98]. Yang *et al.* studied the effects of charge components on fouling behavior by incorporating anionic, cationic, zwitterionic and neutral components in a semi-interpenetrating network (SIPNs) polymer[99]. The zwitterion and anion functionalized SIPN were found to show improved antifouling activity against diatom *Navicula sp* and green alga *D. tertiolecta*. The enhanced non-fouling activity can be attributed to higher hydration capability of anion and zwitterion functionalized coatings.

(c) Amphiphilic Coatings: Amphiphilic polymer surfaces are composed of contrasting hydrophobic and hydrophilic domains at submicron or nano scales**.** The idea is to combine the hydrophobic components that reduce polar interactions of secreted bioadhesives with the surface and protein repellency properties of hydrophilic components. The non-fouling behaviour of the coating can be attributed to the superficial chemical heterogeneity which confuses the approaching fouling organism into evading settlement [63, 100]. Thermodynamically driven phase segregation of immiscible polymer blends creates the compositional heterogeneity at a nanoscale followed by *in situ* cross-linking. Such kinetically and thermodynamically driven phase separation creates surface features comparable to dimensions of secreted bioadhesive [101]. These chemically heterogeneous nanodomains present energetically unfavourable hydrophobic/hydrophilic interaction of secreted bioadhesives with the surface (Figure 2.7) [102]. The size of the chemical heterogeneity must be smaller than that of protein molecules (size -1-10 nm) to restrain their adsorption on a surface [63] effectively.

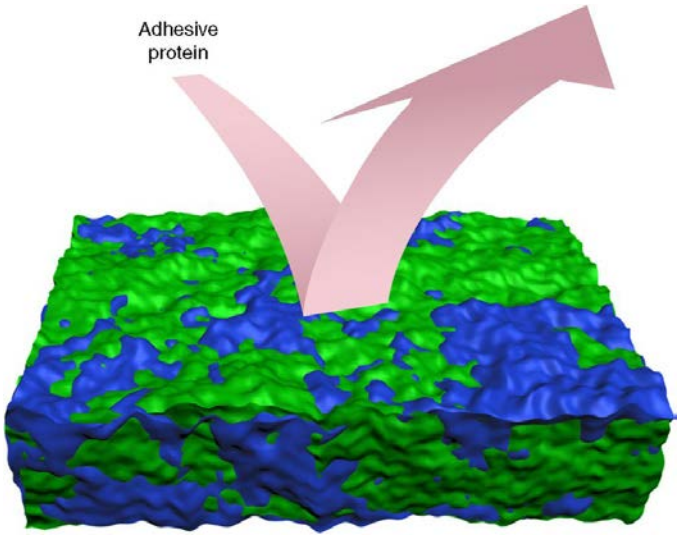

Figure 2.7 Schematic showing the chemically heterogeneous amphiphilic surface that repels proteins. These coatings are based on a combination of hydrophobic (green) and hydrophilic segment (blue) Reprinted from [100].

Table 2. 3 Summary of an AF performance of AA or HA modified TEFA. Adapted with permission from[103]

Organism	AA + TEFA	HA + TEFA
C. marina	Adhesion ↓	Adhesion ●
N. perminuta	Adhesion ●	Adhesion ●
U. linza	Adhesion ↓ Settlement ↓	Adhesion ● Settlement ↓
B. amphitrite	Settlement ↓	Settlement ↓
Field trials	Settlement ↓	Settlement ↓

↓ Reduction

● No significant difference

Underwater surface reconstruction of amphiphilic polymers is another important factor that affects the AF property of the coating. Krishnan fabricated amphiphilic block copolymer with fluorinated side chains and tested it against two algal species (*Ulva* and *Navicula*) which show different adherence behavior to hydrophobic and hydrophilic surfaces [104]. The amphiphilic surface resulted in a high level removal of both the species. The surface rearrangement under water imparting more hydrophilic character to amphiphilic polymers compared to PEGylated surfaces was a possible explanation for the high removal of *Navicula,* which adheres weakly to hydrophilic surfaces. Similarly, the surface reconstructed itself to the hydrophobic configuration by exposing fluoroalkyl chains when it came in contact with *Ulva*, the latter known to adhere weakly to hydrophobic surfaces.

Amphiphillic polymer derived from hydrophobic trifluoroethylamine (TFEA) modification of alginic acid (AA) and hyaluronic acid (HA) showed reduced adhesion of fouling organisms (bacteria, diatoms, and barnacle cypris larvae) [105]. The AF performance of this coating is summarized in table 3.3. Modification with TFEA also enhanced the coating stability due to reduced calcium uptake.

The composition of an amphiphilic polymer, sequencing and position of hydrophobic and hydrophilic moieties have found to affect the AF property of the coating. Wooley *et al.* fabricated amphiphilic coatings based on hyperbranched fluoropolymers (HBFP) and the variable weight percentage of PEG ranging from 14 to 55 %. The coating with 45 % PEG showed maximum resistance to zoospores of *Ulva* and also the most effective zoospores release properties [106]. In

another study, Zoelen *et al.* studied effects of a position and a number of fluorinated moieties in an amphiphilic coating on AF performance against algal species *Ulva*. It was found that the position of fluorinated moieties altered the surface chemistry thus affecting AF behaviour while their number affected the fouling release properties [107]. Keelie *et al.l* fabricated coatings having both amphiphilic and zwitterionic properties from commercially available inexpensive poly(styrene-co-allyl alcohol) (SAA) copolymer [108]. The hydroxyl groups were modified by reaction with 2-chloro-2-oxo-1,3,2-dioxaphospholane while hydrophobic sterynal groups were left unmodified. The resultant coating displayed excellent antifouling performance against zoospores of *Ulva* in comparison to commercialized PDMS based coating (Sylgard 184).

(d) Hydrogel: Hydrogel is a cross-linked, water-swollen polymeric network. These materials can retain a significant amount of water without dissolving. Their use as a marine AF material has been studied because of their environmentally benign nature. Figure 2.8 shows the antifouling mechanism of hydrogel coatings. Hydration layer formation interrupts the initial adhesion of proteins.Peeling off the top layer along with settled organism imparts self-regenerating properties to this coatings. Jiang *et al.* fabricated poly(NIPAM-co-BTM) hydrogel loaded with Ag nanoparticles [109]. These Ag nanocomposite hydrogels showed antimicrobial resistance against *E. coli* and anti-algae performance. Xue fabricated slippery hydrogel-released hydrous surface (SHRHS) by blending sodium polyacrylate (PAAS) powder into a silicone resin [110]. The coating showed lower attachment of microalgae in comparison with a silicone surface. The formation of a strong hydration layer by PAAS resisted the adhesion of organisms. Moreover, the slow hydrolysis of PAAS led to periodic self-regeneration, with exterior surface being peeled and washed away along with the settled organisms. The short-term stability due to poor mechanical properties and difficulty in using the coating over large marine structures have limited further advancements in hydrogel-based coatings. Zhang *et al.* fabricated anionic poly(acrylic acid/sulfopropyl methacrylate) and zwitterionic poly(acrylic acid/ sulfobetaine methacrylate) tethered fibrillar hydrogel coatings [111]. The coatings exhibited about 90-95 % decrease in the attachment of algae *D. tertiolecta* and *Navicula sp*. The fabricated coatings were all oleophobic , with oil contact angle greater than 150 °.

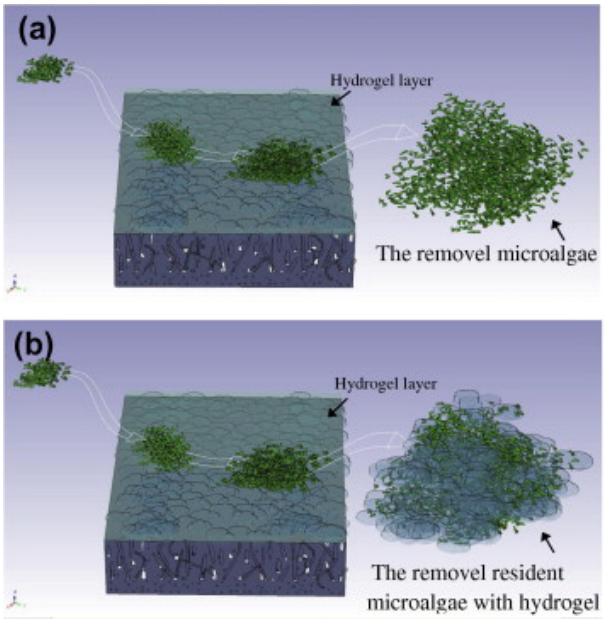

Figure 2.8: Schematic illustration of the underwater self-cleaning mechanism of the SHRHS (a) provides a smooth and highly slippery surface. The trapped water is retained by the hydrogel surface, leading to attachment difficulty for the organism. It also (b) provides a self-regeneration character, where the resident organisms can be carried off with hydrogel peeling. Reprinted from [110]

(e) Peptoid and peptide-based coatings: Another approach involves designing peptoid-based protein-resistant surfaces**.** Peptoids are synthetic peptidomimetic molecules with a peptide-like backbone and side chains appended to nitrogen atoms instead of alpha carbon as in amino acids [112]. Lack of hydrogen bond donors, strong proton-accepting ability and water solubility, are prerequisite for peptoid-based coatings to show effective AF properties. Patterson *et al.* functionalized a PDMS and a PEO surface with peptides and peptoids, respectively. The peptoid-functionalized surface showed the improved removal of *U. linza* and lower settlement of *N.incerta* than the peptide-based surfaces (Figure 2.9). The lack of hydrogen bond donors in peptoid-based coatings may be a possible explanation for their better performance [113]. Ederth investigated the effect of a position, configuration and a number of arginine residues in arginine-rich oligopeptide SAM on their interaction with *Ulva* spores. The position of arginine in SAM was found to influence the settlement of spores. SAM terminating with arginine showed higher settlement of spores than the SAMs where arginine was away from the surface [114].

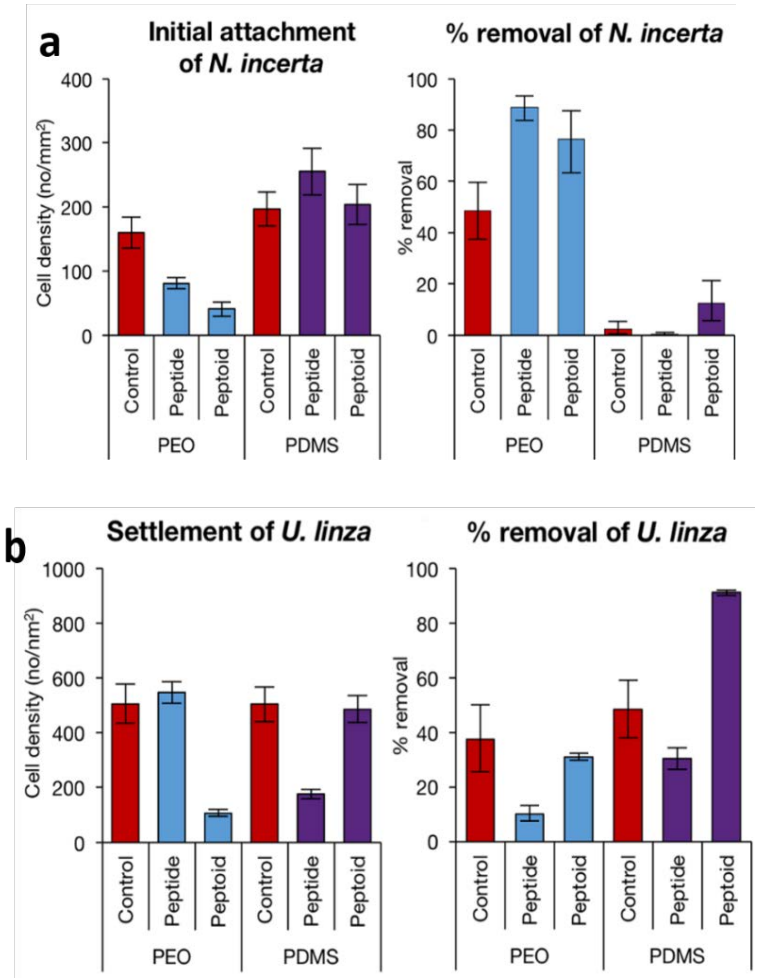

Figure 2.9 (a) Initial attachment and percentage removal of *N. incerta*. (b) Settlement and percentage removal of *U. linza*. Adapted with permission from [113]

(f) Saccharide-based coating: Polysaccharides have been investigated for marine AF because of their intrinsic hydrophilicity. Polysaccharides have shown resistance to protein, mammalian cells and marine organisms [115-117]. Bauer designed hydrophilic and amphiphilic polymeric coatings based on hyaluronic acid (HA) and chondroitin sulfate (CS) and tested against marine organisms for their antifouling potential. The coatings showed reduced settlement and adhesion strength of marine bacteria (*Cobetia marina),* cells of a diatom (*Navicula incerta*) and zoospores of the seaweed *Ulva linza* [103]. Cao *et al.* investigated marine AF potential of three polysaccharides, i.e. alginic acid (AA), pectic acid (PA) and hyaluronic acid (HA) against adhesion and settlement by barnacle cypris larvae and algal zoospores. All three coatings exhibited low settlement of *Ulva* spores. The reduction in settlement of barnacle cyprids on the HA coating was significant [117]. However, the polysaccharides have been known to complex with bivalent ions

such as Ca and Mg which support the growth of bacterial biofilms [118]. Thus, the polysaccharide-based coating would be a poor choice for marine AF applications despite their good protein repelling properties.

2.3.2.4 Anti-fouling Micro topographical surfaces

Topography has a pronounced effect on roughness and wettability of a surface and has been shown to influence bioadhesion [119-121]. It has been observed that many aquatic flora and fauna surfaces inhibit colonization by other species. In an aquatic environment, shark skin and lotus leaves are known to resist fouling because of their distinct micro/nano topography [122]. Thus, the motivation is to fabricate surfaces with similar micro/nano topographies that will resist fouling.

The attachment point theory and topography-induced wettability: Surfaces with micro-topographical features that are smaller than dimensions of the marine organism or their parts used to probe the surface during settling have shown anti-fouling behaviour [123]. Scardinio et al introduced the attachment point theory. The adhesion strength of a marine organism to a surface is related to the number of attachment points this marine organism has on the surface. Figure 2.10 illustrates the attachment point theory. Following this argument, smaller surface topographical features lead to weaker organism-surface interactions and an antifouling effect. Conversely, when the topographical features are of a larger dimension than that of the settling organism, more attachment points are present, facilitating stronger adhesion [124]. The attachment point theory was recorded and validated for spores of the green algae [123], diatoms [125], tubeworms and bryozoan [126].

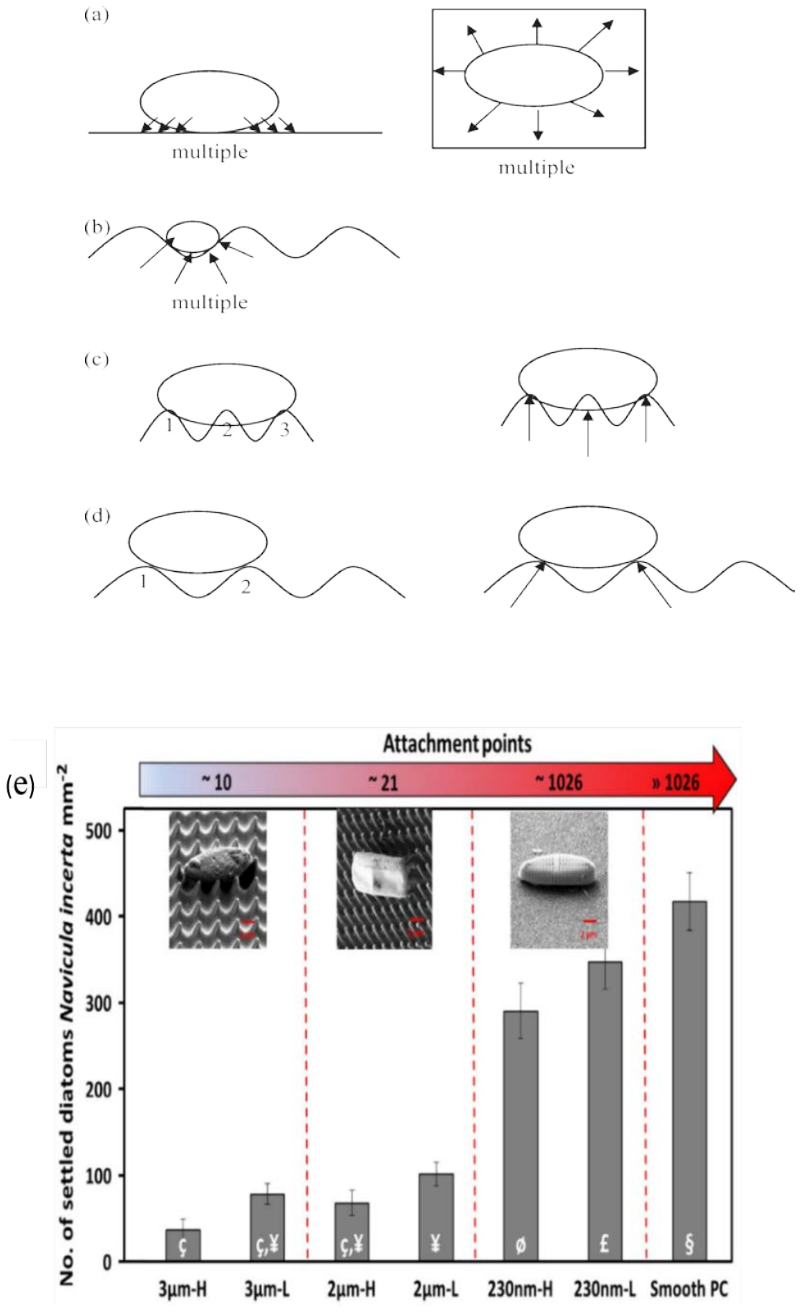

Figure 2.10 A schematic illustration of the attachment point theory of diatoms. (a): multiple attachment points for all diatoms on smooth surface (stronger adhesion); (b): *F. carpentariae* on 2 µm ripples (multiple attachment point, higher adhesion strength); (c): *N. jeffreyi* settling on 2 µm (3 attachment points – lower degree of adhesion); (d): *Amphora sp.* settling on 4 µm ripples (2 attachment points – least adhesion strength) Reprinted from [125]. (e) Attachment behaviour of *N. incerta* on microtextured PC surface validating attachment point theory, with H and L corresponding to height and length of the micro topographies. Reprinted from [127].

Interestingly, exceptions to the attachment point theory were shown by Friedlander *et al*. The adhesion of bacteria *E. coli* was significantly reduced on patterned PDMS substrate during the first 2h, but at longer exposure, the behaviour was significantly reversed [128]. Carman fabricated a multi feature patterned PDMS surface imitating shark skin consisting of ribs of 2 μm wide, 4-16 μm in length and 2 μm spaced. An 85 % reduction in settlement of zoospores of *Ulva Linza* was shown [129].

Barnacle settlement was reduced by almost 100 % on textured PVC as compared to smooth PVC. Cyprid settlement on textured PVC was shown to correlate with the aspect ratio of the surface features [130]. Zhang *et al.* fabricated the textured patterns inspired by taro leaf, rose petal and shark skin on PDMS and evaluated their antifouling activity against algae *N. closterium*, *P. tricornutum* and *Chlorella* [131]. Textures inspired by the shark skin demonstrated to be most effective with respect to antifouling behavior, as shown in figure 2.11 a. Sharkskin pattern has got imbricate boundary structure and V-grove riblets which makes the settlement of microalgae difficult. Rose petal and taro leaf have depressed and raised boundary structures respectively. The raised structure can provide refuge to foulants against hydrodynamic shear, and depressed pattern can increase the number of adhesion points promoting string attachment. Besides, this effect of boundary structure on antifouling performance was more pronounced than the hydrophobicity. Sullivan *et al.* studied the effect of five different microtextured PDMS surface on diatom attachment in static field trials [132]. The study demonstrated that microtexture features were ineffective against the settlement of diatoms because of different settlement strategies showed by diatoms. Also, the arrival of diatoms on surface occurs as agglomerates of planktonic and bacterial cells in field studies which can mask the effect of surface topography in a short time.

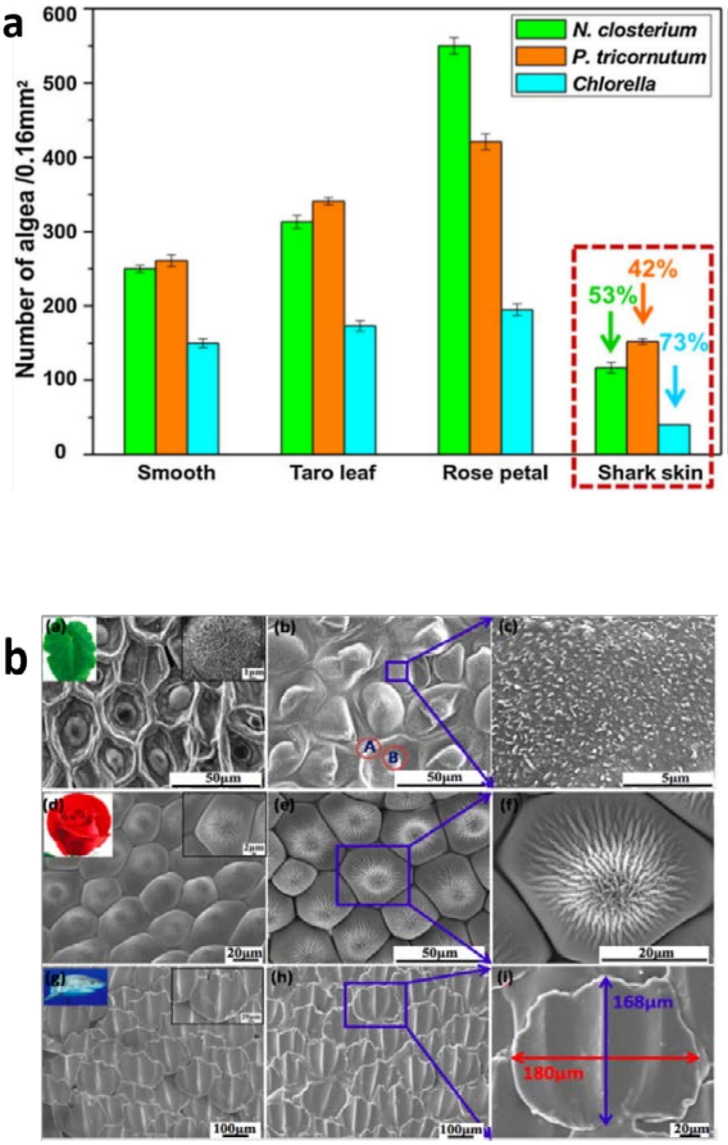

Figure 2.11 a. Settlement of microalgae on the textured coating. (b) SEM images of the created microtextures and original features of taro leaves, rose petals and shark skin. Reprinted from [131]

Topographical features having a single length scale are not likely to display antifouling activity as organisms creating bio-fouling come in varied sizes and shapes [133]. To deal with the aforementioned problem the idea of hierarchically wrinkled surface topography (HWST) was devised. Efimenko *et al.* fabricated uniaxial and biaxial HWST which remained free of fouling for 18 months during the field test in seawater. These coatings comprised of wrinkles of different scales varying from tens of nanometer to the fraction of millimetre arranged in the nested pattern (figure 2.12) [134].

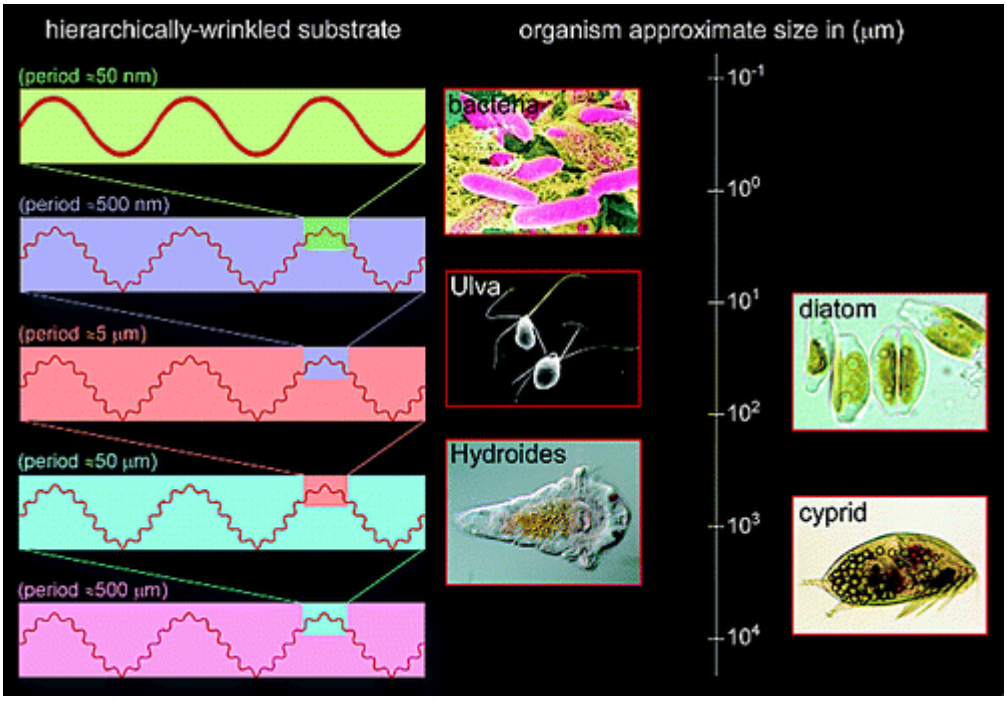

Figure 2.12 Schematic illustrating the design of HWST coatings comprising nested wrinkled topographies ranging from nanometers to a fraction of a millimeter. The right panel shows dimensions of few marine foulants. Reprinted from [134].

The topographical features also change the surface wettability, which can be another factor responsible for anti-fouling behaviour [135]. Increasing the surface roughness of hydrophobic/hydrophilic surfaces makes these surfaces superhydrophobic/superhydrophillic. This enhancement of wettability imparts this surfaces AF property similar to that of hydrophobic FR coating and hydrophilic NF coating. Xiao *et al.* fabricated the tapered microstructure on polycarbonate (PC) and tested their antifouling performance against spores of *Ulva linza* and diatom *N. incerta* [127]. An increase in settlement of *Ulva linza* spores was observed as compared

to the smooth PC surface when the Wenzel roughness of the coating increased. Contrastingly, a decrease in settlement of *N. incerta* was observed on the textured surface as compared to smooth PC because of reduced attachment points. Thus, a fine balance between roughness, attachment points and size range of a microtexture is essential for fabrication of surface topography for superior antifouling performance.

Laser ablation [15] and photolithography [12] in conjugation with nanoparticles modification and surface etching are methods that have been used to create micro-topographies on such substrates as poly (dimethylsiloxane) (PDMS), poly (vinylcholride) (PVC), polycarbonate and polyamide. However, substrate geometry and type limit the applicability of these concepts as these surface modifications require highly specific processing environments and complex fabrication techniques.

2.4 Challenges and future directions

Antifouling technology is transcending from biocide to non-biocide based strategies. However biocidal antifouling coatings (SPC) still dominate the current market. Biocides-based methods are more effective in combating biofouling than non-biocide methods. Winfield *et al.* made a comparative study on the antifouling efficiency of three commercial biocide antifouling (BAF) and fouling release (FR) coatings [136]. A comparative study of the antifouling efficiency of FR coatings (Intersleek 700, Intersleek 900, and Intersleek 1100) and BAF (Intersmooth 7460, Intersmooth 7465, and Intercept 8000) is shown in Figure 2.13. The difference in adherence of marine bacteria and eukaryotes on BAF and FR was observed, and an understanding of the observed differences will influence future developments of novel antifouling technologies.

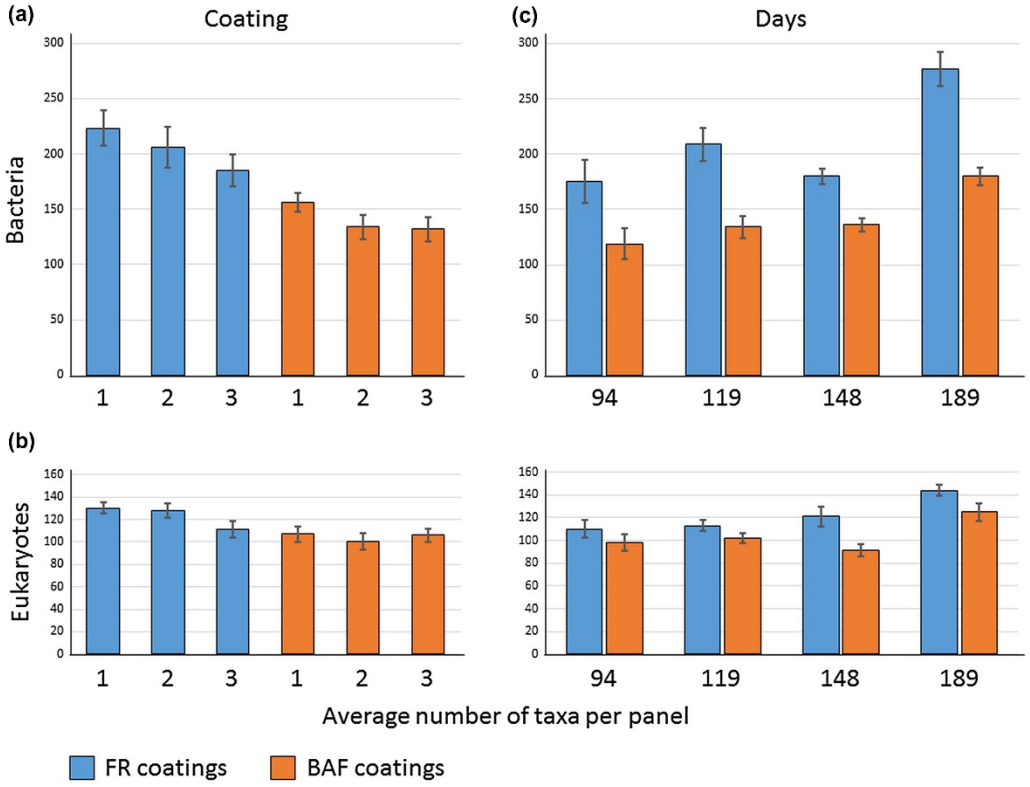

Figure 2.13 Average number of fouling organisms on six different coatings with respect to (a, b) coating types and (c,d) immersion period. Reprinted from [136]

The copper-containing SPC which are widely used may face stringent regulations in future.

The use of antifouling biocides should be regulated because of environmental risks associated with continuous release of such materials into an aquatic environment that can have chronic effects on flora and fauna; the ecotoxicity of commonly used biocides against common fouling species is shown in figure 2.14 [137]. Because of the adverse effects of biocides, regions like Europe, Oceania and some Asian countries have introduced strict rules and regulations on the use of biocides as antifoulants, but regions like South America have no regulations regarding the use of antifouling biocides [137].

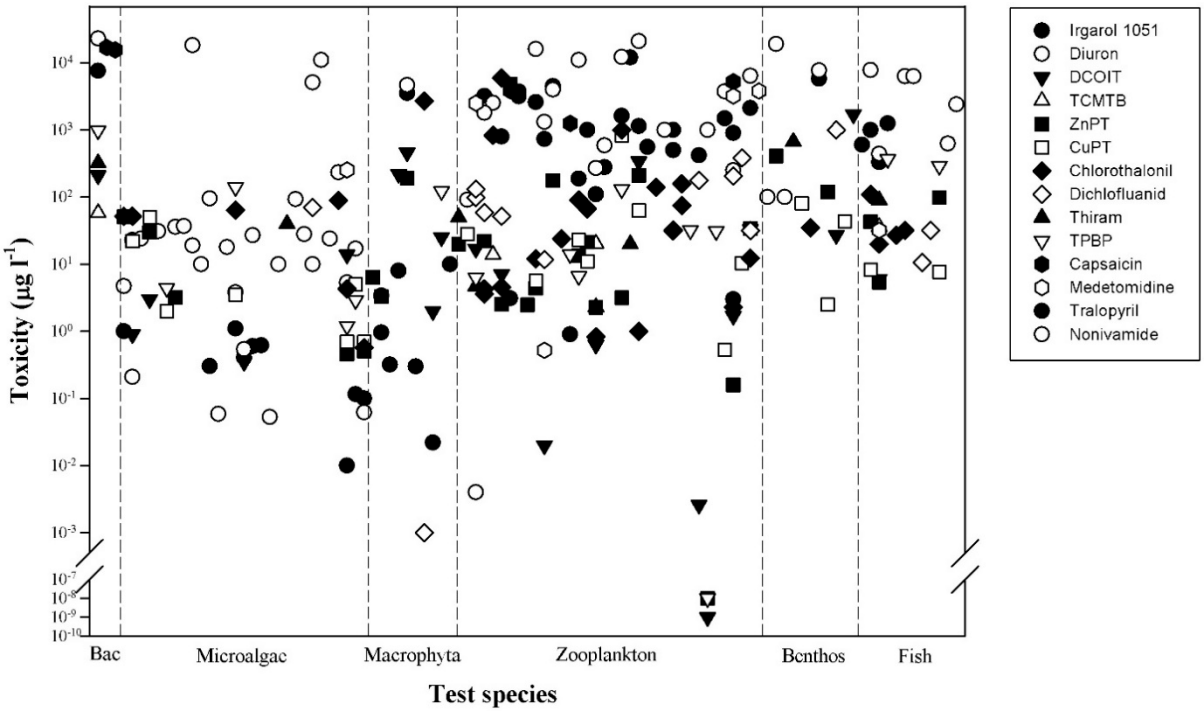

Figure 2. 14 A comparative chart illustrating the ecotoxicity of various biocides on marine fouling species. Reprinted from ref [137]

Concerns associated with the impact of the biocide-containing coatings on the environment is driving current research towards environmentally benign antifouling solutions. Fouling release and non-fouling coatings based on wettability, contrasting surface chemistry, and topography have shown significant antifouling performance but their low stability, high cost and difficulty in large-scale productions are current challenges faced by these environmentally benign coatings. Nanoparticle reinforcement of fouling release coatings has led to improved stability but leaching of nanoparticles from such coatings presents other environmental challenges as toxicity of nanoparticles in aquatic systems is a major issue [138-140]. Textured coating inspired by natural self-cleaning surfaces such as sharkskin, lotus leaf can be promising future candidates. However, these coatings have been found ineffective once the surface features get buried under the fouling assemblage. Besides, the fouling community is diverse in their size, shape and mode of survival. The multifunctional coating can be a better alternative compared to the coatings with a single mode of action. The multifunctional coating can be designed by an optimal blend of surface topography, surface chemistry (hydrophobic, hydrophilic, amphiphilic, and zwitterionic) and natural antifouling products. Chen *et al.* fabricated antifouling coating using nanotopography combined with the capsaicin, a natural biocide derived from pepper, showing promising results [141].

2.5 Conclusion

Biofouling involves interactions between fouling organisms and substrate. The mechanism of the organism attachment to surfaces and biofilm formation requires more in-depth research and understanding. More advanced studies are required to understand and detail effects of surface physcio-chemical properties and texture on the initial attachment of organisms and adhesion strength. Thus, in-depth understanding of material science, chemistry and biology are necessary to combat fouling. The marine antifouling coating market is predicted to reach a value of US $14.25 billion by 2025, which will drive future research towards novel environmentally benign antifouling technologies to overcome current drawbacks of engineered coatings, the antifouling activity of which is often time-dependent, making it difficult to reach long-term goals. These efforts will hopefully help realize nontoxic, durable, commercially viable, environmentally sustainable antifouling coatings that are urgently required.

References

1. Schultz, M.P., *Effects of coating roughness and biofouling on ship resistance and powering.* Biofouling, 2007. **23**(5): p. 331-341.

2. Pogiatzis, T., et al., Identifying optimal cleaning cycles for heat exchangers subject to fouling and ageing. Applied Energy, 2012. **89**(1): p. 60-66.

3. Fitridge, I., et al., The impact and control of biofouling in marine aquaculture: a review. Biofouling, 2012. **28**(7): p. 649-669.

4. Whelan, A. and F. Regan, *Antifouling strategies for marine and riverine sensors.* Journal of Environmental Monitoring, 2006. **8**(9): p. 880-886.

5. Manov, D.V., G.C. Chang, and T.D. Dickey, *Methods for reducing biofouling of moored optical sensors.* Journal of Atmospheric and Oceanic Technology, 2004. **21**(6): p. 958-968.

6. Delauney, L., C. Compere, and M. Lehaitre, *Biofouling protection for marine environmental sensors.* Ocean Science, 2010. **6**(2): p. 503-511.

7. Whelan, A. and F. Regan, *Antifouling strategies for marine and riverine sensors.* J. Environ. Monit., 2006. **8**(9): p. 880-886.

8. Akyildiz, I.F., D. Pompili, and T. Melodia, *Underwater acoustic sensor networks: research challenges.* Ad hoc networks, 2005. **3**(3): p. 257-279.

9. Lee, S., et al., Measurement of pH and dissolved oxygen within cell culture media using a hydrogel microarray sensor. Sensors and Actuators B: Chemical, 2008. **128**(2): p. 388-398.

10. Murphy, K., et al., A low-cost autonomous optical sensor for water quality monitoring. Talanta, 2015. **132**: p. 520-527.

11. Kerr, A., et al., The early stages of marine biofouling and its effect on two types of optical sensors. Environment International, 1998. **24**(3): p. 331-343.

12. Gipperth, L., The legal design of the international and European Union ban on tributyltin antifouling paint: Direct and indirect effects. Journal of environmental management, 2009. **90**: p. S86-S95.

13. Ytreberg, E., J. Karlsson, and B. Eklund, Comparison of toxicity and release rates of Cu and Zn from anti-fouling paints leached in natural and artificial brackish seawater. Science of the Total Environment, 2010. **408**(12): p. 2459-2466.

14. Clare, A.S. and J.T. Høeg, Balanus amphitrite or Amphibalanus amphitrite? A note on barnacle nomenclature. Biofouling, 2008. **24**(1): p. 55-57.

15. Anderson, M. and A. Underwood, *Effects of substratum on the recruitment and development of an intertidal estuarine fouling assemblage.* Journal of Experimental Marine Biology and Ecology, 1994. **184**(2): p. 217-236.

16. Schoener, A. and T.W. Schoener, The dynamics of the species-area relation in marine fouling systems: 1. Biological correlates of changes in the species-area slope. American Naturalist, 1981: p. 339-360.

17. Underwood, A. and M. Anderson, *Seasonal and temporal aspects of recruitment and succession in an intertidal estuarine fouling assemblage.* Journal of the Marine Biological Association of the United Kingdom, 1994. **74**(03): p. 563-584.

18. Hellio, C. and D. Yebra, Advances in marine antifouling coatings and technologies. 2009: Elsevier.

19. Callow, M.E., et al., Use of self-assembled monolayers of different wettabilities to study surface selection and primary adhesion processes of green algal (Enteromorpha) zoospores. Applied and Environmental Microbiology, 2000. **66**(8): p. 3249-3254.

20. Rittschof, D. and J. Costlow, Bryozoan and barnacle settlement in relation to initial surface wettability: A comparison of laboratory and field studies. Sci. Mar., 1989. **53**(2): p. 411-416.

21. Martín-Rodríguez, A.J., et al., From broad-spectrum biocides to quorum sensing disruptors and mussel repellents: Antifouling profile of alkyl triphenylphosphonium salts. PLoS One, 2015. **10**(4): p. e0123652.

22. Dafforn, K.A., J.A. Lewis, and E.L. Johnston, *Antifouling strategies: history and regulation, ecological impacts and mitigation.* Marine Pollution Bulletin, 2011. **62**(3): p. 453-465.

23. Institution, W.H.O. and U.S.N.D.B.o. Ships, *Marine fouling and its prevention*. 1952: United States Naval Institute.

24. Alzieu, C., et al., *Tin contamination in Arcachon Bay: effects on oyster shell anomalies.* Marine pollution bulletin, 1986. **17**(11): p. 494-498.

25. Gibbs, P. and G. Bryan, Reproductive failure in populations of the dog-whelk, Nucella lapillus, caused by imposex induced by tributyltin from antifouling paints. Journal of the Marine Biological Association of the United Kingdom, 1986. **66**(04): p. 767-777.

26. Okoro, H.K., et al., Sources, environmental levels and toxicity of organotin in marine environment - A review. Asian Journal of Chemistry, 2011. **23**(2): p. 473-482.

27. Buma, A.G., et al., Impact of the antifouling agent Irgarol 1051 on marine phytoplankton species. Journal of Sea Research, 2009. **61**(3): p. 133-139.

28. Shtykova, L., et al., Adsorption of antifouling booster biocides on metal oxide nanoparticles: Effect of different metal oxides and solvents. Progress in Organic Coatings, 2009. **64**(1): p. 20-26.

29. Onduka, T., et al., Toxicity of the antifouling biocide Sea-Nine 211 to marine algae, crustacea, and a polychaete. Fisheries science, 2013. **79**(6): p. 999-1006.

30. Thomas, K. and S. Brooks, *The environmental fate and effects of antifouling paint biocides.* Biofouling, 2010. **26**(1): p. 73-88.

31. Chambers, L.D., et al., *Modern approaches to marine antifouling coatings.* Surface and Coatings Technology, 2006. **201**(6): p. 3642-3652.

32. Yebra, D.M., S. Kiil, and K. Dam-Johansen, Antifouling technology—past, present and future steps towards efficient and environmentally friendly antifouling coatings. Progress in organic Coatings, 2004. **50**(2): p. 75-104.

33. Casse, F. and G.W. Swain, The development of microfouling on four commercial antifouling coatings under static and dynamic immersion. International biodeterioration & biodegradation, 2006. **57**(3): p. 179-185.

34. Meseguer Yebra, D., et al., Presence and effects of marine microbial biofilms on biocide-based antifouling paints. Biofouling, 2006. **22**(1): p. 33-41.

35. Almeida, E., T.C. Diamantino, and O. de Sousa, *Marine paints: the particular case of antifouling paints.* Progress in Organic Coatings, 2007. **59**(1): p. 2-20.

36. Marson, F., Anti‐fouling paints. I. Theoretical approach to leaching of soluble pigments from insoluble paint vehicles. Journal of Chemical Technology and Biotechnology, 1969. **19**(4): p. 93-99.

37. Yebra, D.M., et al., Reaction rate estimation of controlled-release antifouling paint binders: Rosin-based systems. Progress in Organic Coatings, 2005. **53**(4): p. 256-275.

38. Finnie, A.A. and D.N. Williams, Paint and coatings technology for the control of marine fouling. Biofouling, 2010. **18**.

39. Milne, A. and G. Hails, *Marine paint*. 1977, Google Patents.

40. Antizar-Ladislao, B., Environmental levels, toxicity and human exposure to tributyltin (TBT)-contaminated marine environment. A review. Environment international, 2008. **34**(2): p. 292-308.

41. Kirchner, S., et al., Prenatal exposure to the environmental obesogen tributyltin predisposes multipotent stem cells to become adipocytes. Molecular endocrinology, 2010. **24**(3): p. 526-539.

42. Lejars, M.n., A. Margaillan, and C. Bressy, *Fouling release coatings: a nontoxic alternative to biocidal antifouling coatings.* Chemical reviews, 2012. **112**(8): p. 4347-4390.

43. Yang, W.J., et al., *Polymer brush coatings for combating marine biofouling.* Progress in Polymer Science, 2014. **39**(5): p. 1017-1042.

44. Omae, I., *General aspects of tin-free antifouling paints.* Chemical reviews, 2003. **103**(9): p. 3431-3448.

45. Noel, R., Antisoiling composition for addition to the coatings of immersed bodies and coating containing it. FR2562554, 1985.

46. Olsen, S.M., et al., *Enzyme-based antifouling coatings: a review.* Biofouling, 2007. **23**(5): p. 369-383.

47. Kristensen, J.B., et al., *Antifouling enzymes and the biochemistry of marine settlement.* Biotechnology Advances, 2008. **26**(5): p. 471-481.

48. Pettitt, M., et al., Activity of commercial enzymes on settlement and adhesion of cypris larvae of the barnacle Balanus amphitrite, spores of the green alga Ulva linza, and the diatom Navicula perminuta. Biofouling, 2004. **20**(6): p. 299-311.

49. Tasso, M., et al., Antifouling potential of Subtilisin A immobilized onto maleic anhydride copolymer thin films. Biofouling, 2009. **25**(6): p. 505-516.

50. Dobretsov, S., et al., *Novel antifoulants: inhibition of larval attachment by proteases.* Marine Biotechnology, 2007. **9**(3): p. 388-397.

51. Chiovitti, A., et al., THE COMPLEX POLYSACCHARIDES OF THE RAPHID DIATOM PINNULARIA VIRIDIS (BACILLARIOPHYCEAE) 1. Journal of Phycology, 2003. **39**(3): p. 543-554.

52. Banerjee, I., R.C. Pangule, and R.S. Kane, Antifouling coatings: recent developments in the design of surfaces that prevent fouling by proteins, bacteria, and marine organisms. Advanced Materials, 2011. **23**(6): p. 690-718.

53. Kristensen, J., et al., Enzymatic generation of hydrogen peroxide shows promising antifouling effect. Biofouling, 2009. **26**(2): p. 141-153.

54. Schultz, M.P., C.J. Kavanagh, and G.W. Swain, Hydrodynamic forces on barnacles: Implications on detachment from fouling‐release surfaces. Biofouling, 1999. **13**(4): p. 323-335.

55. Kim, J., B.J. Chisholm, and J. Bahr, Adhesion study of silicone coatings: the interaction of thickness, modulus and shear rate on adhesion force. Biofouling, 2007. **23**(2): p. 113-120.

56. Brady Jr, R.F. and I.L. Singer, *Mechanical factors favoring release from fouling release coatings.* Biofouling, 2000. **15**(1-3): p. 73-81.

57. Brzozowska, A.M., et al., Effect of variations in micropatterns and surface modulus on marine fouling of engineering polymers. ACS applied materials & interfaces, 2017. **9**(20): p. 17508-17516.

58. Singer, I.L., J.G. Kohl, and M. Patterson, *Mechanical aspects of silicone coatings for hard foulant control.* Biofouling, 2000. **16**(2-4): p. 301-309.

59. Tao, S., L. Xu, and J.C. Fanguy, Optical fiber ammonia sensing probes using reagent immobilized porous silica coating as transducers. Sensors and Actuators B: Chemical, 2006. **115**(1): p. 158-163.

60. Kissa, E., *Fluorinated surfactants and repellents*. Vol. 97. 2001: CRC Press.

61. Baier, R.E., *Surface behaviour of biomaterials: the theta surface for biocompatibility.* Journal of Materials Science: Materials in Medicine, 2006. **17**(11): p. 1057.

62. Griffith, J.R. and J.D. Bultman, *Fluorinated naval coatings.* Industrial & Engineering Chemistry Product Research and Development, 1978. **17**(1): p. 8-9.

63. Krishnan, S., C.J. Weinman, and C.K. Ober, *Advances in polymers for anti-biofouling surfaces.* Journal of Materials Chemistry, 2008. **18**(29): p. 3405-3413.

64. Youngblood, J.P., et al., Coatings based on side-chain ether-linked poly (ethylene glycol) and fluorocarbon polymers for the control of marine biofouling. Biofouling, 2003. **19**(S1): p. 91-98.

65. Brady Jr, R.F., A fracture mechanical analysis of fouling release from nontoxic antifouling coatings. Progress in Organic Coatings, 2001. **43**(1-3): p. 188-192.

66. Edward, R., Ship's hull coated with anti-fouling silicone resin and method of coating. 1961, Google Patents.

67. Milne, A., *Anti-fouling marine compositions*. 1977, Google Patents.

68. Brady, R.F., Properties which influence marine fouling resistance in polymers containing silicon and fluorine. Progress in Organic Coatings, 1999. **35**(1): p. 31-35.

69. Schmidt, D., D. Shah, and E.P. Giannelis, *New advances in polymer/layered silicate nanocomposites.* Current Opinion in Solid State and Materials Science, 2002. **6**(3): p. 205-212.

70. Derbalah, A., et al., Mesoporous Alumina Nanoparticles as Host Tunnel-like Pores for Removal and Recovery of Insecticides from Environmental Samples. ChemPlusChem, 2015. **80**(7): p. 1119-1126.

71. Chakradhar, R.P.S., et al., Fabrication of superhydrophobic surfaces based on ZnO–PDMS nanocomposite coatings and study of its wetting behaviour. Applied Surface Science, 2011. **257**(20): p. 8569-8575.

72. Wouters, M., C. Rentrop, and P. Willemsen, Surface structuring and coating performance: novel biocidefree nanocomposite coatings with anti-fouling and fouling-release properties. Progress in Organic Coatings, 2010. **68**(1): p. 4-11.

73. Martinelli, E., et al., Amphiphilic block copolymer/poly (dimethylsiloxane)(PDMS) blends and nanocomposites for improved fouling-release. Biofouling, 2011. **27**(5): p. 529-541.

74. Selim, M.S., et al., Smart photo-induced silicone/TiO 2 nanocomposites with dominant [110] exposed surfaces for self-cleaning foul-release coatings of ship hulls. Materials & Design, 2016. **101**: p. 218-225.

75. Swain, G.W. and M.P. Schultz, *The testing and evaluation of non‐toxic antifouling coatings.* Biofouling, 1996. **10**(1-3): p. 187-197.

76. Watermann, B., et al., *Performance and effectiveness of non‐stick coatings in seawater.* Biofouling, 1997. **11**(2): p. 101-118.

77. THORLAKSEN[1], P., D.M. YEBRA[1], and P. CATALÀ, Hydrogel-based third generation fouling release coatings. 2010.

78. Holland, R., et al., Adhesion and motility of fouling diatoms on a silicone elastomer. Biofouling, 2004. **20**(6): p. 323-329.

79. Kim, B.Y., et al., Solvent‐resistant PDMS microfluidic devices with hybrid inorganic/organic polymer coatings. Advanced Functional Materials, 2009. **19**(23): p. 3796-3803.

80. Grümping, R., et al., *Microbial degradation of octamethylcyclotetrasiloxane.* Applied and environmental microbiology, 1999. **65**(5): p. 2276-2278.

81. Parrott, M.C. and J.M. DeSimone, *Relieving PEGylation.* Nature chemistry, 2012. **4**(1): p. 13.

82. Morra, M., *On the molecular basis of fouling resistance.* Journal of Biomaterials Science, Polymer Edition, 2000. **11**(6): p. 547-569.

83. Sharma, S., R.W. Johnson, and T.A. Desai, *XPS and AFM analysis of antifouling PEG interfaces for microfabricated silicon biosensors.* Biosensors and Bioelectronics, 2004. **20**(2): p. 227-239.

84. Nurioglu, A.G. and A.C.C. Esteves, Non-toxic, non-biocide-release antifouling coatings based on molecular structure design for marine applications. Journal of Materials Chemistry B, 2015. **3**(32): p. 6547-6570.

85. Chen, S., et al., Surface hydration: principles and applications toward low-fouling/nonfouling biomaterials. Polymer, 2010. **51**(23): p. 5283-5293.

86. Hucknall, A., S. Rangarajan, and A. Chilkoti, *In pursuit of zero: polymer brushes that resist the adsorption of proteins.* Advanced Materials, 2009. **21**(23): p. 2441-2446.

87. Ekblad, T., et al., Poly (ethylene glycol)-containing hydrogel surfaces for antifouling applications in marine and freshwater environments. Biomacromolecules, 2008. **9**(10): p. 2775-2783.

88. Taylor, W. and R.A. Jones, Protein adsorption on well-characterized polyethylene oxide brushes on gold: Dependence on molecular weight and grafting density. Langmuir, 2013. **29**(20): p. 6116-6122.

89. Efremova, N., S. Sheth, and D. Leckband, Protein-induced changes in poly (ethylene glycol) brushes: molecular weight and temperature dependence. Langmuir, 2001. **17**(24): p. 7628-7636.

90. Zhao, C., et al., PEG molecular net-cloth grafted on polymeric substrates and its bio-merits. Scientific reports, 2014. **4**: p. 4982.

91. Yandi, W., et al., Hydration and Chain Entanglement Determines the Optimum Thickness of Poly (HEMA-co-PEG10MA) Brushes for Effective Resistance to Settlement and Adhesion of Marine Fouling Organisms. ACS applied materials & interfaces, 2014. **6**(14): p. 11448-11458.

92. Schilp, S., et al., Physicochemical properties of (ethylene glycol)-containing self-assembled monolayers relevant for protein and algal cell resistance. Langmuir, 2009. **25**(17): p. 10077-10082.

93. Zhang, Z., et al., Polysulfobetaine-grafted surfaces as environmentally benign ultralow fouling marine coatings. Langmuir, 2009. **25**(23): p. 13516-13521.

94. Kitano, H., et al., Structure of water incorporated in sulfobetaine polymer films as studied by ATR‐FTIR. Macromolecular bioscience, 2005. **5**(4): p. 314-321.

95. He, Y., et al., Molecular simulation studies of protein interactions with zwitterionic phosphorylcholine self-assembled monolayers in the presence of water. Langmuir, 2008. **24**(18): p. 10358-10364.

96. Aldred, N., et al., Modulation of barnacle (Balanus amphitrite Darwin) cyprid settlement behavior by sulfobetaine and carboxybetaine methacrylate polymer coatings. Biofouling, 2010. **26**(6): p. 673-683.

97. Ventura, C., et al., Marine antifouling performance of polymer coatings incorporating zwitterions. Biofouling, 2017. **33**(10): p. 892-903.

98. Yang, R., et al., Synergistic Prevention of Biofouling in Seawater Desalination by Zwitterionic Surfaces and Low‐Level Chlorination. Advanced Materials, 2014. **26**(11): p. 1711-1718.

99. Yang, W., et al., *Contribution of Charges in Polyvinyl Alcohol Networks to Marine Antifouling.* ACS applied materials & interfaces, 2017. **9**(21): p. 18295-18304.

100. Callow, J.A. and M.E. Callow, Trends in the development of environmentally friendly fouling-resistant marine coatings. Nature communications, 2011. **2**: p. 244.

101. Gudipati, C.S., et al., Hyperbranched fluoropolymer and linear poly (ethylene glycol) based amphiphilic crosslinked networks as efficient antifouling coatings: an insight into the surface compositions, topographies, and morphologies. Journal of Polymer Science Part A: Polymer Chemistry, 2004. **42**(24): p. 6193-6208.

102. Lin, F.Y., W.Y. Chen, and M.T. Hearn, Thermodynamic analysis of the interaction between proteins and solid surfaces: application to liquid chromatography. Journal of Molecular Recognition, 2002. **15**(2): p. 55-93.

103. Bauer, S., et al., Resistance of Amphiphilic Polysaccharides against Marine Fouling Organisms. Biomacromolecules, 2016. **17**(3): p. 897-904.

104. Krishnan, S., et al., Anti-biofouling properties of comblike block copolymers with amphiphilic side chains. Langmuir, 2006. **22**(11): p. 5075-5086.

105. Bauer, S., et al., Resistance of Amphiphilic Polysaccharides against Marine Fouling Organisms. Biomacromolecules, 2016. **17**(3): p. 897-904.

106. Gudipati, C.S., et al., The antifouling and fouling-release perfomance of hyperbranched fluoropolymer (HBFP)− poly (ethylene glycol)(PEG) composite coatings evaluated by adsorption of biomacromolecules and the green fouling alga Ulva. Langmuir, 2005. **21**(7): p. 3044-3053.

107. van Zoelen, W., et al., Sequence of hydrophobic and hydrophilic residues in amphiphilic polymer coatings affects surface structure and marine antifouling/fouling release properties. ACS Macro Letters, 2014. **3**(4): p. 364-368.

108. Seetho, K., et al., Facile Synthesis of a Phosphorylcholine-Based Zwitterionic Amphiphilic Copolymer for Anti-Biofouling Coatings. ACS Macro Letters, 2015. **4**(5): p. 505-510.

109. Jiang, D., et al., Antimicrobial and antifouling nanocomposite hydrogels containing polythioether dendron: high-loading silver nanoparticles and controlled particle release. Colloid and Polymer Science, 2016. **294**(12): p. 2021-2028.

110. Xue, L., et al., *Bio-inspired self-cleaning PAAS hydrogel released coating for marine antifouling.* Journal of colloid and interface science, 2014. **421**: p. 178-183.

111. Zhang, R., et al., The Tethered Fibrillar Hydrogels Brushes for Underwater Antifouling. Advanced Materials Interfaces, 2017. **4**(7).

112. Simon, R.J., et al., *Peptoids: a modular approach to drug discovery.* Proceedings of the National Academy of Sciences, 1992. **89**(20): p. 9367-9371.

113. Patterson, A.L., et al., Role of Backbone Chemistry and Monomer Sequence in Amphiphilic Oligopeptide-and Oligopeptoid-Functionalized PDMS-and PEO-Based Block Copolymers for Marine Antifouling and Fouling Release Coatings. Macromolecules, 2017.

114. Ederth, T., et al., Interactions of zoospores of Ulva linza with arginine-rich oligopeptide monolayers. Langmuir, 2009. **25**(16): p. 9375-9383.

115. Fyrner, T., et al., Saccharide-functionalized alkanethiols for fouling-resistant self-assembled monolayers: synthesis, monolayer properties, and antifouling behavior. Langmuir, 2011. **27**(24): p. 15034-15047.

116. Ederth, T., et al., Resistance of galactoside-terminated alkanethiol self-assembled monolayers to marine fouling organisms. ACS applied materials & interfaces, 2011. **3**(10): p. 3890-3901.

117. Cao, X., et al., Resistance of polysaccharide coatings to proteins, hematopoietic cells, and marine organisms. Biomacromolecules, 2009. **10**(4): p. 907-915.

118. De Kerchove, A.J. and M. Elimelech, Calcium and magnesium cations enhance the adhesion of motile and nonmotile Pseudomonas aeruginosa on alginate films. Langmuir, 2008. **24**(7): p. 3392-3399.

119. Bazaka, K., R.J. Crawford, and E.P. Ivanova, *Do bacteria differentiate between degrees of nanoscale surface roughness?* Biotechnology journal, 2011. **6**(9): p. 1103-1114.

120. Fletcher, R.L. and M.E. Callow, *The settlement, attachment and establishment of marine algal spores.* British phycological journal, 1992. **27**(3): p. 303-329.

121. Blossey, R., *Self-cleaning surfaces—virtual realities.* Nature materials, 2003. **2**(5): p. 301-306.

122. Kirschner, C.M. and A.B. Brennan, *Bio-inspired antifouling strategies.* Annual review of materials research, 2012. **42**: p. 211-229.

123. Schumacher, J.F., et al., Engineered antifouling microtopographies–effect of feature size, geometry, and roughness on settlement of zoospores of the green alga Ulva. Biofouling, 2007. **23**(1): p. 55-62.

124. Howell, D. and B. Behrends, A review of surface roughness in antifouling coatings illustrating the importance of cutoff length. Biofouling, 2006. **22**(6): p. 401-410.

125. Scardino, A., E. Harvey, and R. De Nys, Testing attachment point theory: diatom attachment on microtextured polyimide biomimics. Biofouling, 2006. **22**(1): p. 55-60.

126. Scardino, A., J. Guenther, and R. De Nys, *Attachment point theory revisited: the fouling response to a microtextured matrix.* Biofouling, 2008. **24**(1): p. 45-53.

127. Xiao, L., et al., Topographic cues guide the attachment of diatom cells and algal zoospores. Biofouling, 2018. **34**(1): p. 86-97.

128. Friedlander, R.S., et al., *Bacterial flagella explore microscale hummocks and hollows to increase adhesion.* Proceedings of the National Academy of Sciences, 2013. **110**(14): p. 5624-5629.

129. Carman, M.L., et al., Engineered antifouling microtopographies–correlating wettability with cell attachment. Biofouling, 2006. **22**(1): p. 11-21.

130. Schumacher, J.F., et al., Species-specific engineered antifouling topographies: correlations between the settlement of algal zoospores and barnacle cyprids. Biofouling, 2007. **23**(5): p. 307-317.

131. Zhang, Y., et al., *Influence of biomimetic boundary structure on the antifouling performances of siloxane modified resin coatings.* Colloids and Surfaces A: Physicochemical and Engineering Aspects, 2017. **528**: p. 57-64.

132. Sullivan, T. and F. Regan, *Marine diatom settlement on microtextured materials in static field trials.* Journal of Materials Science, 2017. **52**(10): p. 5846-5856.

133. Genzer, J. and K. Efimenko, Recent developments in superhydrophobic surfaces and their relevance to marine fouling: a review. Biofouling, 2006. **22**(5): p. 339-360.

134. Efimenko, K., et al., *Development and testing of hierarchically wrinkled coatings for marine antifouling.* ACS applied materials & interfaces, 2009. **1**(5): p. 1031-1040.

135. Vladkova, T., *Surface engineering for non-toxic biofouling control.* Journal of the University of Chemical Technology and Metallurgy, 2007. **42**(3): p. 239-256.

136. Winfield, M.O., et al., Comparative study of biofilm formation on biocidal antifouling and fouling-release coatings using next-generation DNA sequencing. Biofouling, 2018: p. 1-14.

137. Martins, S.E., et al., ecotoxicity of organic and organo-metallic antifouling co-biocides and implications for environmental hazard and risk assessments in aquatic ecosystems. Biofouling, 2018. **34**(1): p. 34-52.

138. Moore, M., Do nanoparticles present ecotoxicological risks for the health of the aquatic environment? Environment international, 2006. **32**(8): p. 967-976.

139. Dale, A.L., et al., Modeling nanomaterial environmental fate in aquatic systems. 2015, ACS Publications.

140. Avelelas, F., et al., Efficacy and ecotoxicity of novel anti-fouling nanomaterials in target and non-target marine species. Marine Biotechnology, 2017. **19**(2): p. 164-174.

141. Lu, Z., et al., Flexible Hydrophobic Antifouling Coating with Oriented Nanotopography and Nonleaking Capsaicin. ACS applied materials & interfaces, 2018. **10**(11): p. 9718-9726.

Chapter 3

High Temperature PECVD of Terpinen-4-ol

In this chapter, the effect of substrate temperature on Plasma enhanced chemical vapor deposition of Terpinen-4-ol is examined. The chapter describes the physical, chemical and optical properties of PECVD deposited Terpinen-4-ol at various substrate temperatures and RF input powers. The results of the study identifies substrate temperature as deposition variables affecting the deposition mechanism and resulting film properties. The result are published as *Avishek kumar, Daniel S. Grant, Kateryna Bazaka, Mohan V. Jacob, Tailoring Terpenoid Plasma Polymer Properties by Controlling the Substrate Temperature during PECVD. Journal of Applied. Polymer. Science, 2018, 135, 45771.*

Tailoring Terpenoid Plasma Polymer Properties by Controlling the Substrate Temperature during PECVD

Abstract

Polymers derived from natural, minimally-processed materials have recently emerged as a more sustainable alternative to synthetic polymers, with promising applications in biocompatible and biodegradable devices. Plasma-enhanced deposition is well-suited to one-step, fast and efficient synthesis of highly cross-linked inert polymers directly from natural resources, however fabrication of biologically-active polymers remains a challenge. Plasma processing parameters influences the properties such as surface energy, roughness, morphology and chemical composition of deposited polymers and thus their final applications. This article reports on the important role of substrate temperature (T_S) in the chemical composition, wettability, refractive index, and cross-linking density of plasma polymers derived from terpenoids. Experiments are conducted as a function of deposition power P_d, and substrate temperature, T_S. T_S is varied from 40-280 °C and is externally controlled. Atomic force microscopy analysis reveals the change in deposition mechanism attributed to shadowing effect at higher T_S and P_d. Increase in band gap (E_g) with high T_s deposition for terpenoid based plasma polymers is observed. Swelling behavior analyzed by in-situ ellipsometry affirms the enhanced cross-link density with increasing deposition rate. Fourier transform infrared (FTIR) analysis exhibits the formation of additional chemical moieties with increasing T_S. Increase in deposition rate with increasing T_S at higher P_d supports the theory of direct incorporation of depositing particles as dominant mechanism of plasma polymerization in current study.

Keywords: Synthesis and processing technique, optical properties, thermal properties

As published in : Avishek kumar, Daniel S. Grant, Kateryna Bazaka, Mohan V. Jacob ,Tailoring Terpenoid Plasma Polymer Properties by Controlling the Substrate Temperature during PECVD. Journal of Applied. Polymer. Science, 2018, 135, 45771.

3.1 Introduction

Polymers from natural materials have emerged as a potentially sustainable and economical alternative to those derived from inorganic or synthetic sources [1]. Those materials that are volatile at room temperature are well-suited for chemical vapor deposition family of techniques. Plasma can act as a catalyst, driving the polymerization of those compounds that are not polymerized under similar conditions in the absence of plasma. Plasma polymerization assists solvent-free, one-step, low-temperature deposition of many kinds of precursor. Thin films produced in such a manner are transparent, smooth, defect free, and have excellent chemical stability and adhesion to substrate [2]. Their thermal, physical and chemical stability substantiates their use as dielectric interlayers and encapsulating layers in electronics [3, 4], and as protective coatings for medical devices [5-9] especially due to the high degree of cross-linking of plasma polymers. The highly cross-linked structure enhances the dielectric break down strength of plasma polymers but causes higher dielectrics loss than conventional polymers [10]. However, comparable dielectrics loss of plasma polymers with conventional polymer material have been observed at frequency less than 1 kHz .Presence of polar moieties and highly cross-linked structure plays a crucial role in affecting the dielectric constant and loss of these materials at higher frequency [11, 12]. Cross-linking also limits the biological activity and biodegradation of plasma polymers, which may be attractive for such applications as bactericidal coatings on medical implants or biodegradable electronics, respectively. This limitation can be addressed by tailoring the degree of crosslinking, which can be attained by controlling plasma processing parameters. Among the processing parameters, applied power and substrate temperature [13-15] significantly affect the mechanism of polymer formation, and hence its chemical composition and structure.

Two different models, namely adsorbed layer and flow-in model have been described to account for mechanisms of plasma deposition as a function of temperature [13-15]. The flow-in model is based on direct incorporation of depositing particles (ions, radicals, and metastable species) in a growing film. Increased deposition rate has been found within the temperature range where direct incorporation is dominant. In plasma polymerization of C:H film obtained from methane, it was found that at substrate temperature above 450 K direct incorporation mechanism was dominant whereas deposition via adsorption is dominant below temperature 450 K [16]. Increase in deposition rate with increasing substrate temperature has been also reported in Plasma enhanced chemical vapor deposition (PECVD) deposition of SiO_X film [17]. Adsorption model is based on chemical reactions between the surface of the substrate and the film formed, with particles physically adsorbed on them during the deposition [13]. There is

adsorption/desorption equilibrium of monomer on the substrate. In this regime, deposition rate decreases with increasing substrate temperature. Residence time of monomer molecules and their flux density are considered as limiting factor which influences the monomer coverage and polymerization rate. Inverse dependence of residence time with substrate temperature accounts for the decrease in growth rate.

Numerous reports are available about the fabrication and properties of Terpenoid derived plasma polymers [4, 18-20]; however the effect of substrate temperature on the properties of the plasma polymer films remain unexplored. A strong correlation has been observed between the deposition variables, and chemical, optical and morphological properties of plasma deposited films. Deposition power was a significant determinant of film properties. With an increase in input RF power from 10W to 100W band gap decreased from 2.93 eV to 2.64 eV [21], and the water contact angle [21] increased.. The biodegradation profile of the plasma polymer sample was controlled by changing the input RF power. The films fabricated at lower deposition power enabled synthesis of biocompatible films with enhanced antimicrobial activity [6, 22].The substrate temperature will also be responsible for tailoring the plasma polymer properties.

The present work investigates the effect of substrate temperature T_S and deposition power on deposition rate, polymerisation mechanism, and fundamental properties of thin films fabricated from terpinen-4-ol. Optical band gap of the films have been analysed which indicates its tunability in given range of T_s and as a potential material for high temperature low dielectric applications.

3.2 Experimental

3.2.1 Materials

An essential oil-derived precursor, terpinen-4-ol ($C_{10}H_{18}O$), purity = 99 %, molecular weight = 154.24 g/mol was sourced from Australian Botanical Products and used without further purification. Microscopic glass slide (75 mm × 25 mm) were used as substrates and were first cleaned using decon (Decon Laboratories Ltd.) and distilled water. Substrates were then ultrasonically cleaned in acetone bath for 30 min, rinsed in propan-2-ol bath for another 30 min, and then air dried.

3.2.2 Plasma polymerization set-up

Terpinen-4-ol films were fabricated in a low pressure, capacitively coupled radio frequency tubular quartz plasma deposition system (5 cm in diameter and 80 cm in length). The power was capacitively coupled by metallic half shells outside the body of the reactor. The flow rate of monomer was controlled through needle valve. The distance between active plasma region and monomer injection site was optimized kept 30 cm for each deposition. The actual flow rate of monomer was estimated to be around 29 cm^3/ min for all the deposition power and temperature and was kept constant. External heating system was used to vary the substrate temperature. The substrate temperature were measured using a thermocouple in contact with substrate holder surface. The temperature was controlled and maintained through variac connected to the heater. Between depositions, reactor was cleaned using 60 W O_2 plasma at the pressure of 0.253 mbar for 30 min.

Films were deposited at 30, 100, 200, 300, 400 W input RF power at different substrate temperature of 40, 140, 180 and 280 °C. For the substrate temperature of 280 °C, film deposition only took place at 30 and 100 W applied power. For each deposition, the deposition time and working pressure were kept constant, at 15 min and 0.066 mbar, respectively

3.2.3 Thin film characterization

3.2.3.1 Physical analysis

Thickness and refractive index of the prepared terpinen-4-ol thin films were measured by variable angle spectroscopic ellipsometry (J. A. Woollam, model M2000 D). Measurements were taken at three different angles of incidence (55 °, 60 °, and 65 °) for all the samples in wavelength range of 200−1000 nm. Three-component optical model consisting of substrate/thin film/surface roughness was used for modelling of terpinen-4-ol thin films. This approach yielded best fit between the model and measured data. The film component was modelled using Cauchy function in optically transparent region. Absorbance studies of thin films were performed using fiber optic UV-visible spectrometer AvaSpec 2048 in wavelength region of 200- 1000 nm.

In-situ ellipsometry was performed to analyze swelling behavior of deposited films when exposed to water to estimate the stability of terpinen-4-ol thin films in aqueous media. The custom built liquid cell configuration was used for the measurement. Dynamic measurements were taken for 7 min to observe the change in thickness using Woollam Complete Ease program.

Static and dynamic water contact angle was measured using optical contact angle measuring system (KSV CAM 101). For each measurement, a water droplet with drop volume of 3 µl was deposited onto the surface of the terpinen-4-ol thin film and observed for 2 min for each sample type. A minimum of five measurements were performed on each sample, and averaged over 5 samples. Young–Laplace fitting method was used to describe the water–surface interactions [23]. Surface energy of the samples were evaluated from contact angle data obtained using three different liquids (water, di-iodomethane, and ethylene glycol) using Van Oss-Chaudhury-Good (VCG) [24] methods.

Topography and roughness of terpinen-4-ol thin films were examined using AFM (NT-MDT, Russian Federation) operated in semi-contact mode. The average roughness was estimated from 5 µm × 5 µm AFM image and all imaging were collected at room temperature.

3.2.3.2 Chemical analysis

Chemical characterization of thin films was performed by FT-IR spectroscopy (Perkin Elmer, spectrum-100) in ATR mode. Microscopic glass slides were used as deposition substrates for FTIR analysis. Spectra were obtained from 4000 to 1250 cm^{-1} with resolution of 4 cm^{-1} averaged over 124 scans.

3.3 Results and discussion

3.3.1 Deposition rate vs temperature

Dependence of deposition rate on substrate temperature and power is shown in figure 3.1. The deposition rate was found to decrease with substrate temperature over the substrate temperature range of 40–140 °C and deposition power P_d of 30, 100, and 200 W. The decrease in deposition rate suggests that in this intermediate temperature regime, the deposition kinetics is adsorption limited [13]. Gursoy et al. showed the decreasing deposition rate with increasing substrate temperature in initiated PECVD of poly(2-hydroxyethylmethacrylate) [25]. However, the deposition rate was found to increase for the substrate temperature of 180 °C for the above deposition powers. The increase in deposition rate with substrate temperature was observed for deposition power of 300 and 400 W. In this power and temperature regime, the film growth is surface reaction limited which is directly correlated to temperature. The particles are directly

incorporated via chemisorption into the growing film as the rate of surface reactions is accelerated in this regime.

Flux of depositing species J_m depends on gas temperature near the substrate which is identical to the substrate temperature T_S and their volume concentration *N* (Equation 1), where B is monomer-dependent constant [13].

$$J_m \approx B \cdot N \cdot \sqrt{T_S} \quad (1)$$

The adsorption of depositing species depends on their sticking coefficient γ and flux density. The sticking coefficient γ can have contributions from both sticking probability of physisorption and direct sticking probability of chemisorption. An activation barrier exists between the physisorption and chemisorption. Surface temperature effects the probability of physisorption whereas the kinetic energy of incoming depositing species plays an important role in chemisorption as extra energy is needed to overcome the activation barrier. The combined effect of high T_S facilitating higher flux of depositing species and high power (300, 400 W in present case) creating species with higher kinetic energy which directly gets incorporated via chemisorption can offer a plausible explanation for the observed increase in deposition rate. Coclite et al. showed increasing deposition rate with increasing substrate temperature in i-PECVD deposition of thin organosilicon films [26].

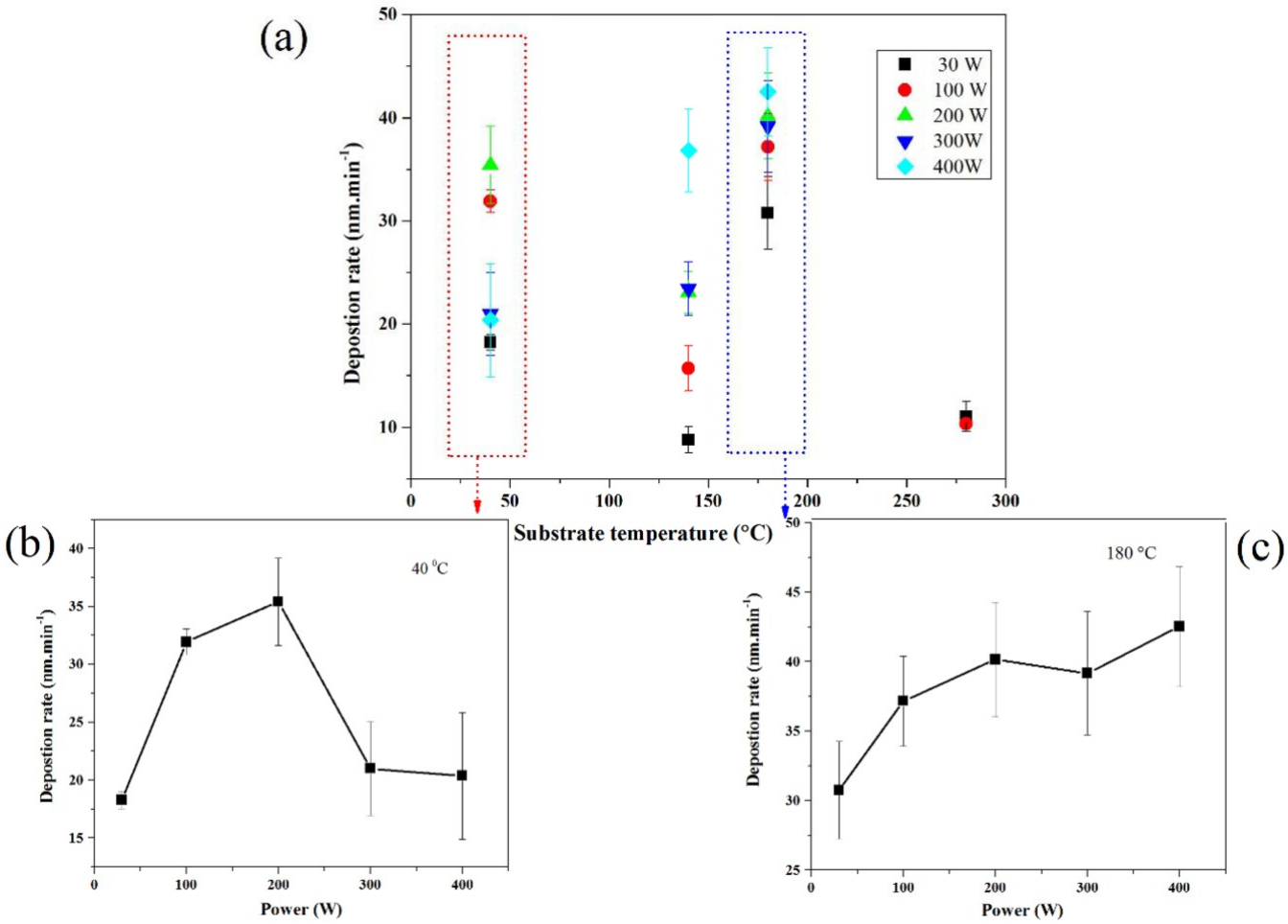

Figure 3. 1(a): Plasma deposition rate at substrate temperatures of 40 ˚C, 140˚C , 180 ˚C and 280˚C and various input plasma power. (b), (c) showing deposition rate vs power for TS of 40 ˚C and 180 ˚C respectively.

3.3.2 FT-IR analysis

FT-IR spectra of terpinen-4-ol films deposited at different temperatures and power levels of (a) 100 and (b) 400 W, respectively, are shown in figure 3.2. The broad transmission feature in 3100–3700 cm^{-1} region is attributed to –O–H stretching. Absorption of moisture from ambient air can give rise to broadening of –O–H peaks, however this possibility was ruled out by vacuum annealing of the sample after deposition for 24 hr and performing FT-IR analysis immediately after the annealing. There is significant decrease in –O–H vibration as the deposition temperature is increased. Increasing the substrate temperature eliminates the hydroxyl groups which are not

thermally stable [27]. In the spectra region 3000–2850 cm^{-1}, there are three distinct peaks which seem to converge into one broad peak. The peaks at 2952, 2869, and 2928 cm^{-1} can be attributed to asymmetric/symmetric stretching of C– H in $–CH_3$ and asymmetric stretching in $–CH_2$, respectively. With increasing substrate temperature it can be observed that IR absorption by $–CH_x$ group (3000-2850) increases but there is no significant change in intensity above the substrate temperature of 40 C. With increasing substrate temperature there is enhancement in cross-linking which makes the film denser and closely packed with molecules. The bands in 3000–2800 cm^{-1} region are preserved in resultant polymers, however their intensity changes when compared to that of the monomer. The peak in 1640–1680 cm^{-1} region observed in spectra of films deposited at 40 °C can be attributed to alkenyl C=C stretch. The shift of this peak to 1700–1710 cm^{-1} region with increasing deposition temperature indicates the formation of carbonyl (C=O) group which is much more pronounced in film fabricated at 400 W. The possible explanation for this phenomena can be an increase in reaction rate of –OH moieties with alkenyl C=C sites in growing film assisted by higher substrate temperature. The peak at 1455/1377 cm^{-1} corresponds to methyl C-H asymmetric/symmetric bend and is preserved in deposited polymers.

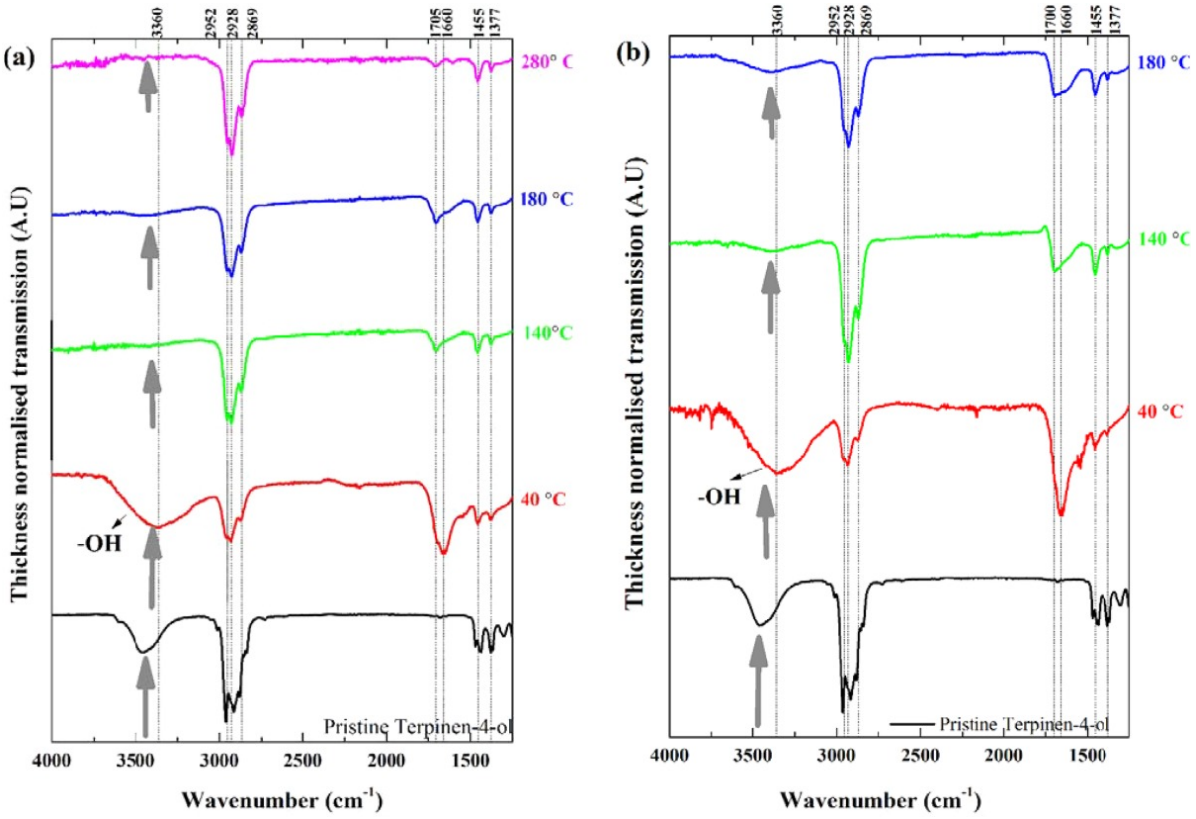

Figure 3. 2 Thickness normalized FTIR transmission spectra of terpinen-4-ol films deposited at two power levels (a) 100 W and (b) 400 W at various substrate temperatures. With increase in deposition temperature decrease in –OH peak intensity is observed (grey arrow). The spectrum of precursor material is added for comparison. Dashed lines indicate

absorption by various chemical moieties in polymer

3.3.3 UV-vis spectrometry

Films deposited at different substrate temperatures and applied powers were analyzed with UV-vis spectroscopy. Figure 3.3 shows UV-vis spectra of RF-PECVD deposited terpinen-4-ol thin films deposited at 100 and 400 W. The absorption peak appears at ~290 nm for all the samples except for that deposited at 400 W and substrate temperature of 180 °C, where a shift of 10 nm towards the visible region of the spectrum is observed. The peak absorption at 290 nm can be attributed to $n \rightarrow \pi^*$ transition of carbonyl group, which is conjugated to unsaturated C=C bond. The absorption peak shifts to ~300 nm for films fabricated at 400 W, T_S = 180 °C, which is attributed to higher degree of conjugation. Broadening of the peak with increasing power and substrate temperature suggests high degree of cross-linking [28]. Intramolecular charge transfer can be one of the reasons for the appearance of low intensity shoulder between 400–500 nm for the samples deposited at 400 W and T_S of 40 and 180 °C.

Optical band gap values of terpinen-4-ol films fabricated under different conditions are presented in table 3.1. The band gap was calculated from UV-vis absorption spectra using Tauc plot. The best fit was obtained for n = 2, indicating an indirect allowed band transition in all terpinen-4-ol polymers. The optical band gap decreased with increasing substrate temperature except at deposition temperature of 140 °C. Decrease of E_g in amorphous carbon based material due to increase in sp^2 carbon content and varying hydrogen content has been reported by Oppedisano et al [29]. Optical band gap values changed from 3.52 eV to 3.38 eV as the substrate temperature increased for deposition power of 400 W. The electronic dielectric constant (ε_r) of the films were obtained by using simple relation, $\varepsilon_r = n^2$ in visible region as extinction coefficient k is negligible in this region[30].

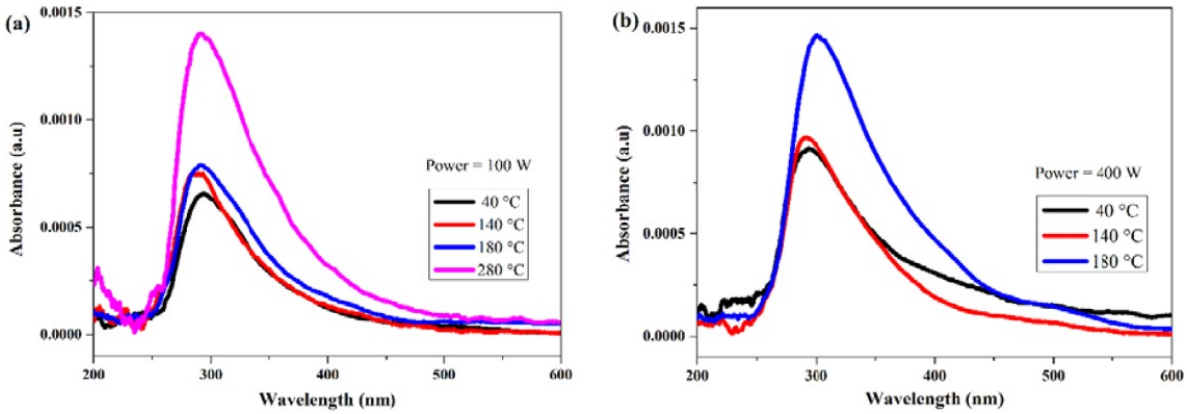

Figure 3. 3 UV-vis spectra of terpinen-4-ol plasma polymers at various substrate temperature and power level of (a) 100W, and (b) 400 W.

3.3.4 Wetting behavior and stability

The wettability of terpinen-4-ol thin films were measured as a function of substrate temperature and deposition power, as shown in figure 3.4. The static and dynamic water contact angle was found to increase with increasing substrate temperature across all deposition powers, with the most significant increase taking place as the deposition temperature changes from 40 to 140 °C. Table 3.1 shows the static and dynamic contact angle along with surface energy for deposited films along with their surface energy. The contact angle hysteresis *(Advancing contact angle - Receding contact angle)* is greater for the films deposited at 400 W which is indicative of pinning of liquid drop to greater extent while receding. The columnar morphology of films fabricated at 400 W can lead to greater pinning of liquid probe while receding. The receding contact angle at substrate temperature of 40 ^{0}C was almost zero for both the deposition power. Receding contact angle was observed to decrease with the increasing substrate temperature which indicates greater fraction of high energy areas in the films[31, 32]. As the deposition temperature increases to 140, 180 and 280 °C, the static contact angle values remain relatively stable within 75–85 °C range. The higher contact angle at higher substrate temperature can be attributed to a decrease in hydrophilic –OH species within the film matrix and an increase in hydrophobic $-CH_x$ species, particularly when substrate temperature increases from 40 to 140 °C. A decrease in polar groups in the film increases the hydrophobicity of the films. Increase in static contact angle from ~87 ° to ~99 ° as substrate temperature varied from 25 °C to 60 °C have been reported in PECVD-deposition of poly(2,2,3,4,4,4-hexafluorobutyl acrylate) [33].

Table 3. 1 The effect of substrate temperature and applied power on wettability and surface energy

Deposition power	Substrate temperature (°C)	Static contact angle (Θ)	Advancing contact angle *Adv* (Θ)	Receding contact angle *Rec* (Θ)	Surface energy ($J.m^{-2}$)
100 W	40	40.81	46.84	-	44.48
	140	85.1	91.96	66.69	43.82
	180	83.66	89.17	63.21	44.22
	280	82.5	85.75	46.35	44.08
400 W	40	37.65	43.56	-	55.71
	140	79.25	87.21	45.35	45.37
	180	77.62	84.31	37.36	45.46

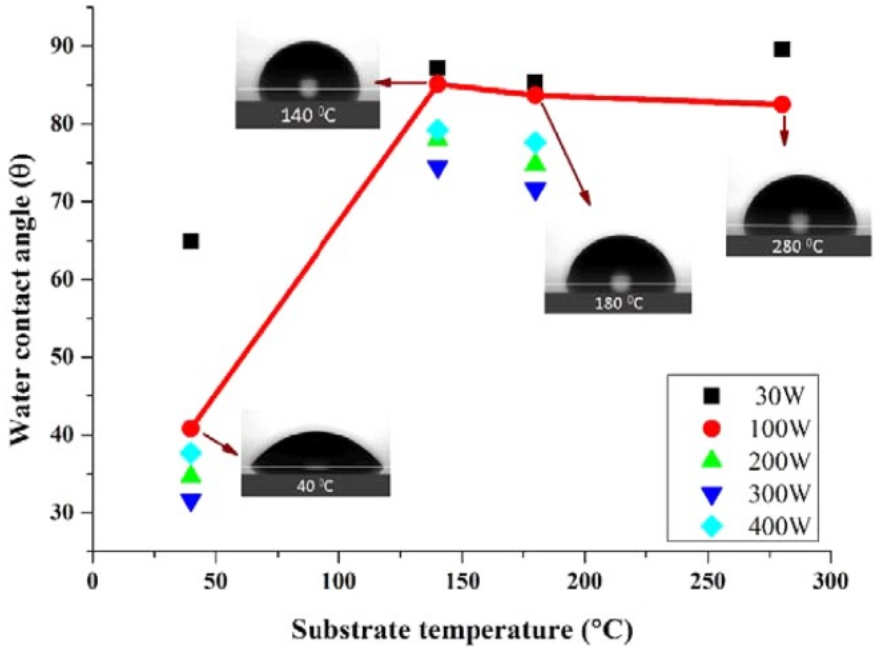

Figure 3. 4 Water contact angle at various substrate temperatures and deposition powers. Photographs of deionized water droplets (V = 3 µl) on terpinen-4-ol polymers deposited at power of 100 W and varied substrate temperature are shown in the graph..

Figure 3.5 shows the swelling behavior of films as a function of deposition rate. The degree of swelling is given by H (thickness of swelled polymer)/ H_0 (thickness of dry polymer) and was determined by in-situ ellipsometry measurements. The dissolution behavior of films showed inverse relationship with deposition rate. The swelling behavior of the film has direct correlation

to the degree of cross-linking in the film. Lower degree of swelling indicates towards more crosslinked structure in plasma polymers. Free volume in deposited thin films decreases with increasing degree of cross-linking. Decrease in free volume leads to a decrease in space for chain movements and also the dissolution of unbound trapped species in the film. Previous studies have shown a direct relationship between refractive index and the degree of cross-linking in acetylene plasma polymers [34]. Sulyaeva et al. showed an increase in refractive index of boron carbonitride films fabricated by PECVD from 1.5 to 2.8 with increasing temperature of deposition [35]. Higher refractive index indicates higher crosslinking in films, which in turn is associated with superior stability in aqueous media. The positive change in refractive index of films with increasing deposition rate, though small, corroborates the analysis of swelling behavior by in-situ ellipsometry. Table 3.2 shows the effect of substrate temperature on deposition rate, refractive index, band gap, electronic dielectric constant and the degree of swelling.

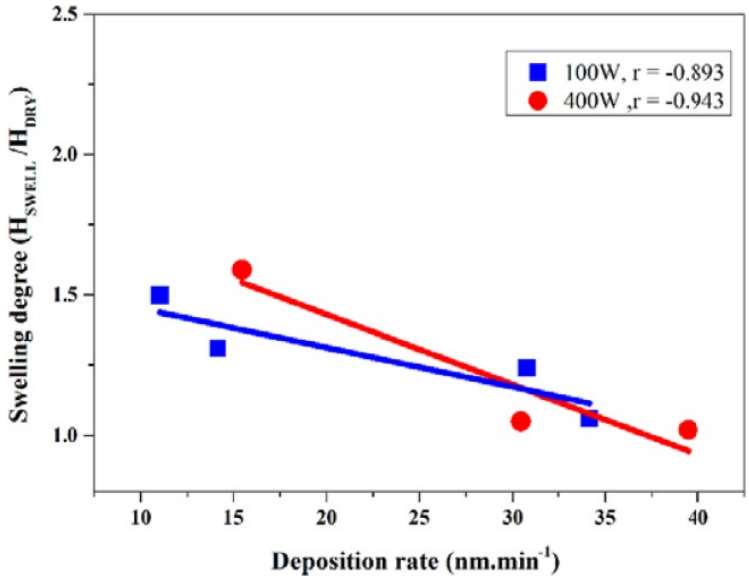

Figure 3. 5 Comparison of swelling degree of films deposited at different power levels at various deposition rates.

Table 3. 2 The effect of substrate temperature and applied power on refractive index, optical band gap, electronic dielectric constant and the degree of swelling

Deposition power	Substrate temperature (°C)	Deposition Rate (nm/ Min)	Refractive index (n) at 500 nm	Band gap E_{og} (eV)	Swelling degree	ε_r
100 W	40	31.92	1.58	3.54	1.24	2.49
	140	15.7	1.56	3.79	1.31	2.43
	180	37.16	1.59	3.52	1.06	2.52
	280	10.34	1.61	3.51	1.50	2.59
400 W	40	20.36	1.59	3.52	1.59	2.52
	140	36.18	1.60	3.57	1.05	2.56
	180	42.51	1.66	3.39	1.02	2.75

3.3.5 Thin film morphology

AFM micrographs of terpinen-4-ol thin films deposited at 400 W and substrate temperatures (T_S) of 40, 140, and 180 °C are shown in figure 3.6. The corresponding SEM images are shown in figure 3.7. The surfaces were found to be very smooth, with RMS roughness values below 1 nm for various substrate temperatures, with slight increase in roughness observed as the substrate temperature increased. As the substrate temperature increases, the film surface evolves from granular to columnar morphology. The change in morphology with increasing deposition rate indicates the change of growth mechanism in terpeinen-4-ol plasma films. It is possible that desorption of highly volatile species and ion bombardment contributed to chain scissioning at the surface of the growing polymer. Small polymer fragmented units may also aggregate on the substrate surface to induce greater surface roughening [36-38], facilitated by increased mobility of these units at higher substrate temperature. The shift towards columnar morphology suggests the shadowing effect [39, 40] outcompetes the surface diffusion effects, which has reverse impact of reducing roughness. Due to shadowing effects, the crest of the surface receives more building units than the troughs due to its larger receiving solid angle, which promotes higher growth rate at the crest than the trough. A qualitatively opposite evolution of film topography as a function of

deposition temperature was observed in roll-to-roll deposition of silica-like moisture barrier coatings at atmospheric pressure [41]. The low roughness films can be used in applications where smooth coatings are desired, such as antifouling coatings [42, 43] and as interfacial layers in organic electronics [44].

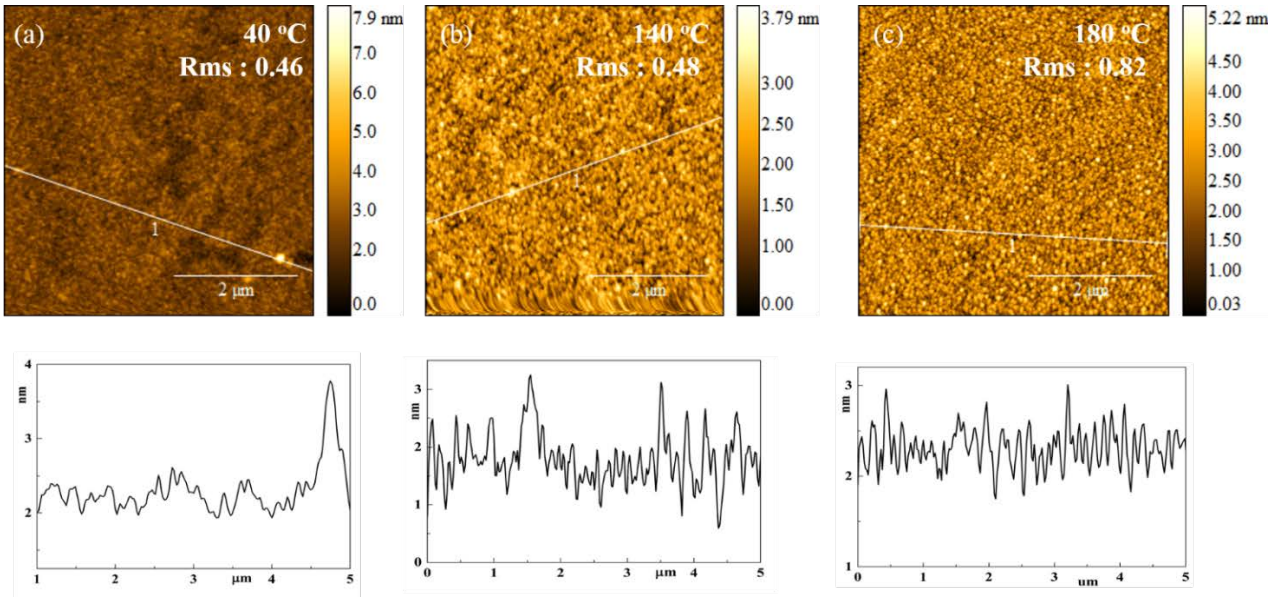

Figure 3. 6 Atomic force microscopy images and line profile showing the effect of substrate temperature on the morphology and roughness of terpinen-4-ol films deposited at the power of 400 W at T_S 40 ˚C , 140 ˚C and 180 ˚C.

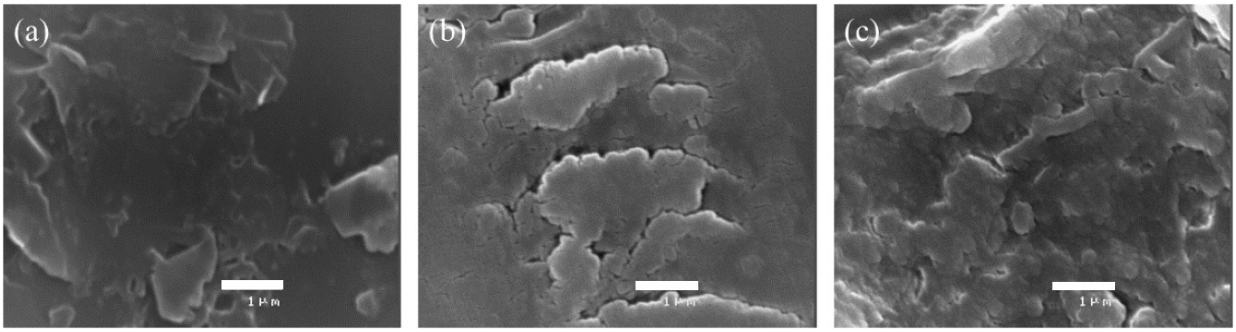

Figure 3. 7 Scanning electron microscope images of terpinen-4-ol films deposited at the power of 400 W at T_S (a) 40 ˚C , (b) 140 ˚C and (c) 180 ˚C . *Inset scale: 1µm*

3.3.6 Comparison with literature and discussion

The findings from the set of experiments gives the critical information about impact of substrate temperature on chemistry and structure of terpinen-4-ol plasma polymers. Table 3.3 summarizes the effect of controlled substrate temperature on contact angle, optical band gap, and refractive index, as well as provides a comparison with that the previously reported values [21].

Table 3. 3. Comparison of properties of terpinen-4-ol plasma polymers with substrate temperature as an uncontrolled and controlled processing parameter

	Reported values [21] P_d = 100 W	P_d = 100 W				P_d = 400 W		
T_s (°C)	Uncontrolled	40	140	180	280	40	140	280
θ (°)	75.2	40.8	85.2	83.7	82.5	37.7	79.3	77.6
E_g (eV)	2.64	3.54	3.79	3.52	3.50	3.52	3.56	3.38
n	1.55	1.58	1.56	1.59	1.61	1.59	1.60	1.66

From the results of two sets of experiments (variable P_d and fixed T_S; variable T_S and fixed P_d) the chemical composition of films seems to be substrate temperature dependent only while other properties such as wettability & refractive index ,are dependent on both P_d and T_S. Substrate temperature affects the adsorption/desorption process at the surface during deposition, which in turn controls the rate and mechanism of deposition. The increase in deposition rate with substrate temperature hints towards the direct incorporation of depositing particles as deposition mechanism at high P_d. Formation of carbonyl functionalities in the growing film was assisted by increasing substrate temperature. An increase in CH_X species in films with increasing substrate temperature is a plausible explanation for the observed increase in value of the water contact angle. Decrease in the swelling degree with increasing deposition rate indicates the latter as one of the key variables affecting the degree of cross-linking in films. Substrate temperature at higher deposition power has pronounced effect on morphology of thin films. Though there was slight increase in roughness with increasing substrate temperature, the topography change from granular to columnar structure was pronounced, indicating the shadowing effect during growth. This study exhibits increase in optical band gap of plasma polymerized terpinene-4-ol films from 2.67 to 3.54 when deposited at elevated substrate temperature. This shows the highest optical

band gap tunability of the terpinene-4-ol plasma polymer film by controlling the substrate temperature.

Gaining a wide control over the properties of terpinen-4-ol plasma polymers makes them a promising material for a wider range of applications .Use of plasma polymer as dielectrics have been widely proposed in literature [12]. Polymers with band gap > 3 eV have been found suitable for use as dielectric material [45]. Applications such avionic power conditioning [46] , pulse power system [47] and many require dielectrics which are stable over wide temperature range. Biaxially oriented poly-propylene is currently most used polymer capacitor but has maximum operation temperature less than 100 ^{0}C. Aromatic poly urea (ArPU) showed relatively high dielectric constant (4.2) and breakdown strength (690 MV/m) but values were consistent only till 180 C [48]. Dielectrics property of Aromatic polythiourea fabricated by Wu.et.al showed no significant change till temperature of 150^{0}C [49]. Figure3.8 shows the maximum working temperature of reported polymer dielectrics along with their dielectric constants. Boxed region displays the expected place of terpinene-4-ol plasma polymers as dielectric material in figure 3.8. Polyimide (PI) and fluorine polyester (FPE) are recent additions in this chart and have been extensively studied. However these materials possess difficulty in terms of their solution processbility as they are insoluble in most organic solvents because of their rigid molecular structure. Plasma polymerization overcomes the issues related with solution processbility as it is compatible to majority of organic and inorganic precursor materials. The electronic dielectric constant of the terpinene-4-ol films fabricated at various deposition temperature are in range of 2.5-2.75 with E_g > 3 eV which makes them a potential material for low k dielectrics application. These films can find a potential use as high temperature low dielectric material as it is thermally stable in high temperature range (approx. ~100-300 ^{0}C). Besides this the sub nanometer roughness and low water wettability of this films are important properties which will facilitate their better incorporation in device structure. Ultra-smooth surface and minimal moisture sensitivity are critical to ensuring low loss and high breakdown strength[49, 50].

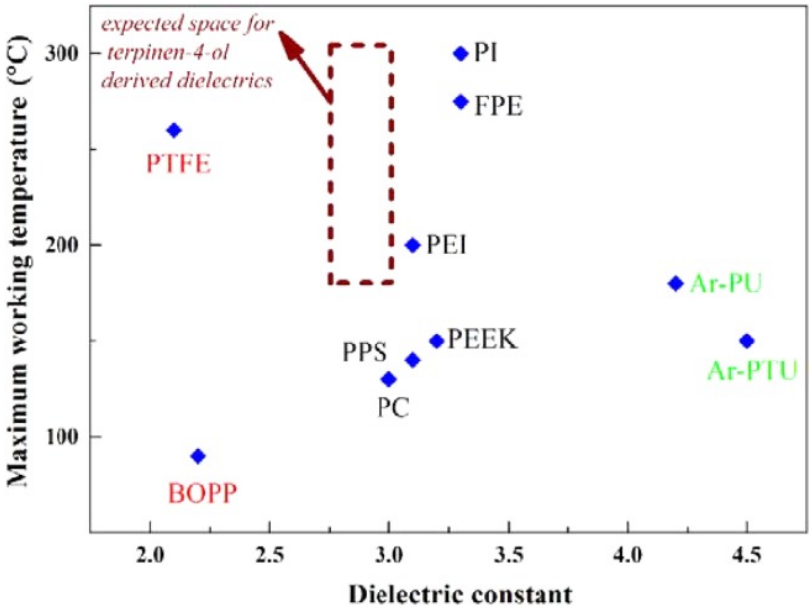

Figure 3. 8 Dielectric constant and maximum working temperature of some high temperature organic polymers dielectrics: Biaxially oriented polypropylene (BOPP)[51], polycarbonate (PC)[51] ,polyphenylsulfide (PPS)[52] ,polyetheretherketone (PEEK)[53] ,polytetrafluoroethylene (PTFE)[52] ,polyetherimide (PEI)[52] ,fluorene polyester (FPE)[54, 55] ,polyimide (PI)[56] , aromatic polyurea (Ar-PU)[48] , aromatic polythiourea (Ar-PTU)[49]. The boxed region displays the expected place of terpinene-4-ol plasma polymers in the graph.

.

3.4 Conclusion

The deposition kinetics, structure, morphology and physio-chemical properties of Terpinen-4-ol thin films have been investigated as function of deposition temperature. Thermally stable Terpinen-4-ol thin films of uniform properties are fabricated over wide temperature range (40 - 300 ^{o}C). Increase in deposition rate with T_S at higher power indicates towards different film forming mechanism. Direct incorporation of film forming species via chemisorption in this particular power-temperature regime seems to be plausible explanation. Increase in optical band gap (E_g) of about 1 eV and decrease in water wettability of films deposited at high temperature can be explained on account of enhanced cross-linking of thin films and loss of –OH species respectively. It is shown that in addition to deposition power, substrate temperature determines both the deposition rate and deposition mechanism, and consequently, influences the chemistry, stability, and morphology of the resultant films. Plasma processing parameters such as power and substrate temperature plays crucial role in tailoring the properties of deposited polymer.

Applications of plasma polymers depends on their properties such as surface energy, roughness, morphology, and chemical composition which is dependent on the choice of suitable plasma process parameters during deposition. As such, substrate temperature can be considered an important process control that can be used to tune the assembly and subsequent performance of thin films fabricated from terpinen-4-ol using PECVD.

References

1. Bazaka, K., M.V. Jacob, and K. Ostrikov, *Sustainable Life Cycles of Natural-Precursor-Derived Nanocarbons.* Chemical reviews, 2015. **116**(1): p. 163-214.

2. Tsougeni, K., et al., "Smart" polymeric microfluidics fabricated by plasma processing: controlled wetting, capillary filling and hydrophobic valving. Lab on a Chip, 2010. **10**(4): p. 462-469.

3. Ozaydin-Ince, G., A.M. Coclite, and K.K. Gleason, CVD of polymeric thin films: applications in sensors, biotechnology, microelectronics/organic electronics, microfluidics, MEMS, composites and membranes. Reports on Progress in Physics, 2011. **75**(1): p. 016501.

4. Jacob, M.V., et al., Plasma polymerised thin films for flexible electronic applications. Thin Solid Films, 2013. **546**: p. 167-170.

5. Ershov, S., et al., Free radical-induced grafting from plasma polymers for the synthesis of thin barrier coatings. RSC Advances, 2015. **5**(19): p. 14256-14265.

6. Bazaka, K., et al., Plasma-assisted surface modification of organic biopolymers to prevent bacterial attachment. Acta biomaterialia, 2011. **7**(5): p. 2015-2028.

7. Gulati, K., et al., Biocompatible polymer coating of titania nanotube arrays for improved drug elution and osteoblast adhesion. Acta biomaterialia, 2012. **8**(1): p. 449-456.

8. Wertheimer, M.R., *Plasma processing and polymers: a personal perspective.* Plasma Chemistry and Plasma Processing, 2014. **34**(3): p. 363-376.

9. Jacobs, T., et al., Plasma surface modification of biomedical polymers: influence on cell-material interaction. Plasma Chemistry and Plasma Processing, 2012. **32**(5): p. 1039-1073.

10. Jiang, H., et al., The relationship between chemical structure and dielectric properties of plasma-enhanced chemical vapor deposited polymer thin films. Thin Solid Films, 2007. **515**(7): p. 3513-3520.

11. Lee, S., et al., Effects of hydroxyl groups in polymeric dielectrics on organic transistor performance. Applied physics letters, 2006. **88**(16): p. 162109.

12. Bhattacharyya, D., et al., Plasma-Polymerized Multistacked Organic Bipolar Films: A New Approach to Flexible High-κ Dielectrics. Advanced Materials, 2008. **20**(12): p. 2383-2388.

13. Deutsch, H., et al., *On the temperature dependence of plasma polymerization.* Contributions to Plasma Physics, 1988. **28**(2): p. 149-155.

14. Kersten, H., et al., The energy balance at substrate surfaces during plasma processing. Vacuum, 2001. **63**(3): p. 385-431.

15. Kersten, H. and G. Kroesen, *On the temperature dependence of the deposition rate of amorphous, hydrogenated carbon films.* Journal of Vacuum Science & Technology A, 1990. **8**(1): p. 38-42.

16. Von Keudell, A. and W. Möller, *A combined plasma-surface model for the deposition of C: H films from a methane plasma.* Journal of applied physics, 1994. **75**(12): p. 7718-7727.

17. Wuu, D., et al., Plasma-deposited silicon oxide barrier films on polyethersulfone substrates: temperature and thickness effects. Surface and Coatings Technology, 2005. **197**(2): p. 253-259.

18. Bazaka, K. and M.V. Jacob, Solubility and surface interactions of RF plasma polymerized polyterpenol thin films. Materials Express, 2012. **2**(4): p. 285-293.

19. Bazaka, K. and M. Jacob, Synthesis of radio frequency plasma polymerized non-synthetic Terpinen-4-ol thin films. Materials Letters, 2009. **63**(18): p. 1594-1597.

20. Jacob, M.V., et al. RF plasma polymerised thin films from natural resources. in International Journal of Modern Physics: Conference Series. 2014. World Scientific.

21. Bazaka, K., M.V. Jacob, and B.F. Bowden, Optical and chemical properties of polyterpenol thin films deposited via plasma-enhanced chemical vapor deposition. Journal of Materials Research, 2011. **26**(08): p. 1018-1025.

22. Bazaka, K., N. Ketheesan, and M.V. Jacob, *Polymer encapsulation of magnesium to control biodegradability and biocompatibility.* Journal of nanoscience and nanotechnology, 2014. **14**(10): p. 8087-8093.

23. Adamson, A.W. and A.P. Gast, *Physical chemistry of surfaces.* 1967.

24. Owens, D.K. and R. Wendt, *Estimation of the surface free energy of polymers.* Journal of applied polymer science, 1969. **13**(8): p. 1741-1747.

25. Gürsoy, M., et al., Initiation of 2-Hydroxyethyl Methacrylate Polymerization by Tert-Butyl Peroxide in a Planar PECVD System. Plasma Processes and Polymers, 2015. **13**: p. 438-446.

26. Coclite, A.M. and K.K. Gleason, Initiated PECVD of organosilicon coatings: a new strategy to enhance monomer structure retention. Plasma Processes and Polymers, 2012. **9**(4): p. 425-434.

27. Petersen, J., et al., Organosilicon coatings deposited in atmospheric pressure Townsend discharge for gas barrier purpose: Effect of substrate temperature on structure and properties. ACS applied materials & interfaces, 2012. **4**(11): p. 5872-5882.

28. Kim, M., et al., High-rate deposition of plasma polymerized thin films using PECVD method and characterization of their optical properties. Surface and Coatings Technology, 2003. **169**: p. 595-599.

29. Oppedisano, C. and A. Tagliaferro, Relationship between sp2 carbon content and E04 optical gap in amorphous carbon-based materials. Applied Physics Letters, 1999. **75**(23): p. 3650-3652.

30. Dakhel, A., *Mechanisms of dc-current transfer in tris (acetylacetonato) iron (III) films.* Journal of non-crystalline solids, 2007. **353**(16): p. 1529-1533.

31. Strobel, M. and C.S. Lyons, *An essay on contact angle measurements.* Plasma Processes and Polymers, 2011. **8**(1): p. 8-13.

32. Morra, M., E. Occhiello, and F. Garbassi, *Knowledge about polymer surfaces from contact angle measurements.* Advances in Colloid and Interface Science, 1990. **32**(1): p. 79-116.

33. Karaman, M. and E. Yenice, Plasma Enhanced Chemical Vapor Deposition of Poly (2, 2, 3, 4, 4, 4-hexafluorobutyl acrylate) Thin Films. Chemical Vapor Deposition, 2015. **21**(7-8-9): p. 188-195.

34. Zají, L., et al., Study of plasma polymerization from acetylene in pulsed rf discharges. Thin Solid Films, 2003. **425**(1): p. 72-84.

35. Sulyaeva, V., et al., PECVD synthesis and optical properties of BC X N Y films obtained from N-triethylborazine as a single-source precursor. Surface and Coatings Technology, 2013. **230**: p. 145-151.

36. Sumiya, M., et al., Study of 193nm photoresist degradation during short time fluorocarbon plasma exposure. I. Studies of modified layer formation. Journal of Vacuum Science & Technology B, 2008. **26**(5): p. 1637-1646.

37. Nest, D., et al., Role of polymer structure and ceiling temperature in polymer roughening and degradation during plasma processing: a beam system study of P4MS and PαMS. Journal of Physics D: Applied Physics, 2010. **43**(8): p. 085204.

38. Chung, T., et al., Electron, ion and vacuum ultraviolet photon effects in 193? nm photoresist surface roughening. Journal of physics D: Applied physics, 2010. **43**(27): p. 272001.

39. Drotar, J.T., et al., Surface roughening in shadowing growth and etching in 2+ 1 dimensions. Physical Review B, 2000. **62**(3): p. 2118.

40. Kokkoris, G., et al., Dual nanoscale roughness on plasma-etched Si surfaces: Role of etch inhibitors. Physical Review B, 2007. **76**(19): p. 193405.

41. Starostin, S.A., et al., Towards Roll-to-Roll Deposition of High Quality Moisture Barrier Films on Polymers by Atmospheric Pressure Plasma Assisted Process. Plasma Processes and Polymers, 2015. **12**(6): p. 545-554.

42. Demirel, Y.K., et al., A CFD model for the frictional resistance prediction of antifouling coatings. Ocean Engineering, 2014. **89**: p. 21-31.

43. Muir, B.W., et al., Characterization of low-fouling ethylene glycol containing plasma polymer films. Langmuir, 2008. **24**(8): p. 3828-3835.

44. Wu, G., A. Sahoo, and J. Lin, Effects of e-beam deposited gate dielectric layers with atmospheric pressure plasma treatment for IGZO thin-film transistors. Surface and Coatings Technology, 2016.

45. Sharma, V., et al., *Rational design of all organic polymer dielectrics.* Nature communications, 2014. **5**.

46. Venkat, N., et al., High temperature polymer film dielectrics for aerospace power conditioning capacitor applications. Materials Science and Engineering: B, 2010. **168**(1): p. 16-21.

47. Chen, P. and B. Chu, Improvement of dielectric and energy storage properties in Bi (Mg 1/2 Ti 1/2) O 3-modified (Na 1/2 Bi 1/2) 0.92 Ba 0.08 TiO 3 ceramics. Journal of the European Ceramic Society, 2016. **36**(1): p. 81-88.

48. Wang, Y., et al., *High-energy density in aromatic polyurea thin films.* Applied Physics Letters, 2009. **94**(20): p. 202905.

49. Wu, S., et al., Aromatic polythiourea dielectrics with ultrahigh breakdown field strength, low dielectric loss, and high electric energy density. Advanced Materials, 2013. **25**(12): p. 1734-1738.

50. Fritz, S.E., T.W. Kelley, and C.D. Frisbie, Effect of dielectric roughness on performance of pentacene TFTs and restoration of performance with a polymeric smoothing layer. The Journal of Physical Chemistry B, 2005. **109**(21): p. 10574-10577.

51. Qi, L., L. Petersson, and T. Liu, *Review of recent activities on dielectric films for capacitor applications.* Journal of International Council on Electrical Engineering, 2014. **4**(1): p. 1-6.

52. Tan, D., et al., *High-Temperature Capacitor Polymer Films.* Journal of electronic materials, 2014. **43**(12).

53. Ho, J. and T.R. Jow. Effect of crystallinity and morphology on dielectric properties of PEEK at elevated temperature. in Solid Dielectrics (ICSD), 2013 IEEE International Conference on. 2013. IEEE.

54. Liang, Z., *High-Temperature Electronics.* High Temperature Materials and Mechanisms, 2014: p. 467.

55. Stricker, J., et al., *Evaluation of fluorene polyester film capacitors.* CARTS USA-2010, 2010: p. 15-18.

56. Zhou, Z., et al., Amphiphilic triblock copolymers with PEGylated hydrocarbon structures as environmentally friendly marine antifouling and fouling-release coatings. Biofouling, 2014. **30**(5): p. 589-604.

Chapter 4

Marine Antifouling Coating fabrication

Terpinen-4-ol bilayer films fabricated on glass substrate using different deposition parameters are studied for their marine antifouling behavior. The samples are deployed at the proposed site for one month to study their antifouling characteristics. The experimental data is interrogated using a 3-way analysis of variance (ANOVA) to determine if statistically significant differences exist between Terpinen-4-ol bilayer treated and untreated substrates. The objective is to fabricate environmentally benign antifouling coatings from naturally derived materials. The study has been published as *Avishek kumar, Scott Mills, Kateryna Bazaka, Nigel Bajema, Ian Atkinson, Mohan V. Jacob., Biodegradable Optically Transparent Terpinen-4-ol Thin Films for Marine Antifouling Applications. Surface & Coatings Technology 349, (2018), 426–433*

Biodegradable Optically Transparent Terpinen-4-ol Thin Films for Marine Antifouling Applications

Abstract

Sustainable marine antifouling strategies aim to minimize long term environmental impacts while effectively preventing surface colonization. In this study, we report upon a biodegradable antifouling coating for marine applications. In two stages, thin bilayers were produced using plasma-enhanced chemical vapor deposition of terpinen-4-ol, at applied powers of 100 W initially and then 10 or 25 W. The resulting coatings were characterized for solubility, surface energy, surface roughness and optical transmission. Both coatings exhibited similar solubility over the initial 14 days of observation, though structures deposited at 25 W were significantly more stable after 14 days. Coatings were smoother than the control surface upon which they were deposited and had higher hydrophobicity with transmission efficiencies greater than 90 % (400-1000 nm). Field assessments of the samples were carried out in Curralea Lake (Townsville, Australia) to assess their real world performance. Results indicate that the environmentally friendly coatings, terpinen-4-ol plasma polymer influenced antifouling. The proposed mechanism for this effect is the dissolution of the coating coupled with possible antimicrobial properties of the terpinen-4-ol. These results point to the potential usefulness of developing multilayer coatings for extended deployments.

Key Words: Polymer thin film, RF plasma polymerization, Marine antifouling, Plasma polymer

As published in: Avishek kumar, Scott Mills, Kateryna Bazaka, Nigel Bajema, Ian Atkinson, Mohan V. Jacob., Biodegradable Optically Transparent Terpinen-4-ol Thin Films for Marine Antifouling Applications. Surface & Coatings Technology 349, (2018), 426–433

4.1 Introduction

Marine biofouling is the undesirable colonization of immersed artificial surfaces by marine micro-organisms, plants and animals [1-4]. Biofouling is a highly dynamic process and the type of fouling community depends on the physico-chemical properties of the substrate [5], geographic location [6], environmental conditions such as seasonal changes [7], resource competition and predation. Biofouling of shipping vessels, heat exchangers, oceanographic sensors and aquaculture systems carries significant economic and performance implications [8-10]. An increase in the roughness of a ship's hull by fouling can cause powering penalties of up to 86% at cruising speed [8]. Biofouling of environmental monitoring equipment, e.g. oceanographic sensors used to measure dissolved oxygen, turbidity, conductivity, pH and fluorescence, is another major challenge [11, 12]. Here, fouling of optical windows in cameras and optical sensors degrade the interface, thereby notably limiting the deployment period of these devices, and considerably affecting the accuracy of the collected measurements [13-15].

Self-polishing biocidal tri-butyl tin polymer was used extensively to combat marine fouling, but was banned in 2008 due to its adverse environmental effects [16]. Copper and Zinc based biocides are less toxic, nevertheless they present a major source of heavy metal transfer to biota in bay areas, which may prevent their use in the near future [17]. The development of environmentally benign solutions, such as those modeled on antifouling biological surfaces [18-21], natural enzyme based coatings [22, 23] ,low surface energy coatings [24, 25] and crosslinked hydrogel coating [26] are gaining momentum.

Natural antifouling products may provide a good alternative to biocide-based antifouling strategies as they are biodegradable and often less toxic. Qian and colleagues reviewed the efficacy of 214 naturally occurring antifouling agents derived from marine habitats [27], suggesting that marine organisms were a promising source of antifouling agents. In another study, Wang *et al.* demonstrated that di(1H-indol-3-yl)methane (DIM) extracted from marine bacteria (*Pseudovibrio denitrificans)* showed potential antifouling properties against the barnacle cyprids (*Balanus amphitrite),* when loaded into paint and applied as an antifouling marine coating on PVC panels. The antifouling activity of DIM was comparable to commercially available biocide Sea Nine [28].

Similarly, avarone and avarol, quinone and sesquiterpenoid hydroquinone extracted from the Mediterranean sponge *Dysidea avara* also exhibited antifouling activity against the cyprids of *Balanus Amphitrite* [29-31]. Piazza and colleagues showed that a terpene extracted from the red

algae *Sphaerococcus coronopifolius* inhibited the settlement of barnacles (A amphitrite) [32]. The extracted terpene bromosphaerol showed the antifouling activity through a non-toxic mechanism.

Terpinen-4-ol is extracted from *Melaleuca alternifolia* essential oil (tea tree oil) and is inherently antimicrobial in nature [33-35]. Plasma polymerized terpinen-4-ol thin films synthesized at lower power of 10 W have shown antimicrobial activity against human pathogens *Pseudomonas aeruginosa* and *Staphylococcus aureus*, preventing surface colonization, production of extracellular polymer substances, and biofilm formation [36, 37]. The antimicrobial and antifouling properties of these coatings were attributed to a favorable combination of surface chemistry and morphology, and elution of unfragmented monomer units [37, 38]. Interestingly, unlike most other plasma polymers, those of terpinen-4-ol are optically transparent [38]. These two characteristics suggest that terpinen-4-ol coatings may be effective for the inhibition of biofouling on the surface of optical windows used in sensing applications.

Plasma deposition is a clean and environmentally friendly technique that can be used to fabricate pin hole free coatings with better stability and adhesion to substrates when compared to other film forming techniques, such as spin coating, graft polymerization and drop casting [39, 40]. Plasma polymerization is an effective means for surface immobilization of biologically-active natural terpenes [41] and fabrication of antifouling coatings [42, 43]. Surface properties, e.g. surface energy, chemistry, and morphology, and mechanical properties of the coating influence the bio-adhesion of micro-organisms to the substrate. The chemical composition and thickness of the coating can easily be controlled by varying the deposition parameters, affording a much greater degree of versatility and control compared to other synthesis methods. In the research described here, terpine-4-ol bilayer thin films were fabricated and their efficacy as optically transparent antifouling coatings for sensor windows examined.

4.2 Experimental Design

4.2.1 Materials

An essential oil precursor, namely terpinen-4-ol ($C_{10}H_{18}O$), with a purity of 99 % and molecular weight of 154.24 g/mol, was purchased from Australian Botanical Products and used without any further modification. Microscope cover slips (24 mm^2) made from hydrolytic class borosilicate glass were used as a deposition substrate. These substrates were first cleaned with 5 % solution of decon 90 (Decon laboratories limited)and distilled water (D.I) followed by ultrasonic cleaning

(43 kHz ± 2 kHz) in an acetone bath for 30 min and propan-2-ol for an additional 30 min, all cleaned substrates were air dried prior to use.

4.2.2 Coating fabrication and characterization

Terpinen-4-ol bilayers were fabricated in a low pressure (6.6×10^{-2} mbar) tubular quartz plasma deposition system (5 cm in diameter and 80 cm in length). Terpinen-4-ol vapors was used for plasma generation. Power was capacitively coupled across the sample stage inside the tube using copper plates (3 × 20 cm) wrapped around the outside of the tube as described elsewhere [44]. The frequency of capacitive coupling was 13.56 MHz. No external heating was used for terpinen-4-ol vaporization. Between each deposition, the reactor was cleaned by flushing the chamber with oxygen at a power of 60W for 30 min with the resultant plasma maintained under vacuum (1.3×10^{-1} mbar). The first terpinen-4-ol layer was deposited at an input power of 100 W, followed by a second layer fabricated at either 10 or 25 W. The time gap between layers being deposited was 15 minutes, the system was vented between each layer. The thickness of each layer was 300 nm.

The thickness and refractive index of the prepared bilayer terpinen-4-ol coatings were measured by variable angle spectroscopic ellipsometry (VASE J. A. Woollam, M2000 D). Measurements were performed at three different angles (55°, 60° and 65°) for all samples in the wavelength range of 200 to 1000 nm.

A three component optical model was employed (substrate, thin film and surface roughness) for modelling single layers. Additionally, a graded layer model was investigated that comprised of five components (substrate, first layer, graded interphase, second layer and surface roughness). This gave the best agreement between modelled and measured data. The film component was modelled using the Cauchy function.

Pristine and fouled bilayer films and controls were characterized using AvaSpec 2048 fiber optic UV/VIS/NIR spectrometer (wavelength range 200–1100 nm, resolution 0.8 nm).

Chemical characterization of the bilayer coatings were performed by FT-IR spectroscopy (Perkin Elmer, spectrum-100) in ATR mode, KBr pellets were used as the deposition substrate for the analysis. Spectra were obtained from 4000 to 600 cm^{-1} with a resolution of 4 cm^{-1} averaged over 124 scans. The Raman spectra of bilayer coating were recorded using WITEC spectrometer (alpha 300 access) in the range of 100-4000 cm^{-1}.

The sessile drop contact angle and surface free energy were measured using an optical contact angle measuring system (KSV, CAM 101). Three different liquids (water, di-iodomethane, and

ethylene glycol) were used to measure the contact angle with a drop volume of 3 µl, five measurements were performed per sample and averaged over five samples. The values were reported as mean value ± the standard deviation. The Young Laplace fitting [45] and Van Oss-Chaudhury-Good (VCG) [46] methods were used to evaluate contact angle and surface free energy, respectively.

The topography and roughness of the bilayer coating were examined using NT-MDT AFM. Roughness and topography were examined in semi-contact mode. The average roughness was estimated from 3 μm^2 AFM images with all imaging conducted at room temperature (23 ^oC).

Underwater stability testing of the polymer coating was conducted in an artificial sea water (ASW) tank at 25 °C. Bilayer thin films were deposited on a 25 mm^2 glass substrate. The thickness of each dry coating was measured prior to immersion in the ASW tank. The content of the ASW tank was changed after two weeks. Samples were taken out of the ASW at scheduled intervals of 1, 7, 14, and 28 days, rinsed with deionized water, oven dried at 50 °C for 8 hours and their dry thickness measured. The reduction in thickness was expressed as the percentage of remaining thickness. For each deposition power, three replicates were fabricated, tested and measured, and data points were averaged.

4.2.3 Biofouling study site and sampling

Biofouling study involved sample deployment in Curralea Lake in Townsville, Australia (Latitude -19.27033°, Longitude 146.78865°). The depth of the deployment site was approximately 5 meters. The samples were floated out to each trial location using a system of light ropes and small pulleys to a depth of 1 m below the water surface. In this manner, samples could readily be retrieved at predefined time intervals. Sampling was conducted during the period August to September 2016.

In total 60 samples were deployed to study their antifouling characteristics. Three types of samples were deployed; the two bilayer terpene coatings and controls (untreated substrates). Each sample group contained a minimum of 5 replicates for each of 4 exposure intervals (1, 7, 14 and 28 days).

The extent of biofouling was visualized using an optical microscope at 10 locations per sample at a magnification of 10× with a specially modified camera to yield a flat field of view (2000 microns). Images at different focus levels were captured and stacked to produce an output image

in TIFF format at a resolution of 1280 × 720 pixels. Captured images were converted to gray-scale binary images and automatic thresholding was applied to differentiate between biomass and void space using program Image J. Automatic thresholding methods such as the iterative selection method, the Renyi entropy method, the Otsu method and the max entropy method were applied to each image and the result from the method giving the maximum resemblance between the original and the threshold image was chosen.

The experimental data was interrogated using a 3-way analysis of variance (ANOVA) to determine if statistically significant differences existed between the coatings, exposure period and method of characterization.

4.3 Results and discussion

4.3.1 FTIR and Raman analysis

The ATR-FTIR spectra of plasma polymerized terpinen-4-ol coating at two different deposition powers are shown in figure 4.1 (a). The broad transmission peak between 3700–3100 cm^{-1} corresponds to –OH vibrations. The peaks at 2952, 2869, and 2928 cm^{-1} can be attributed to asymmetric/symmetric stretching of C– H in $–CH_3$ and asymmetric stretching in $–CH_2$, respectively. The vibrations characteristics of carbonyl group are present in the 1700-1710 cm^{-1} region. The band present around 1650 can be attributed to alkenyl C=C stretch and is more prominent for the 25 W sample. The vibrations at 1455/1377 cm^{-1} correspond to the methyl C-H asymmetric/symmetric bend in the deposited coating. The weak intensity peaks in 1000–1250 cm^{-1} region can be ascribed to aromatic –C–H in plane bend. There is also a possibility of C–O stretch and C–O–H bend in these regions. Peak broadening is observed within 1300–1000 cm^{-1} region, which can be due to overlapping intensity from all the bands occurring in this region.

The Raman spectra of films is shown in figure 4.1 (b). Peak G around 1550–1600 cm^{-1} corresponds to bond stretching of sp^2 atoms in chains and rings. Peak D around 1350 cm^{-1} can be attributed to breathing modes of aromatic rings[47]. The intensity of both the G and D peaks are almost similar for both the films as can be seen in the inset of figure 4.1b. Similarity of peak intensity suggests a similar degree of amorphization in both the films. The Raman spectra of essential oils as reported by Baranska et al. [48] show a large number of vibrational intensity analogs, many of which are absent from the spectra for plasma polymerized films.

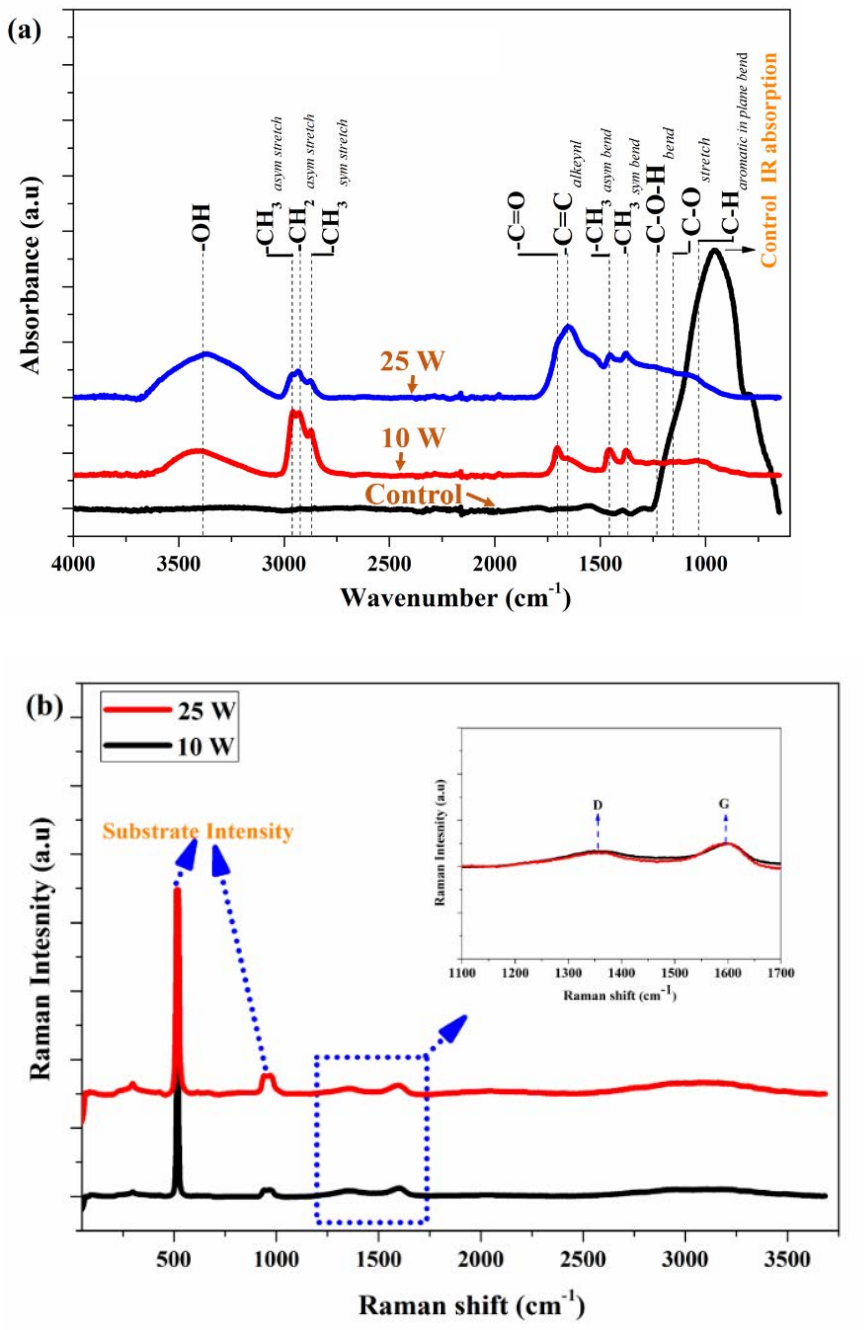

Figure 4. 1 (a) Thickness-normalized FTIR transmission spectra of terpinen-4-ol films deposited at two power levels 10 W and 25 W along with control. (b) Raman spectra of terpinen-4-ol films deposited at power levels of 10 W(black) and 25 W (red).

4.3.2 Film stability

Terpinen-4-ol coatings were immersed in sterile artificial sea water (ASW) with similar pH and salinity in order to assess their stability under natural marine conditions. This immersion test eliminated the effect of marine organism upon the test surfaces. Figure 4.2 (a) shows the percentage reduction in thickness of coating immersed in ASW over a period of 28 days. Up to a period of 7 days, coatings exhibited an average reduction in thickness of 15 %. Both coatings exhibit similar dissolution curves up to 14 days (≈25 %) of immersion. By day 28, the coatings showed a significant difference, with the 10 W coating reduced to almost half of its initial thickness, while the 25 W coatings maintained approximately 75% of the initial thickness.

Figure 4.2 (b) shows the contact angles of the coatings after immersion in ASW for different time periods, except for period zero that were examined prior to immersion. The contact angles of both coatings were initially hydrophilic and decreased over time, with the decrease being more prominent in 25 W coating.

Films deposited via plasma polymerization at a lower input power are known to be less crosslinked than those deposited at higher power [49, 50]. Hydrophilic uncross-linked oligomers trapped in the coating matrix dissolve readily. These results are consistent with higher rates of crosslinking in the 25 W coatings in comparison with the less crosslinked 10 W samples, the latter being more susceptible to film rearrangement and relaxation due to hydration of unbound oligomers with increased exposure time to the ASW, see figure 4.2 (c).

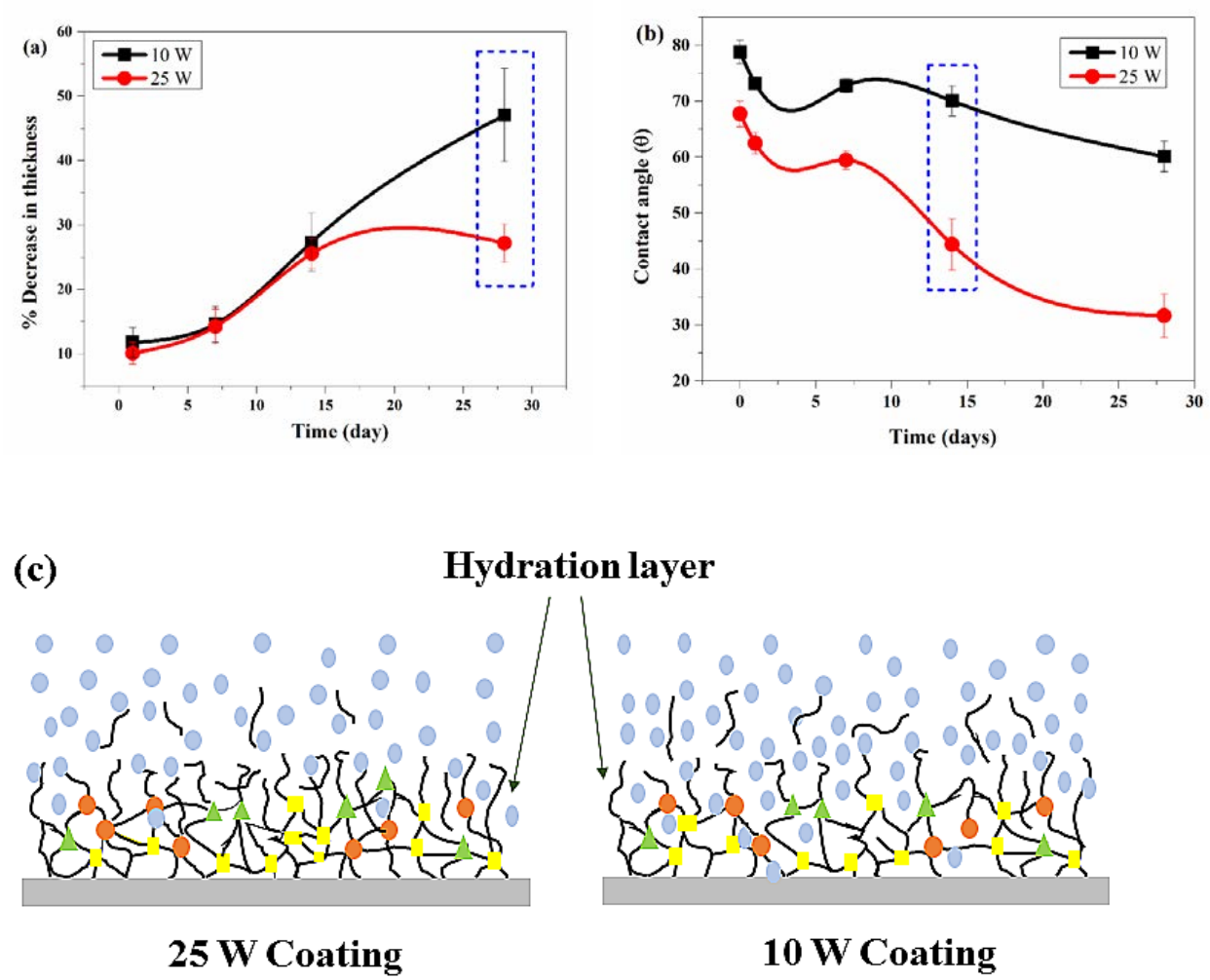

Figure 4. 2 (a) Coating thickness decrease vs time of different terpinen-4-ol coating fabricated at different power levels. (b) Dependence of contact angle of terpinen-4-ol coating on exposure time in ASW. Error bar corresponds to standard deviation. (c) Schematic showing hydration and dissolution behavior of coatings.

4.3.3 Wetting behavior and roughness

Hydrophobicity of the coated surfaces was evaluated by measuring the static water contact angle (θ_w). Both the terpinen-4-ol coatings and control were found to be hydrophilic in nature, the 10 W , 25 W and control surfaces exhibited a θ_w of 78.75 °, > 67.73 ° and > 36.31 ° respectively, see table 4.1. The increase in hydrophobic $-CH_X$ species and decrease in hydrophilic –OH species in the 10 W coating makes it less hydrophilic than the 25 W variant, as evident in the FT-IR spectra of films, figure 4.1.

The surface energy of the coating is strongly related to the degree and strength of adhesion of marine organisms[51]. Ideally surface energy of coating should be 22-24 mN/m for the minimal bioadhesion to occur as discovered by Baeir [52]. The surface energy of the films was evaluated using a VCG approach by analyzing contact angle data of coatings measured for three solvents: water, diiodomethane, and ethane-di-ol. The Young–Dupree equation for solid-liquid systems was used to calculate the surface energy (Y_s) for coatings as shown in equation 1 and 2:

$$Y_S = y_s^{LW} + 2\sqrt{Y_s^+ Y_s^-} \quad (1)$$

$$(1 + \cos\theta)\, Y_l = 2\left(\sqrt{y_s^{LW} y_l^{LW}} + \sqrt{y_s^+ y_l^-} + \sqrt{y_l^+ y_s^-}\right) \quad (2)$$

where Y_l is surface tension liquid, Y_s is the surface tension of solid, y_s^{LW},y_l^{LW} are the dispersive component of solid and liquid, and y_i^+ , y_i^- represents the electron-acceptor parameter and electron–donor parameter of substance, respectively. The surface free energy was estimated to be 45.38 mJ m^{-2} and 46.08 mJ m^{-2} for 10 W and 25 W coating, respectively. As surface energy of both the bilayer films are in same range it can be inferred that its influence on antifouling behavior of both the coating would be similar.

Coating roughness is an important parameter affecting antifouling behavior in number of ways. Roughness alters the wetting behavior of the surface. AFM was used to evaluate the roughness of coating and unmodified control samples. The roughness of both the coating and the control was below 1 nm. Table 4.1 lists important surface properties, such as contact angle, surface energy and roughness of the coatings.

Table 4. 1 Terpinen-4-ol coating characteristics: static contact angle, surface energy and roughness

Plasma Treatment	Static contact angle (°)			Surface free energy (mJ m^{-2})	Roughness /rms (nm)
	Water	Ethane-diol	Diiodomethane		
10 W surface	78.75 ± 2.09	55.94 ± 1.67	37.86 ± 1.39	45.38 ± 4.76	0.44 ±0.15
25 W surface	67.73 ± 2.33	47.58 ±2.27	36.57 ± 0.83	46.08 ± 3.73	0.65 ± 0.18
Control	36.31 ± 3.09	45.66 ±2.98	47.77 ± 1.29	55.71	0.69 0.16

4.3.4 Biofouling studies

Figure 4.3 shows photographs of bio-fouled samples after different immersion periods, displaying a steady increase in biofouling across the test period. Figure 4.4 (a) shows the degree of biofouling as the percentage of the surface area covered, significant differences ($p < 0.05$) were found between immersion periods and coatings. The control exhibited the highest degree of fouling compared to the coated samples (66 % by day 28). Of the coated samples, the 25 W variant had the highest degree of coverage, increasing from 32 % at the end of 7 days to 63 % at the end 28 days. In contrast, the 10 W treated surface was most effective against fouling with only 17 % coverage after 7 days and 53 % by day 28. This kind of behavior has also been shown by terpien-4-ol films when they were tested for antibacterial activity against *S. aureus*. The 25 W treated surface exhibited the highest attachment of *S. aureus* compared with the 10 W and control samples. The biological activity of terpinen-4-ol has shown to be preserved in polyterpenol films fabricated at low power. Diffusion and accumulation of terpinen-4-ol in bacterial cytoplasmic membrane leads to loss of membrane integrity [53] .

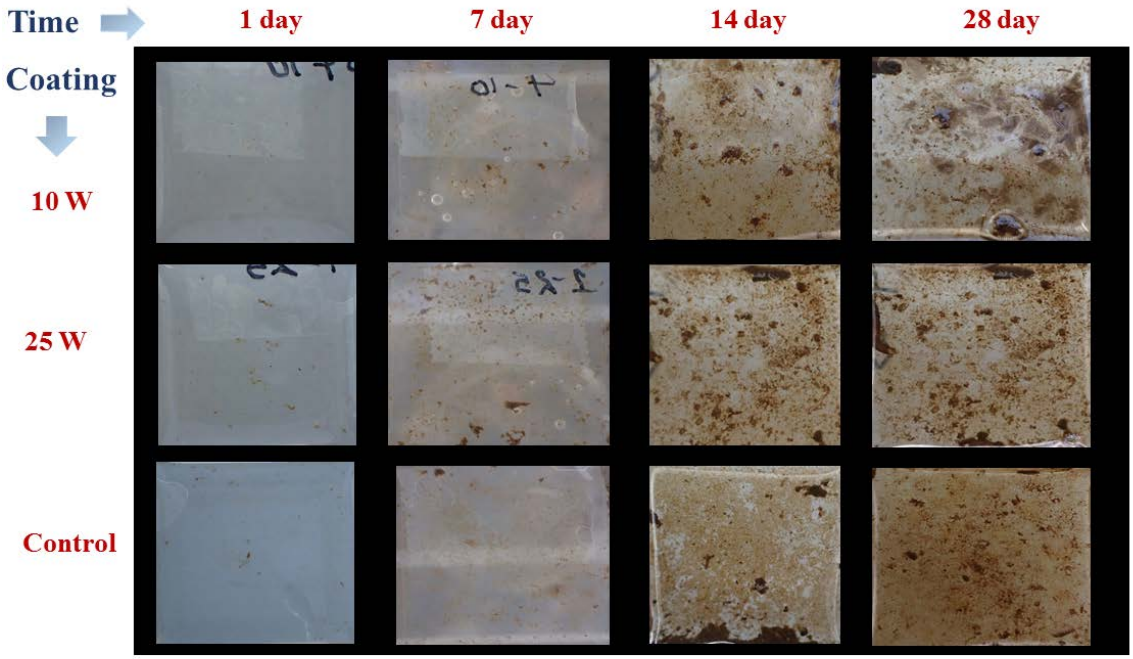

Figure 4. 3 Photographs of bio-fouled samples after different immersion period. The dimension of each sample is 2.5 × 2.5 cm

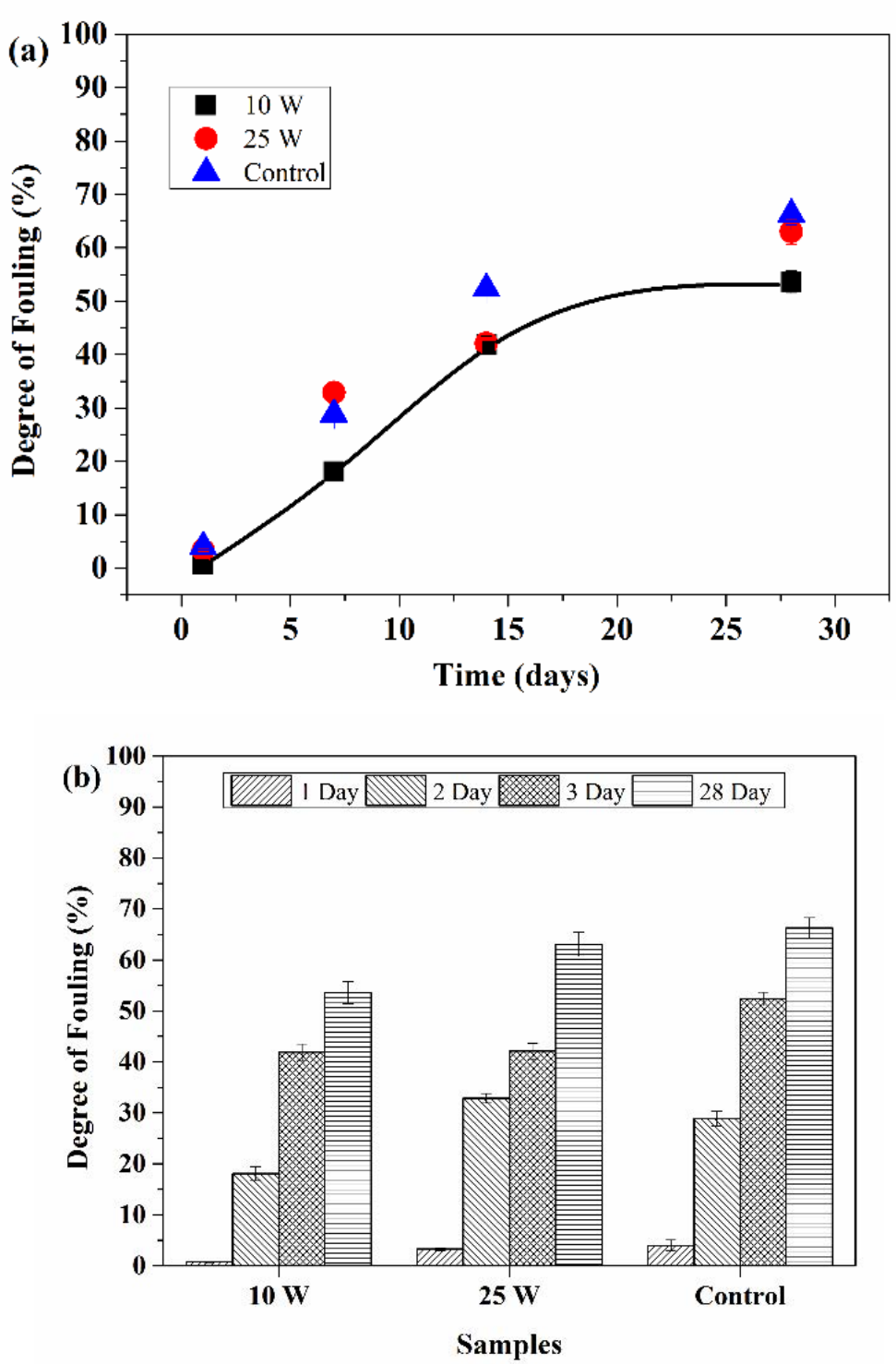

Figure 4. 4 Fouling coverage: (a) With respect to time (b) with respect to coating for different terpinen-4-ol coating surfaces. Bars shows standard deviation

From visual analysis of the control and films the biofouling process starts immediately after aquatic immersion. Surface colonization by cells of various species takes place in the initial fouling

period, however, only those species tolerant to the surface properties of the substrate are able to attach and proliferate [54]. In the first week, biofilm formation was reduced significantly by the 10 W terpinen-4-ol coatings compared to the control, the proposed mechanism involves both antimicrobial and mechanical action. The 10 W terpinene-4-ol film would act as a biocidal self-polishing coating, whereby organisms that attach to its surface would be deactivated on contact, followed by subsequent dissolution of the topmost layer of the polymer to rid the surface from the dead microorganisms and their debris. Furthermore, it should be noted that the decrease in the coating thickness is estimated at approximately 13 % per week for the first 15 days of immersion for 10 W samples, whereas the degree of fouling per week increases from 17 % to 21 % over the sample period of time. The observed increase in fouling coverage in the second week relative to the first week of immersion despite similar polymer dissolution rates suggests monomer elution and contact killing as the primary antifouling mechanisms.

Antimicrobial activity of terpinen-4-ol results from its ability to compromise microbial membrane structures [34, 55-57]. Like typical lipophilles they partition through cytoplasmic membranes and cell walls, disrupting the structure of phospholipids, fatty acids and layers of polysaccharides. In prokaryotic cells like bacteria, the permeabilization of membranes leads to a reduction of membrane potential through loss of ions leading to proton pump dysfunction [58, 59]. In due course, macromolecules can leak trough the damaged cell wall and membranes, potentially leading to cell lysis [56]. Essential oils have also been found to damage lipids and proteins while facilitating cytoplasmic coagulation [60]. In eukaryotic cells, essential oils have been found to decrease mitochondrial membrane potential, thus promoting their depolarization. The mitochondria membrane becomes exceptionally permeable, resulting in a leakage of proteins, cytochrome C, calcium ions and radicals, and ultimately leading to cell death [61]. Therefore, disruption of the membrane integrity leading to loss of cytoplasmic material, respiration inhibition, damage to DNA and protein lysis may be plausible mechanisms for the anti-biofouling properties of terpinen-4-ol in aquatic environments, see figure 4.5.

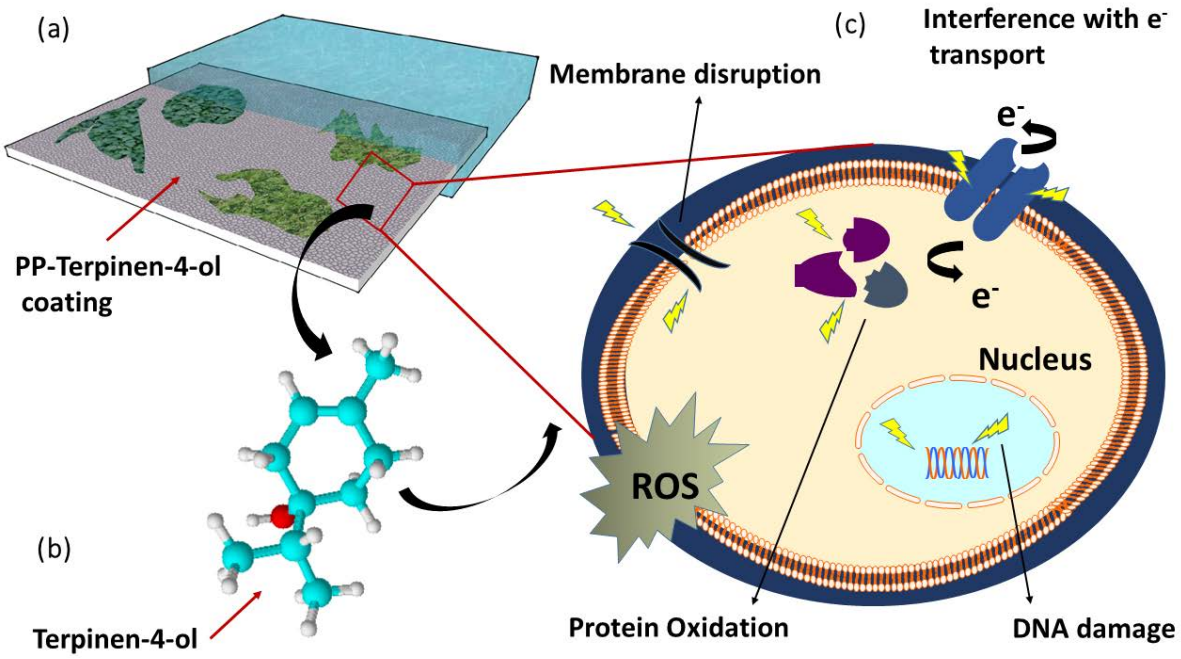

Figure 4. 5 Proposed hypothetical mechanisms of antifouling action of terpinen-4-ol coatings under aquatic conditions. (a) Immersion in marine environment; (b) Dissolution of terpinen-4-ol; (c) Plausible effects of terpinen-4-ol on cellular functioning of marine biofouling organisms. The mechanical dissolution of the coatings is likely to work in tandem with the anti-microbial action of the terpinen-4-ol, essentially dislodging bio-fouling organism over time.

4.3.5 Transmittance:

UV-Vis spectroscopy was performed to quantify light transmission efficiency of pristine and bio-fouled samples. Antifouling coatings with favorable transparency are important for aquatic sensor applications. Figure 4.6 (a) shows the optical transparency of 10 W and control fouled surfaces in the wavelength range of 400–1000 nm for each time period. The transmittance measurements were made immediately after samples were taken out of the water. Figure 4.6 (b) shows the comparison of light transmittance of all three substrate treatments as a function of time at wavelength of 500 nm. Optical transparency of pristine surfaces is also shown for comparison. The transparency of all of the pristine samples is well above 90 %. For the 1 and 7 day time points the transparency of the 10 W fouled surfaces were above 60 % as shown in figure 4.6(a). Transparency reduced to less than 50 % for the control after 7 days of immersion. Light transmission efficiency was reduced well below 30 % for the coatings and control after immersion periods of 14 days or more.

It is possible that further optimization of the coating could extend the antifouling efficacy of 10 W terpienen-4-ol coating beyond 7 days. For instance, thicker films may sustain high levels of polymer dissolution and/or elution of the unreacted monomer into the ambient environment. Furthermore, reduction in the degree of cross-linking may facilitate elimination of biologically active terpinen-4-ol units from the polymer matrix without compromising its mechanical and optical properties.

It is worth noting that Curralea Lake represents a marine environment conducive to extreme levels of biofouling. Adding to this, the chosen deployment site exhibited little water circulation around the samples, potentially contributing to the accumulation of organisms due to reduced dislodgment by localised flows. It is therefore plausible that these coatings would deliver far greater antifouling protection in locations with higher level of circulation.

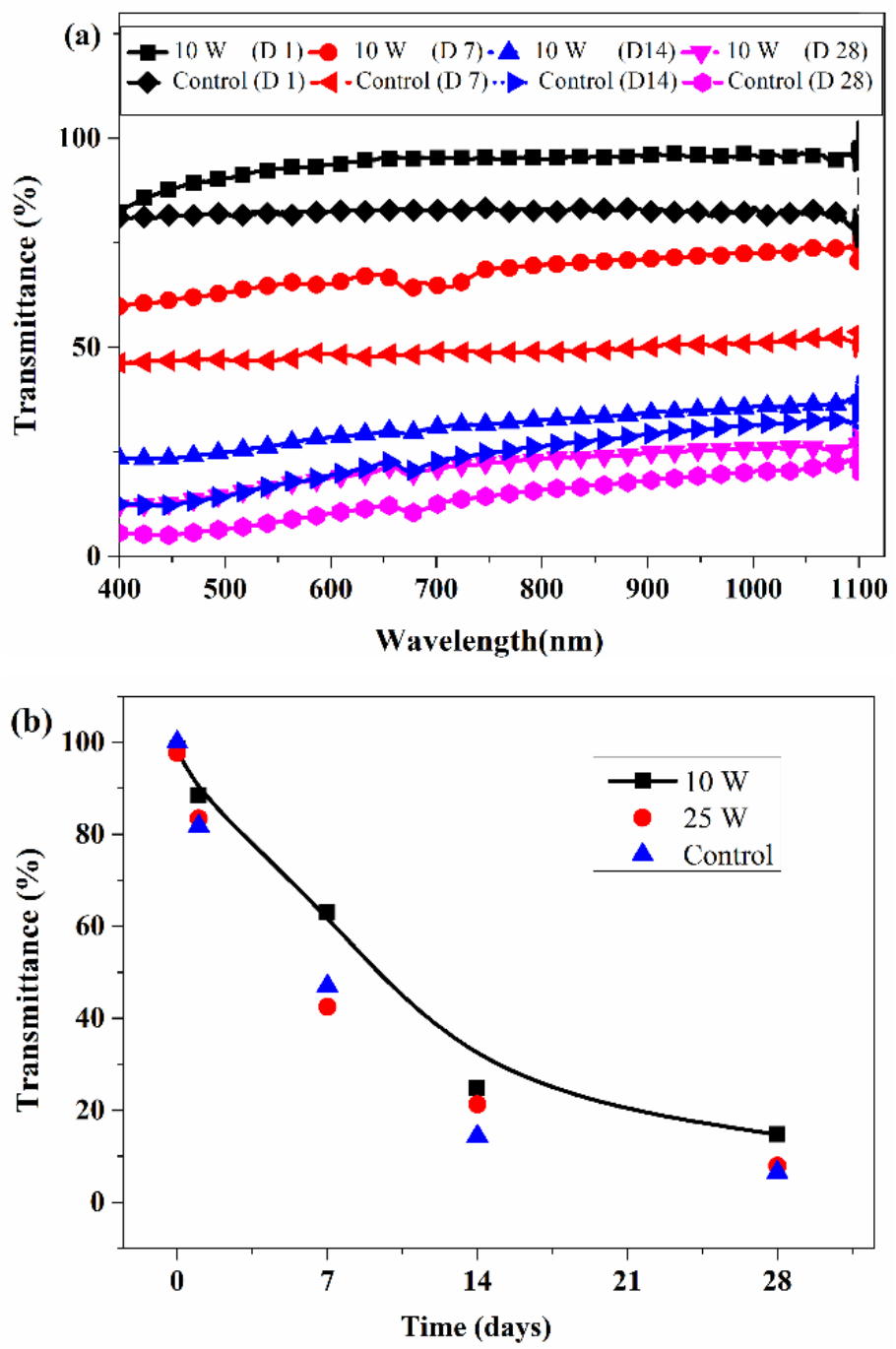

Figure 4. 6 (a) Light transparency of 10 W terpinen-4-ol coatings and control as function of different testing wavelengths after different immersion periods (D1, D7, D14 & D28 represents the number of days). (b) Comparison of transmittance of all the coatings along with control as a function time at fixed wavelength of 500 nm.

4.4 Conclusion

The present study aimed to consider an alternative environmentally-friendly solution to inhibit the preliminary stages of biofouling. Terpinen-4-ol films with light transmission efficiency of 90–99 % at wavelengths of 400–1000 nm were fabricated by PECVD. The bioactive coating (fabricated at 10 W) showed good stability in artificial sea water for up to one week. The degree of fouling coverage was significantly reduced on 10 W terpinen-4-ol samples for the first week and was consistently lower than that for the control and other tested surfaces (25 W), however the degree of anti-biofouling afforded by the coating would require further improvement for real-life applications. The light transmission efficiency of the fouled 10 W sample was above 60 % for the first week of deployment. The present work has demonstrated for the first time the use of plasma polymerized terpinen-4-ol as an antifouling coating for marine applications. The further development of multilayer coatings designed to dissolve over time hold promise for reductions in biofouling, through mechanical dislodgment and anti-microbial activity. Importantly, these coatings are biodegradable and do not pose long term threats to aquatic ecosystems.

References

1. Asuri, P., et al., *Polymer–nanotube–enzyme composites as active antifouling films.* Small, 2007. **3**(1): p. 50-53.

2. Yebra, D.M., S. Kiil, and K. Dam-Johansen, Antifouling technology—past, present and future steps towards efficient and environmentally friendly antifouling coatings. Progress in organic Coatings, 2004. **50**(2): p. 75-104.

3. Chambers, L.D., et al., *Modern approaches to marine antifouling coatings.* Surface and Coatings Technology, 2006. **201**(6): p. 3642-3652.

4. Almeida, E., T.C. Diamantino, and O. de Sousa, *Marine paints: the particular case of antifouling paints.* Progress in Organic Coatings, 2007. **59**(1): p. 2-20.

5. Anderson, M. and A. Underwood, *Effects of substratum on the recruitment and development of an intertidal estuarine fouling assemblage.* Journal of Experimental Marine Biology and Ecology, 1994. **184**(2): p. 217-236.

6. Schoener, A. and T.W. Schoener, The dynamics of the species-area relation in marine fouling systems: 1. Biological correlates of changes in the species-area slope. American Naturalist, 1981: p. 339-360.

7. Underwood, A. and M. Anderson, *Seasonal and temporal aspects of recruitment and succession in an intertidal estuarine fouling assemblage.* Journal of the Marine Biological Association of the United Kingdom, 1994. **74**(03): p. 563-584.

8. Schultz, M.P., Effects of coating roughness and biofouling on ship resistance and powering. Biofouling, 2007. **23**(5): p. 331-341.

9. Pogiatzis, T., et al., Identifying optimal cleaning cycles for heat exchangers subject to fouling and ageing. Applied Energy, 2012. **89**(1): p. 60-66.

10. Fitridge, I., et al., The impact and control of biofouling in marine aquaculture: a review. Biofouling, 2012. **28**(7): p. 649-669.

11. Whelan, A. and F. Regan, *Antifouling strategies for marine and riverine sensors.* Journal of Environmental Monitoring, 2006. **8**(9): p. 880-886.

12. Manov, D.V., G.C. Chang, and T.D. Dickey, *Methods for reducing biofouling of moored optical sensors.* Journal of Atmospheric and Oceanic Technology, 2004. **21**(6): p. 958-968.

13. Delauney, L., C. Compere, and M. Lehaitre, *Biofouling protection for marine environmental sensors.* Ocean Science, 2010. **6**(2): p. 503-511.

14. Whelan, A. and F. Regan, *Antifouling strategies for marine and riverine sensors.* J. Environ. Monit., 2006. **8**(9): p. 880-886.

15. Akyildiz, I.F., D. Pompili, and T. Melodia, *Underwater acoustic sensor networks: research challenges.* Ad hoc networks, 2005. **3**(3): p. 257-279.

16. Evans, S., A. Birchenough, and M. Brancato, *The TBT ban: out of the frying pan into the fire?* Marine Pollution Bulletin, 2000. **40**(3): p. 204-211.

17. Al-Naamani, L., et al., Chitosan-zinc oxide nanocomposite coatings for the prevention of marine biofouling. Chemosphere, 2017. **168**(Supplement C): p. 408-417.

18. Kirschner, C.M. and A.B. Brennan, *Bio-inspired antifouling strategies.* Annual review of materials research, 2012. **42**: p. 211-229.

19. Nir, S. and M. Reches, Bio-inspired antifouling approaches: the quest towards non-toxic and non-biocidal materials. Current Opinion in Biotechnology, 2016. **39**: p. 48-55.

20. Liu, K. and L. Jiang, *Bio-inspired self-cleaning surfaces.* Annual Review of Materials Research, 2012. **42**: p. 231-263.

21. Xu, J., et al., Investigation of the biofouling properties of several algae on different textured chemical modified silicone surfaces. Applied Surface Science, 2014. **311**(Supplement C): p. 703-708.

22. Kristensen, J.B., et al., *Antifouling enzymes and the biochemistry of marine settlement.* Biotechnology advances, 2008. **26**(5): p. 471-481.

23. Hu, Y., et al., Antifouling Zwitterionic Coating via Electrochemically Mediated Atom Transfer Radical Polymerization on Enzyme-Based Glucose Sensors for Long-Time Stability in 37° C Serum. Langmuir, 2016. **32**(45): p. 11763-11770.

24. Pollack, K.A., et al., Hyperbranched fluoropolymer-polydimethylsiloxane-poly (ethylene glycol) cross-linked terpolymer networks designed for marine and biomedical applications: heterogeneous nontoxic antibiofouling surfaces. ACS applied materials & interfaces, 2014. **6**(21): p. 19265-19274.

25. Detty, M.R., et al., *Environmentally benign sol–gel antifouling and foul-releasing coatings.* Accounts of chemical research, 2014. **47**(2): p. 678-687.

26. Wang, J. and J. Wei, Hydrogel brushes grafted from stainless steel via surface-initiated atom transfer radical polymerization for marine antifouling. Applied Surface Science, 2016. **382**(Supplement C): p. 202-216.

27. Qian, P.-Y., et al., Mini-review: marine natural products and their synthetic analogs as antifouling compounds: 2009–2014. Biofouling, 2015. **31**(1): p. 101-122.

28. Wang, K.-L., et al., *Low-Toxicity Diindol-3-ylmethanes as Potent Antifouling Compounds.* Marine Biotechnology, 2015. **17**(5): p. 624-632.

29. Tsoukatou, M., et al., Evaluation of the activity of the sponge metabolites avarol and avarone and their synthetic derivatives against fouling micro-and macroorganisms. Molecules, 2007. **12**(5): p. 1022-1034.

30. Joshi, M., et al., *Need of Natural Biocides in Antifouling Paints for Prevention of Marine Pollution.* International Journal of Innovative Research and Development, 2015. **4**(7).

31. Fusetani, N., *Antifouling marine natural products.* Natural product reports, 2011. **28**(2): p. 400-410.

32. Piazza, V., et al., Terpenes from the red alga Sphaerococcus coronopifolius inhibit the settlement of barnacles. Marine biotechnology, 2011. **13**(4): p. 764-772.

33. Calcabrini, A., et al., Terpinen-4-ol, the main component of Melaleuca alternifolia (tea tree) oil inhibits the in vitro growth of human melanoma cells. Journal of Investigative Dermatology, 2004. **122**(2): p. 349-360.

34. Carson, C., K. Hammer, and T. Riley, Melaleuca alternifolia (tea tree) oil: a review of antimicrobial and other medicinal properties. Clinical microbiology reviews, 2006. **19**(1): p. 50-62.

35. Mondello, F., et al., In vivo activity of terpinen-4-ol, the main bioactive component of Melaleuca alternifolia Cheel (tea tree) oil against azole-susceptible and-resistant human pathogenic Candida species. BMC infectious diseases, 2006. **6**(1): p. 1.

36. Bazaka, K., et al., Plasma-assisted surface modification of organic biopolymers to prevent bacterial attachment. Acta biomaterialia, 2011. **7**(5): p. 2015-2028.

37. Bazaka, K., et al., Plasma-enhanced synthesis of bioactive polymeric coatings from monoterpene alcohols: a combined experimental and theoretical study. Biomacromolecules, 2010. **11**(8): p. 2016-2026.

38. Bazaka, K., M.V. Jacob, and B.F. Bowden, Optical and chemical properties of polyterpenol thin films deposited via plasma-enhanced chemical vapor deposition. Journal of Materials Research, 2011. **26**(08): p. 1018-1025.

39. Bazaka, K., M.V. Jacob, and K. Ostrikov, *Sustainable Life Cycles of Natural-Precursor-Derived Nanocarbons.* Chemical reviews, 2015.

40. Jacob, M.V., et al., Plasma polymerised thin films for flexible electronic applications. Thin Solid Films, 2013. **546**: p. 167-170.

41. Bazaka, K., et al., Anti-bacterial surfaces: natural agents, mechanisms of action, and plasma surface modification. Rsc Advances, 2015. **5**(60): p. 48739-48759.

42. Kumar, V., et al., Amphiphilic Copolymer Coatings via Plasma Polymerisation Process: Switching and Anti-Biofouling Characteristics. Plasma Processes and Polymers, 2011. **8**(5): p. 373-385.

43. Bhatt, S., et al., Nanostructure protein repellant amphiphilic copolymer coatings with optimized surface energy by inductively excited low pressure plasma. Langmuir, 2011. **27**(23): p. 14570-14580.

44. Jacob, M., et al., *Fabrication of a novel organic polymer thin film.* Thin Solid Films, 2008. **516**(12): p. 3884-3887.

45. Adamson, A.W. and A.P. Gast, *Physical chemistry of surfaces.* 1967.

46. Owens, D.K. and R. Wendt, *Estimation of the surface free energy of polymers.* Journal of applied polymer science, 1969. **13**(8): p. 1741-1747.

47. Ferrari, A.C. and J. Robertson, *Raman spectroscopy of amorphous, nanostructured, diamond–like carbon, and nanodiamond.* Philosophical Transactions of the Royal Society of London A: Mathematical, Physical and Engineering Sciences, 2004. **362**(1824): p. 2477-2512.

48. Baranska, M., et al., *Chemotaxonomy of aromatic plants of the genus Origanum via vibrational spectroscopy.* Analytical and bioanalytical chemistry, 2005. **381**(6): p. 1241-1247.

49. Kim, M., et al., High-rate deposition of plasma polymerized thin films using PECVD method and characterization of their optical properties. Surface and Coatings Technology, 2003. **169**: p. 595-599.

50. Chan, K. and K.K. Gleason, Initiated chemical vapor deposition of linear and cross-linked poly (2-hydroxyethyl methacrylate) for use as thin-film hydrogels. Langmuir, 2005. **21**(19): p. 8930-8939.

51. Molena, E., et al., *Protein antifouling and fouling-release in perfluoropolyether surfaces.* Applied Surface Science, 2014. **309**(Supplement C): p. 160-167.

52. Baier, R.E., *Surface behaviour of biomaterials: the theta surface for biocompatibility.* Journal of Materials Science: Materials in Medicine, 2006. **17**(11): p. 1057.

53. Bazaka, K., et al., The effect of polyterpenol thin film surfaces on bacterial viability and adhesion. Polymers, 2011. **3**(1): p. 388-404.

54. Dobretsov, S., R.M. Abed, and M. Teplitski, *Mini-review: Inhibition of biofouling by marine microorganisms.* Biofouling, 2013. **29**(4): p. 423-441.

55. Carson, C.F., B.J. Mee, and T.V. Riley, Mechanism of action of Melaleuca alternifolia (tea tree) oil on Staphylococcus aureus determined by time-kill, lysis, leakage, and salt tolerance assays and electron microscopy. Antimicrobial agents and chemotherapy, 2002. **46**(6): p. 1914-1920.

56. Cox, S., et al., The mode of antimicrobial action of the essential oil of Melaleuca alternifolia (tea tree oil). Journal of applied microbiology, 2000. **88**(1): p. 170-175.

57. Morcia, C., M. Malnati, and V. Terzi, In vitro antifungal activity of terpinen-4-ol, eugenol, carvone, 1,8-cineole (eucalyptol) and thymol against mycotoxigenic plant pathogens. Food Additives & Contaminants: Part A, 2012. **29**(3): p. 415-422.

58. Turina, A.d.V., et al., *Natural terpenes: self-assembly and membrane partitioning.* Biophysical chemistry, 2006. **122**(2): p. 101-113.

59. Di Pasqua, R., et al., *Membrane toxicity of antimicrobial compounds from essential oils.* Journal of Agricultural and Food Chemistry, 2007. **55**(12): p. 4863-4870.

60. Gustafson, J., et al., *Effects of tea tree oil on Escherichia coli.* Letters in applied microbiology, 1998. **26**(3): p. 194-198.

61. Bakkali, F., et al., *Biological effects of essential oils–a review.* Food and chemical toxicology, 2008. **46**(2): p. 446-475.

Chapter 5

Pulse PECVD of Terpinen-4-ol

In this chapter effect of deposition conditions on the antibacterial performance of plasma polymerized Terpinen-4-ol films is investigated. Antibacterial activity of the pulse-PECVD fabricated terpinen-4-ol films is compared against continuous PECVD deposited counterparts. The changes in films antibacterial performance and physico-chemical properties are measured concerning monomer fragmentation and wettability properties. The result of this work is to submitted as *Avishek kumar, Ahmed AL-Jumaili, Kateryna Bazaka, Peter Mulvey, Jeffery Warner, Mohan V. Jacob . Enhanced Antibacterial Activity of Terpinen-4-ol Derived Films Fabricated via Pulse Plasma Deposition. Applied surface science*

Enhanced Antibacterial Activity of Terpinen-4-ol Derived Films Fabricated via Pulse Plasma Deposition

Abstract

Antifouling/antibacterial coating derived from sustainable natural resource for biomedical devices have showed promising outcomes especially to prevent bacterial growth. Herein pulse-plasma chemical vapour deposition method is used to fabricate antimicrobial coating from Terpinen-4-ol, a tea tree oil based precursor. The aim of this research is to retain the pristine monomer structure to maximum extent in developed stable coating enhancing its antibacterial activity. The developed films have tunable physical and chemical properties. Diverse film surface properties were obtained by varying the plasma deposition parameters, mainly the deposition mode (pulse and continuous wave) and duty cycle. The role of film wettability on degree of bacterial attachment has been elucidated. Overall, the number of viable bacteria on all the deposited coatings (25-30 %) were reduced to half with respect to the control (56 %).

Keywords: Pulse-PECVD, Polymer thin films, Antibacterial coatings, Plasma polymers

As to be submitted : Avishek kumar, Ahmed AL-Jumaili, Kateryna Bazaka, Peter Mulvey, Jeffery Warner, Mohan V. Jacob . Enhanced Antibacterial Activity of Terpinen-4-ol Derived Films Fabricated via Pulse Plasma Deposition. Applied surface science

5.1 Introduction

Bacterial colonization and subsequent biofilm formation on solid surfaces pose a challenging problem to public health and negatively affect performance of many industrial processes [1, 2]. Approximately 650,000 patients are affected by hospital acquired infections (HAI) annually which costs about $40 billion to healthcare system in US alone [3, 4]. Approximately 80 % of microbial infections are related to bacterial colonization and biofilm formation on medical implants [5, 6]. Pathogens such as *Escherichia coli* and *Pseudomonas aeruginosa* have been isolated from these infections [5, 7]. *P. aeruginosa* in particular have been found to cause a variety of biofilm mediated infections, such as tracheal stent and catheter-associated urinary tract infections [8], the bacterial infection of implantable medical devices act as reservoir of infections, impede the device correct performance and can diminish the host defence mechanism [9]. These shortcomings pose a major challenge in their future developments. Therefore, development of bioactive coatings that inhibit bacterial attachment on medical device surfaces without contributing to the development of antibiotic resistance appears as an attractive strategy to alleviate the incidence of implant-associated microbial infections.

To date, two coating strategies that notably differ in terms of their mechanism of action have been used to mitigate fouling by biological entities. Non-biocidal techniques employ surfaces that prevent the initial stages of microorganism attachment, tackling the problem at its source. PEG-based surfaces are commonly employed in this approach [10, 11], however the stability of PEG-based surfaces still remains a concern [12, 13]. Furthermore, specific antibodies against PEG were detected in patients during therapeutic treatment, which was not observed earlier with PEG-based drugs [14]. Biocidal coatings [15] rely on a direct interaction between microorganism and antimicrobial molecules, antibiotics or biocides incorporated in a coating [16].

Essential oils are a class of compounds which are extensively researched for their antimicrobial properties [17]. However, fabrication of solid surfaces from essential oils by conventional coating techniques like spin coating is difficult. The precise control of the molecular and macromolecular chemical structure of the polymers derived from essential oil is still a limiting factor [18]. Plasma enhanced chemical vapour deposition(PECVD) is a versatile technique for immobilization of this class of compounds on solid surfaces [19, 20]. Plasma polymerized thin films from these compounds are smooth, transparent, and have excellent chemical stability and adhesion to substrate. Their physical and chemical properties substantiate their use as protective coatings for medical devices [20-24], dielectric interlayers and encapsulating layers in electronics [25, 26]. Furthermore, tuning of plasma parameters in PECVD allows one to tailor chemical *(*e.g. *surface*

energy) and physical (e.g. *thickness*) properties of the polymer film based on their desired applications.

Plasma polymers of terpinen-4-ol have a demonstrated antimicrobial behaviour [20, 27]. Polymers fabricated at a low power of 10 W have been shown to be effective in reducing surface colonization and biofilm formation when tested against human pathogens *P. aeruginosa and S. aureus* [20, 27]. However, film fabricated at power of 25 W could not retain the inherent antimicrobial nature of terpinne-4-ol [28-30]. Thus, deposition power is an important parameter, which is likely to dictate the antimicrobial behaviour of terpinen-4-ol plasma polymers. Higher power leads to greater fragmentation of the monomer and reduced antimicrobial behaviour, whereas films deposited at power (less than 10 W) were found to be hydrolytically unstable. Previous work was focused on continuous wave plasma deposition, which leads to higher monomer fragmentation and loss of some monomer functionalities. Pulse plasma deposition partly overcomes these drawbacks of continuous wave plasma deposition. Polymers fabricated by pulse –PECVD technique are more chemically structured and consists of more unfragmented monomer molecules. The greater retention of monomer structure in deposited film becomes of great importance in plasma deposition of bioactive monomer molecules. The duty cycle (DC) is one of the very important parameter for pulse plasma deposition and is defined as DC = ton/ toff + ton. In this work, pulsed PECVD of terpinen-4-ol thin films at a peak power of 10 W is investigated. A set of 4 duty cycles (DC-10, DC-20, DC-40, DC-100) is chosen to study the effect of the duty cycle and effective power on physical and chemical properties, namely chemical composition, surface wettability and morphology. Biological activity of the fabricated films was studied by assessing the attachment and viability of gram - negative bacteria *P. aeruginosa* on their surface. The selected species of bacteria is a strong biofilm former of clinical relevance.

5.2 Experimental Section

5.2.1 Materials

Terpinen-4-ol (*$C_{10}H_{18}O$, M.W.=154.24 g/mol, Purity > 99 %, Australian Botanical Products Ltd.*) was used without any further modification. Microscope cover slips *(dia (Φ)=19 mm, ProSciTech, Australia)* made of borosilicate glass were used as a deposition substrate. The substrates were sequentially ultrasonically (43 kHz ± 2 kHz) cleaned for 30min in baths of 5% decon 90 solution (*Decon laboratories limited*), distilled water (D.I), acetone and, finally, propanol.

5.2.2 Sample Preparation

Pulse plasma Terpinen-4-ol (pp-Terpinen-4-ol) films were fabricated in a custom built tubular plasma reactor [31]. The separation between electrodes was kept at 8 cm for all the depositions. Clean substrates were placed in a plasma reactor and the chamber was brought to a steady pressure of 7 × 10-2 mbar. Plasma discharge was ignited using terpinen-4-ol vapors in a pulse wave mode at various duty cycles (DC) of 10, 20, 40 and 100 % at a peak power of 10 W. The pulse repetition frequency was set at 500 Hz. The monomer was introduced into the reactor chamber after achieving a steady pressure of 7 × 10-2 mbar after plasma ignition. The monomer flow rate was kept steady at 29 cm3/min by means of a needle valve. Thin films were deposited for 15 minutes at a process pressure of 2 × 10-1 mbar for all the duty cycles.

5.2.3 Thin film characterization

Coating thickness was confirmed by variable angle spectroscopic ellipsometry (VASE J. A. Woollam, M2000 D, USA). Measurements were taken in a wavelength range of 200-1000 nm at three different angles of incidence (55°, 60° and 65°). The polymer film thickness was modelled using a Cauchy function.

FT-IR spectroscopy was performed using a spectrum-100 spectrometer (Perkin Elmer,USA) operated in an ATR mode. Samples were deposited on KBr pellets for FT-IR charcteization. All FT-IR data were thickness normalized. Spectra were obtained at a resolution of 4 cm^{-1} averaged over 124 scans. XPS was performed using Specs SAGE 150 (Specs, Germany) using a monochromatic Al Kα source (hυ=1486.6 eV). The spectra were collected using a 90° take-off angle. Casa XPS software was used for data analysis and C1s spectra were charge corrected relative to C-C at the binding energy of 285.0 eV.

The static contact angle was measured using a KSV CAM 101 optical contact angle measuring instrument. Wettability of all surfaces was measured for three different liquids, namely deionized water, ethylene glycol (Ajax chemicals, Australia) and di-iodomethane (Merck Schuchardt OHG, Germany). A 3 µl drop of liquids was placed on the film surface and images were captured with an equipped camera. The contact angle was calculated using the Young-Laplace fitting [32]. The values reported here are a mean of fifteen measurements per sample type obtained from three independent samples. Surface energy was estimated following the Van Oss-Chaudhury-Good (VCG) method [33].

Roughness and topography of the film surface were examined using NT-MDT AFM instrument operated in a tapping mode. The roughness values were obtained from 3 μm ×3 μm AFM images and were averaged over three samples.

5.2.4 Antimicrobial activity

Pseudomonas aeruginosa (ATCC-589) cells were cultured overnight in Luria–Betani (L B) broth at 37 ^{o}C to reach a log phase. The culture was diluted to 10^{-5} colony forming units (CFU/ml) in a fresh LB medium. The biocidal response of pp-Terpinen-4-ol films and control (unmodified cover glass) was studied *in vitro*. pp-Terpinen-4-ol films were UV-sterilized by placing them at distance of 5 cm away from UV light source for duration of 20 minutes. UV-sterilized films and control samples were placed in 12-well cell cultured plates (Falcon, USA). 2ml of bacterial suspension was placed into each well. The samples were incubated at 37 ^{o}C for 24 hours after which they were rinsed with sterile deionized water to wash away any unattached bacteria. 3μl of each propidium iodide (PI) and SYTO9 (live/dead bacterial viability kit, Thermo Fisher Scientific, USA,) were added to a sterile 1 ml of deionized water for staining dead/live cells, respectively. A 200 μl aliquot of the staining solution was placed on the surface of the samples and allowed to incubate in the dark for 20 minutes. PI stains the dead bacterial cells red, whereas SYTO9 stains live cells as green. Samples were rinsed with sterile deionized water after incubation to wash away any excess stain.

The samples were visualized using an epifluorescence microscope (Axiovision, Zeiss). Images were captured at five random locations per sample. A minimum of three samples for each duty cycle were assessed. Images were processed using Image J software package (National Institutes of Health, USA). Bright field microscopic images were converted to 8 bit images. Threshold was adjusted in converted image to resemble the original image. An 'analyze particle plugin' was used to count the number of bacterial cells as dead (red) or alive (cyan). Viable bacterial adhesion assay data are analysed by one way analysis of variance (ANOVA) using origin pro software (version 9.). Tukey test were carried out to analyse the difference between groups.

5.3 Results and Discussion

5.3.1 Deposition rate

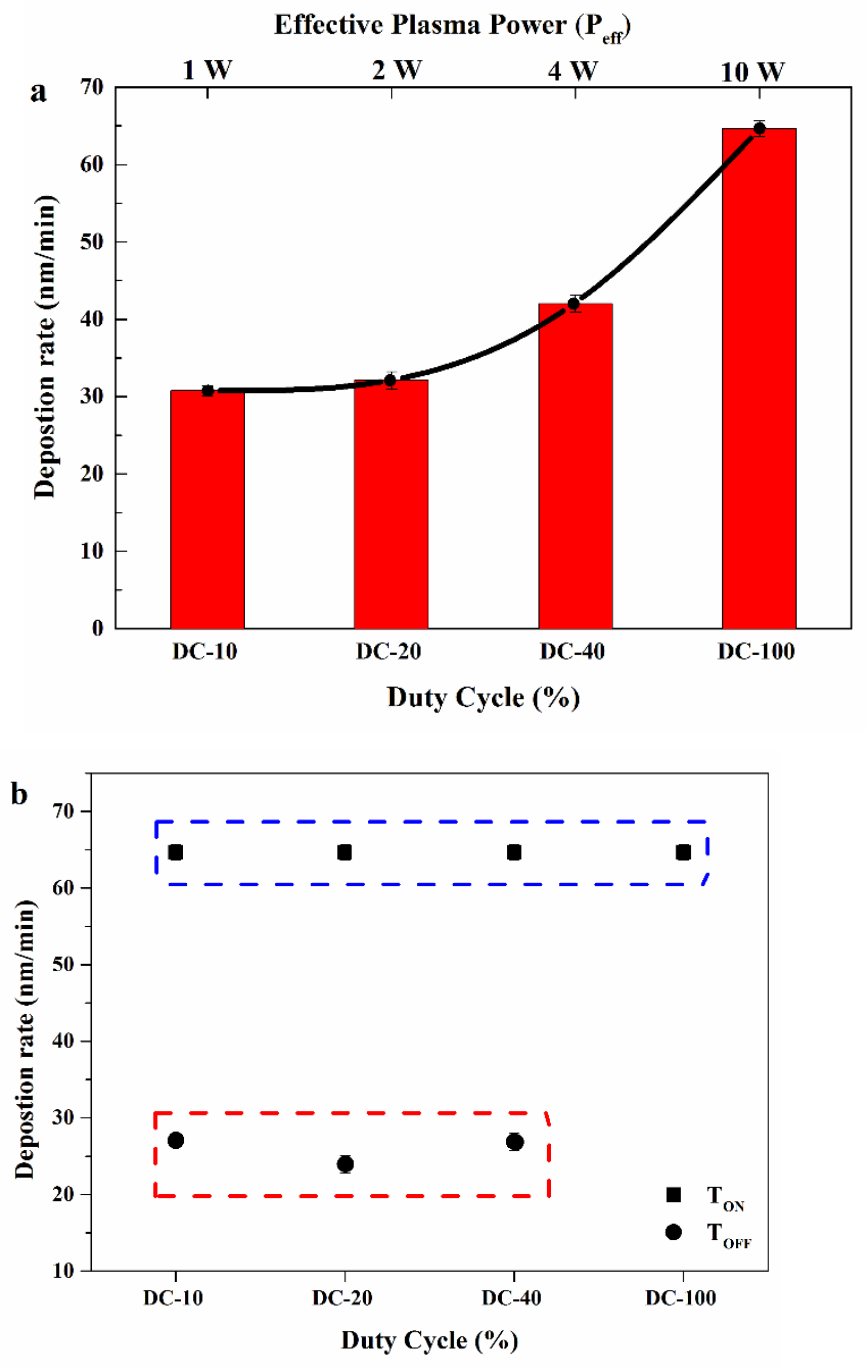

Figure 5. 1 (a). Deposition rate as a function of the duty cycle. (b) Influence of the duty cycle

on the deposition rate during the T_{off} period.

Plasma deposition conditions influence the film chemical and physical properties [34, 35]. Figure 5.1 (a) shows the deposition rate of plasma polymerized terpinen-4-ol films deposited using pulse RF power at DC-10, DC-20 , DC-40, DC-100 at a peak power of 10 W. The monomer flow rate and deposition pressure were kept constant during the process. Deposition rate (Rm) was calculated using the following equation 1 [36]:

$$R_m = \frac{R_{Mon}\, T_{on} + R_{Moff}\, T_{off}}{T_{tot}} = \frac{\text{Thickness}}{T_{tot}} \qquad (1)$$

where R_{Mon} and $R_{M\ off}$ are deposition rates during 'plasma on' and 'plasma off' periods, respectively. R_{Mon} was considered equal to R_{cw}, which is the deposition rate in a continuous wave mode (CW) at the same peak power; $R_{Mon} = R_{cw}$. The strong dependency of the film growth rate on the duty cycle suggests an occurrence of different polymerization mechanisms (e.g. plasma polymerization, chemical radical chain reaction, dissociation, etching, and ionization) during pulse PECVD of terpinen-4-ol. An increase in the deposition rate with the duty cycle indicates deposition is occurring in the power deficient region of the plasma. An increase in the deposition rate can be attributed to the increasing T_{on} with an increase in the duty cycle. At lower duty cycles (long T_{off}), there is a sharp decrease in the concentration of film-forming species (i.e. free radicals and ions), which may account for the low deposition rate. Plasma polymerization dominates the chemical radical chain reaction at a higher duty cycle (short T_{off}). Each molecule is fragmented to a greater degree as result of passing through a greater number of plasma discharges before arriving at the substrate. There is an increase in the polymeric chain terminations at the surface of the substrate due to high production of radicals with an increasing duty cycle. Figure 5.1 b shows the deposition rate during 'plasma on' and 'plasma off' periods. R_{Moff} was calculated using the following equation 2.

$$R_{Moff} = \frac{R_M\, T_{tot} - R_{Mcw}\, T_{on}}{T_{off}} \qquad (2)$$

The graph shows the deposition rate in the 'plasma off' period is lower than that in the 'plasma on' period. The flux of energetic particles (ions or electrons) decreases during the 'plasma off' period. Also, combining of the plasma phase-formed radicals with those on the surface of the growing film leads to the chain termination during T_{off} period, thus lowering the deposition rate. The chemical radical chain reaction polymerization is a favoured mechanism at the lower duty

cycles [35, 37]. The deposition rate at the low duty cycle (long T_{off}) period is influenced by the concentration of the adsorbed monomer ([M]), active growing chains ([M*), and initiating species, with the deposition rate in the 'plasma off' period estimated to be approximately 24–27 nm/min.

5.3.2 Film composition

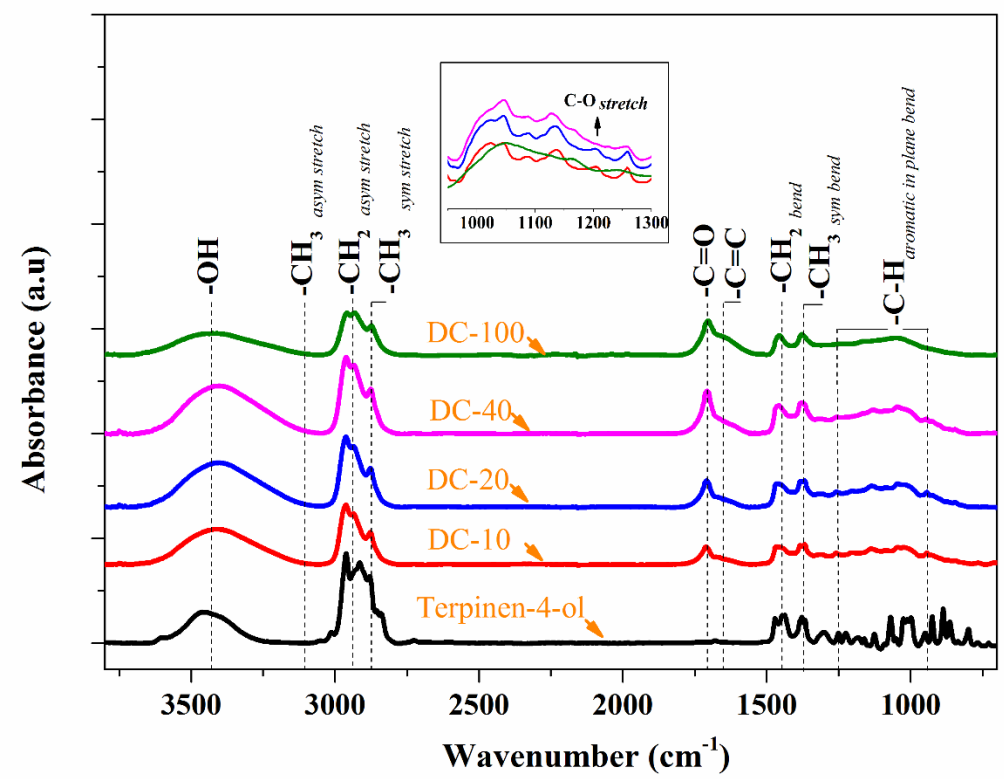

Figure 5. 2 FT-IR spectra of pulse polymerized terpinen-4-ol thin films at different duty cycles. The spectrum for the liquid precursor has been added as a reference

Different chemical reactions, such as free radical polymerization, random cross-linking, dissociation or etching occur during a PECVD process. The specific reaction mechanisms affect the growth rate, structure and chemical composition of the deposited films. Figure 5.2 shows the FTIR/ATR spectra of the precursor terpinen-4-ol monomer (reference spectrum) along with pp-terpinen-4-ol films deposited at various duty cycles at a peak power of 10 W. The absorbance peak for a –C-H aromatic in plane bend [38] is observed in the 1250-950 cm-1 region in films deposited at a duty cycle of 10 , 20, and 40, while it disappears in polymers deposited at a higher duty cycle of 100. This indicates the incorporation of an intact precursor ring structure in the film at a lower duty cycle. With an increasing duty cycle, every molecule of the monomer is subjected to a greater number of plasma discharges (TON) and thus is more likely to undergo a greater degree of dissociation. This may provide an explanation for the disappearance of the –C-H aromatic in plane bend with an increasing duty cycle. Phenolic -C-O stretch is observed at 1200

cm-1 in the films deposited at DC-10 and DC-20. An increase in the peak intensity corresponding to the methyl stretch [38](2871-2879 and 2961 cm-1) and methylene C-H stretch (2935 cm-1) is observed with an increasing duty cycle. An increase in the peak intensity of methylene stretch bands with respect to methyl stretching bands is indicative of a more cross-linked structure of the polymers fabricated at higher duty cycles. An increase in peak intensities at 1380 and 1460 cm -1 corresponds to an increase in symmetric –C-H bend in methyl and methylene group, respectively. Formation of a more irregular cross-linked structure at higher duty cycles seems to provide a possible explanation for the drop in the intensity of this band in films deposited at DC-100. The intensity of the peak at 1705 cm-1 representing –C = O [38] stretching in carboxyl group increases with an increasing duty cycle. A broad peak at 1660 cm-1 corresponds to –C = C stretching, which is only observed in films deposited at DC-100 as a likely consequence of more carbon bond substitutions. The broad peak centered around 3440 cm-1 is indicative of the –O-H stretch.

Table 5. 1 Wettability, surface roughness, surface O/C ratio and binding composition of pulsed plasma polymerized terpinen-4-ol thin films.

Films	Roughness (r.m.s) ,nm	WCA (deg)	O/C	% C-C /C-H C1s	%C-OH/C-OR C2	% C=O C3
pp-DC-10	0.25 ± 0.02	42.16 ± 0.66	0.22	68.60	21.67	9.73
pp-DC-20	0.24 ± 0.015	47.91 ± 0.31	0.17	70.28	19.44	10.27
pp-DC-40	0.25 ± 0.02	79.42 ± 1.56	0.10	69.51	17.95	12.54
pp-DC-100	0.44 ± 0.15	67.38 ± 3.8	0.20	81.73	5.33	12.93
Control (bare cover glass)	0.69 ± 0.16	36.31 ± 3.09	-	-	-	-

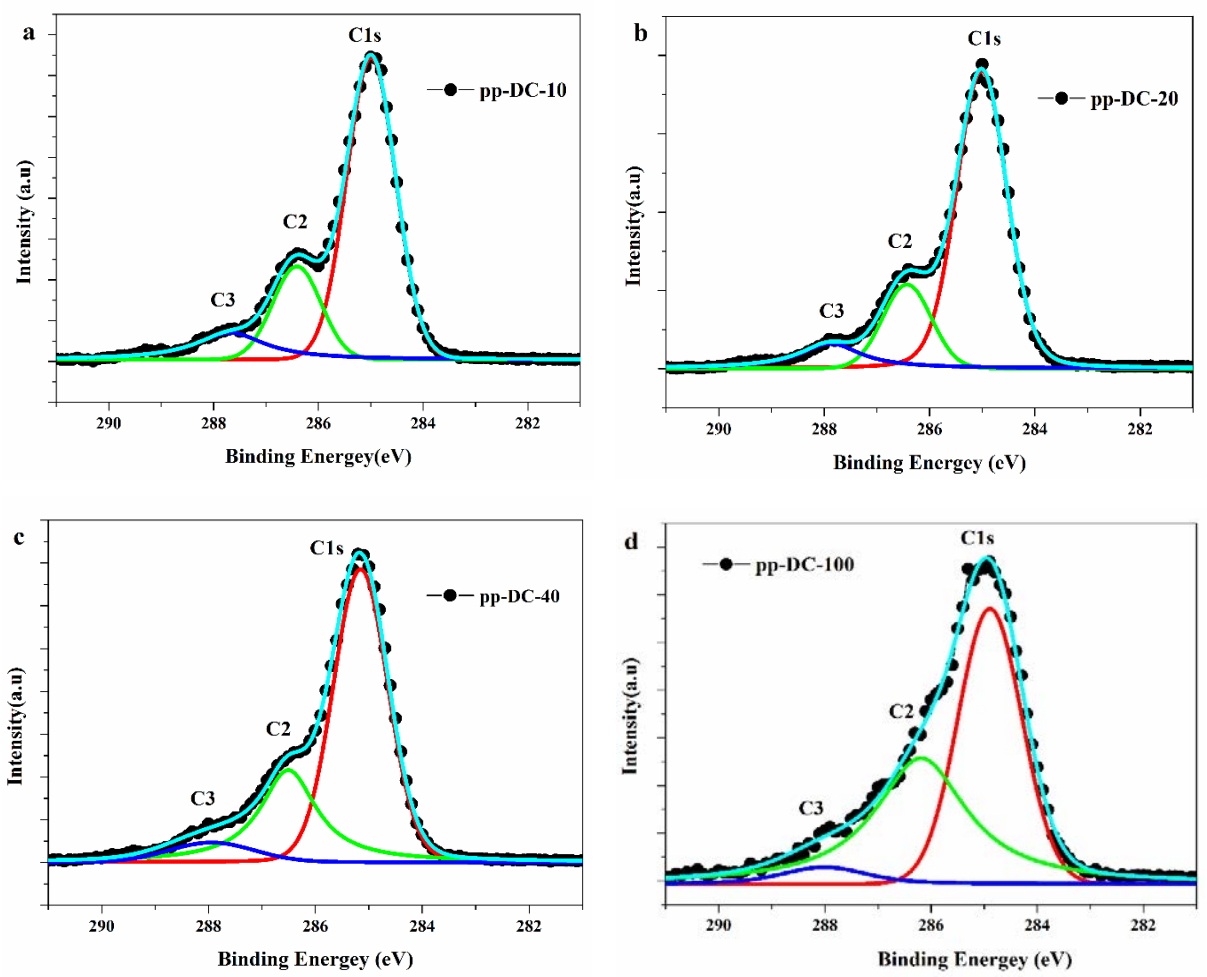

Figure 5. 3 High resolution C1s XPS spectra of pulse –PECVD deposited Terpinen-4-ol films at various duty cycles (a)-pp-DC-10, (b)-pp-DC-20, (c)-pp-DC-40, and (d)- pp-DC-100.

Figure 5.3 shows the high-resolution C1s spectra of pp-terpinen-4-ol films deposited at different duty cycles. Spectra reveals a decreasing O/C ratio with an increasing duty cycle, which is corroborated by an increasing peak intensity at 285 eV. A high O/C ratio is observed in pp-DC-100. A higher number of aliphatic carbons incorporated in films accounts for this phenomenon. There is a decrease in the –C-O component with an increasing duty cycle. The C-O bonds are more prone to rearrangement, which can in part account for this observation [39]. The C=O component increases with an increasing duty cycle.

5.3.3 Film wettability

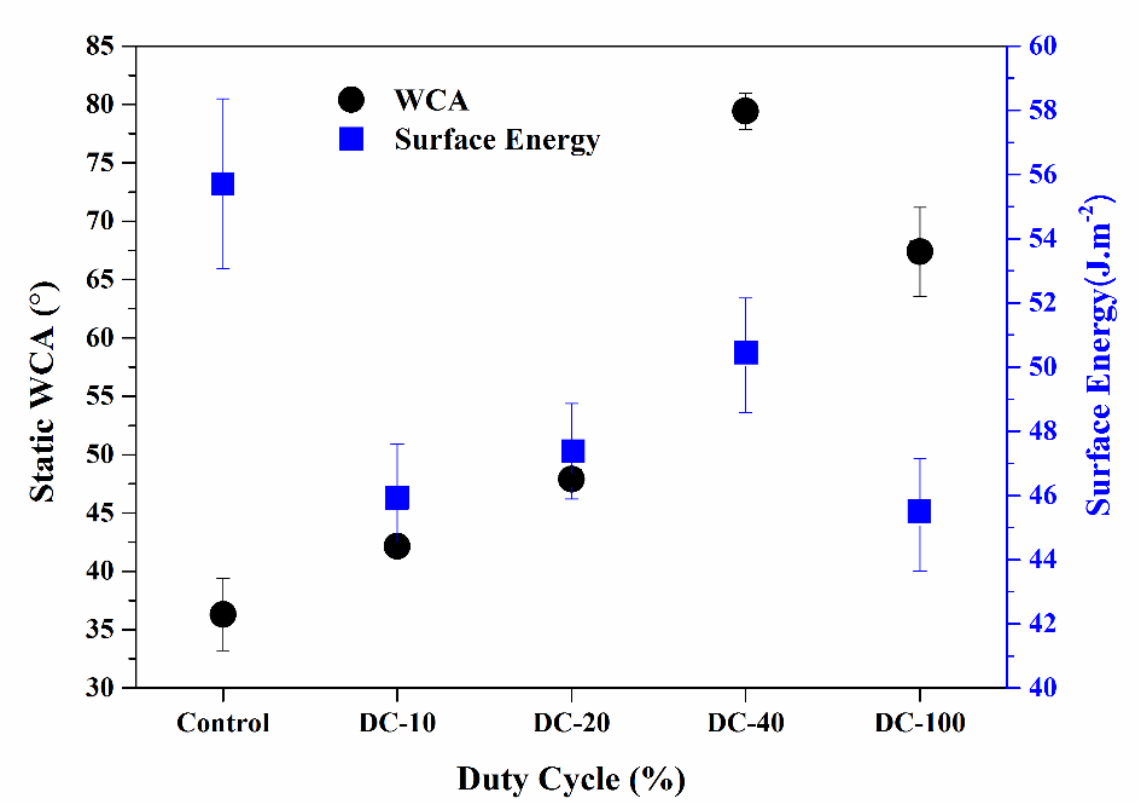

Figure 5. 4 Static water contact angle and surface energy of films deposited at DC-10, DC-20, DC-40 and DC-100.

The biocompatibility of a material is influenced by its wettability and surface energy. Water contact angles (WCA) of pp-terpinen-4-ol are listed in table 5.1. The influence of the duty cycle on the WCA and surface energy are shown in figure 5.4. WCA on an unmodified substrate has also been added for reference. Both contact angle and surface energy of the pp-terpinen-4-ol films were found to increase with the duty cycle except that for DC-100 films. The variation in wettability can be ascribed to changes in the chemical composition of the films. The effect of surface roughness (table 5.1), which is less than one nm for all the pp-terpinen-4-ol surfaces, on wettability would be negligible.

An increase in hydrophobicity with the duty cycle can be attributed to a higher degree of fragmentation of monomer rings, which results in a more cross-linked polymer structure as evident from the FTIR analysis. A slight decrease in the contact angle at DC-100 can be attributed to an increased concentration of hydrophilic –C=O groups. A greater degree of fragmentation and recombination of molecules at a higher duty cycle leads to the formation of more hydrophilic

functionalities (-C=O in present case). This phenomenon becomes more pronounced under a deposition regime with a high level of fragmentation [36].

5.3.4 Antibacterial activity

P. aeruginosa, a gram negative pathogenic bacterium, was used to evaluate the antimicrobial activity of pp-terpinen-4-ol. This strain is a potent biofilm former and is clinically relevant. Figure 5.5 shows the fluorescence microscope images of attached *P. aeruginosa* cells on the surfaces of pp-terpinen-4-ol and control samples. Viable (cyan) and non-viable (red) cells are observed on surfaces of both polymer and control samples. It can be observed that there is no colony formation on the surfaces of pp-DC-10 and pp-DC-20. These films were found to be unstable in aqueous media, which can at least in part account for the low attachment of cells on these surfaces. pp-DC-40 shows a high degree of attachment of *P. aeruginosa* cells. The number of non-viable cells was the highest on pp-DC-40 among all the samples tested. Figure 5.6(a) shows the percentage of live bacterial cells attached on the surface of pp-terpinen-4-ol as a function of duty cycle. The percentage of viable bacteria on glass coverslips (used as a control) were found to be around 61 %. A significant decrease in the number of viable bacteria, to 35 %, 19 %, 22 % and 24 %, was observed on pp-terpinen-4-ol deposited at the duty cycle of DC-100, DC-40, DC-20, and DC-10, respectively. There is no significant difference in bacterial viability on polymers deposited at DC-10 and DC-20. Polymers fabricated at DC-40 showed the lowest percentage of viable bacteria on their surface compared to the other samples and the control. Bacterial adhesion to a surface is an intricate process that depends upon the wettability, roughness, charge and chemistry of the surface, as well as the properties of the microorganism [40-42]. Hydrophobic surfaces are thermodynamically favourable to settlement by hydrophobic cells and likewise is observed for hydrophilic surfaces also [43, 44]. *P. aeruginosa* strains have been found to be relatively hydrophobic in nature [45, 46]. This explains the relatively high level of attachment of the cells to pp-terpinen-4-ol deposited at DC-40, which is relatively more hydrophobic compared to other pp-terpinen-4-ol polymers (Figure 5.6b). Hydrophobic surfaces favours the water elimination at solid-liquid interface, facilitating close approach of bacterial cells to surface [47].

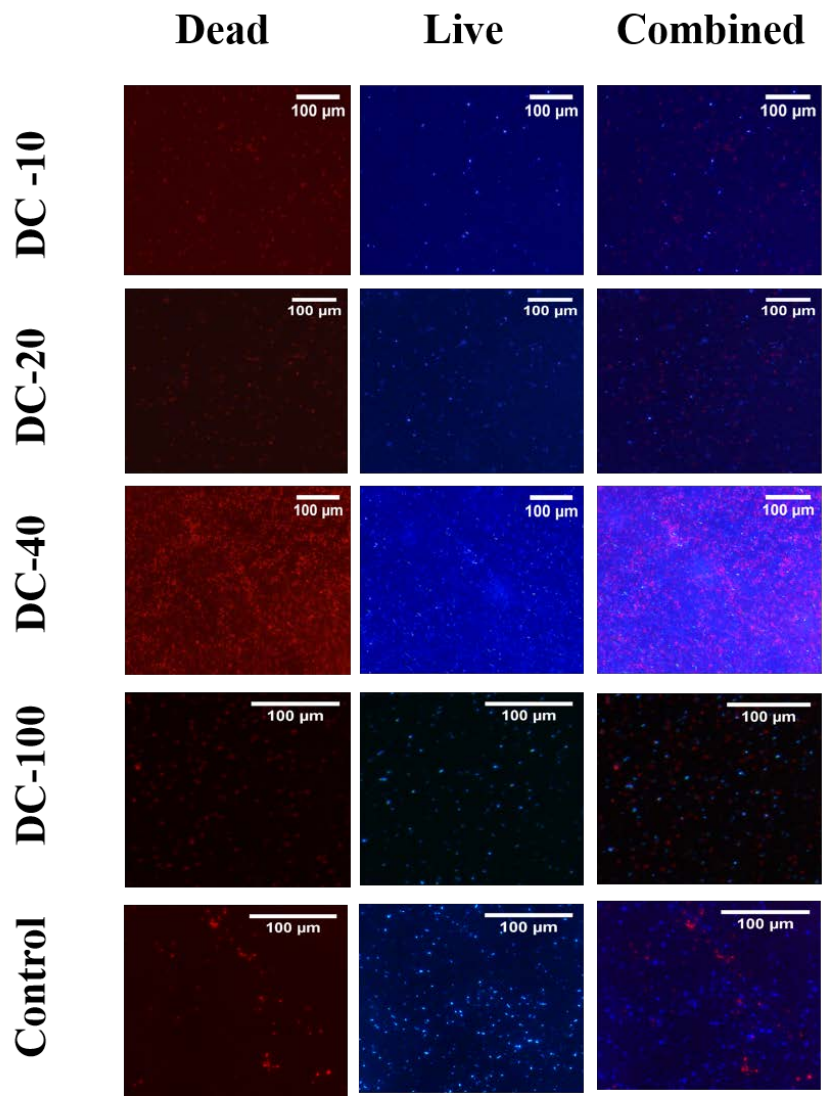

Figure 5. 5 Fluorescence microscopy images of *P. aeruginosa* cells attached to the surfaces of plasma polymers fabricated at different duty cycles and a control (glass slides) after 24 hr of incubation. Red is indicative of dead bacteria and cyan indicates viable cells.

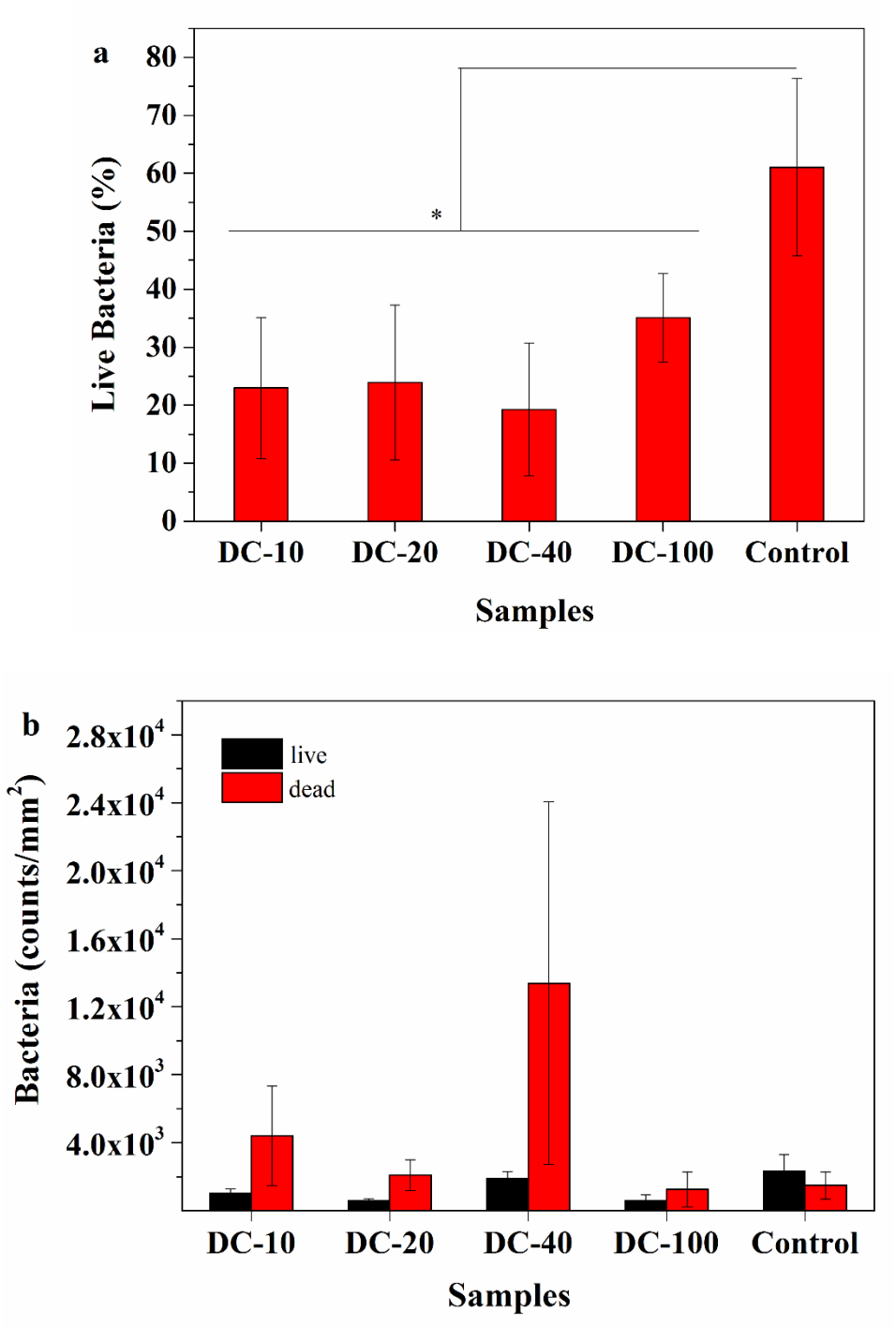

Figure 5. 6(*a*) Percentage of live bacteria (* = P < 0.05). Bacterial viability between control and deposited terpinen-4-ol coatings are significantly different. (b) Total number of bacteria attached to the surface of deposited films and control after 24 hr of incubation.

5.3.5 Stability test

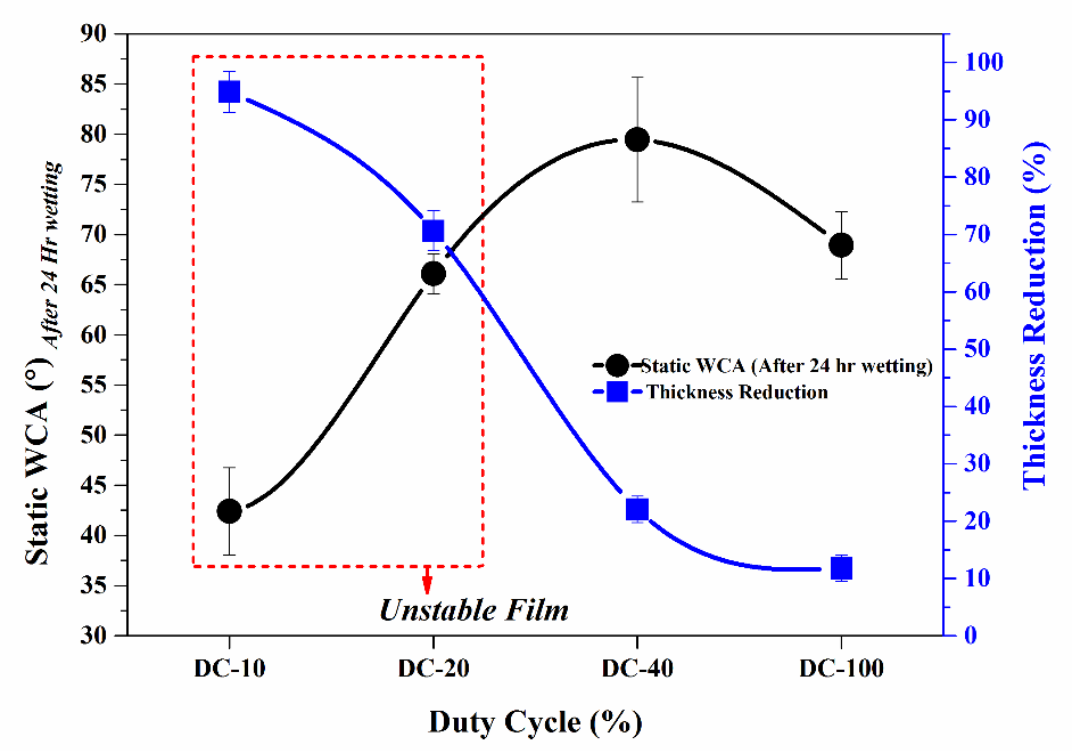

Figure 5. 7 Static water contact angle and percentage loss in thickness of deposited films after 24 hr immersion in aqueous media.

The values for the static WCA and loss of thickness after an incubation in deionized water for 24 hr are shown in figure 5.7. For pp-terpinen-4-ol films, stability in water increased with the increasing duty cycle. The thickness loss of coatings deposited at DC-10 and DC-20 were around 90 % and 70 %, respectively. A relatively low degree of cross-linking and high hydrophilic character of these films make them highly dissolvable under aqueous conditions. Elution of low molecular weight chains from the films leads to a significant decrease in the thickness of these films. Similar behaviour has been previously reported for other types of plasma polymers [48].

There was a minimal increase in the WCA for films after 24 hrs of incubation for coatings deposited at DC-40 and DC-100. However, there was a significant increase in the water contact angle for films deposited at DC-20 after 24 hr of immersion. A high rate of elution of hydrophilic moieties observed in DC-20 coatings would leave behind a carbon rich matrix, which can to some extent explain an increase in contact angle for these films. This reasoning can be extended to a

WCA increase observed for coatings fabricated at DC-40 and DC-100, although the increase was minimal because of the lower rate of dissolution.

5.4 Conclusion

Antimicrobial terpinen-4-ol films were fabricated by the pulsed PECVD method. XPS characterization revealed an increase in the carbon content of films with an increasing duty cycle. FT-IR spectra suggested a possible polymerization mechanism, where at a lower duty cycle C-O bond dissociation is followed by radical chain reactions. Complete monomer ring fragmentation was observed at higher duty cycles. Polymer fabricated at a duty cycle of DC-40 (P_{eff} = 4W) and DC-100 were found to be more stable and robust when immersed in aqueous media. There was a link between surface wettability and attachment of *P. aeruginosa*. High bacterial attachment was observed on polymers deposited at DC-40 because of higher hydrophobicity of these surfaces. These polymers also showed the highest antibacterial activity among all the tested samples. The greater degree of preservation of monomer molecules at lower duty cycles enhances the antibacterial activity of these films, however, their low stability under aqueous conditions may limit their applications.

Reference

1. Banerjee, I., R.C. Pangule, and R.S. Kane, Antifouling coatings: recent developments in the design of surfaces that prevent fouling by proteins, bacteria, and marine organisms. Advanced Materials, 2011. **23**(6): p. 690-718.

2. Callow, J.A. and M.E. Callow, Trends in the development of environmentally friendly fouling-resistant marine coatings. Nature communications, 2011. **2**: p. 244.

3. Scott, R.D., The direct medical costs of healthcare-associated infections in US hospitals and the benefits of prevention. 2009.

4. Magill, S.S., et al., *Multistate point-prevalence survey of health care–associated infections.* New England Journal of Medicine, 2014. **370**(13): p. 1198-1208.

5. Monroe, D., Looking for chinks in the armor of bacterial biofilms. PLoS biology, 2007. **5**(11): p. e307.

6. Davies, D., *Understanding biofilm resistance to antibacterial agents.* Nature reviews Drug discovery, 2003. **2**(2): p. 114.

7. Nouraei, S.R., et al., Bacterial colonization of airway stents: a promoter of granulation tissue formation following laryngotracheal reconstruction. Archives of Otolaryngology–Head & Neck Surgery, 2006. **132**(10): p. 1086-1090.

8. Saini, H., et al., Azithromycin-ciprofloxacin-impregnated urinary catheters avert bacterial colonization, biofilm formation, and inflammation in a murine model of foreign-body-associated urinary tract infections caused by Pseudomonas aeruginosa. Antimicrobial agents and chemotherapy, 2017. **61**(3): p. e01906-16.

9. Percival, S.L., et al., Healthcare-associated infections, medical devices and biofilms: risk, tolerance and control. Journal of medical microbiology, 2015. **64**(4): p. 323-334.

10. Zanini, S., et al., *Polyethylene glycol grafting on polypropylene membranes for anti-fouling properties.* Plasma chemistry and plasma processing, 2007. **27**(4): p. 446.

11. Ma, H., et al., "Non-Fouling" Oligo (ethylene glycol)-Functionalized Polymer Brushes Synthesized by Surface-Initiated Atom Transfer Radical Polymerization. Advanced Materials, 2004. **16**(4): p. 338-341.

12. Tugulu, S. and H.-A. Klok, Stability and nonfouling properties of poly (poly (ethylene glycol) methacrylate) brushes under cell culture conditions. Biomacromolecules, 2008. **9**(3): p. 906-912.

13. Roosjen, A., et al., *Stability and effectiveness against bacterial adhesion of poly (ethylene oxide) coatings in biological fluids.* Journal of Biomedical Materials Research Part B: Applied Biomaterials, 2005. **73**(2): p. 347-354.

14. Armstrong, J.K., et al., Antibody against poly (ethylene glycol) adversely affects PEG-asparaginase therapy in acute lymphoblastic leukemia patients. Cancer, 2007. **110**(1): p. 103-111.

15. Cavallaro, A., et al., Influence of immobilized quaternary ammonium group surface density on antimicrobial efficacy and cytotoxicity. Biofouling, 2016. **32**(1): p. 13-24.

16. Tiller, J.C., et al., *Designing surfaces that kill bacteria on contact.* Proceedings of the National Academy of Sciences, 2001. **98**(11): p. 5981-5985.

17. Murbach Teles Andrade, B.F., et al., *Antimicrobial activity of essential oils.* Journal of Essential Oil Research, 2014. **26**(1): p. 34-40.

18. Wilbon, P.A., F. Chu, and C. Tang, *Progress in renewable polymers from natural terpenes, terpenoids, and rosin.* Macromolecular rapid communications, 2013. **34**(1): p. 8-37.

19. Bazaka, K., et al., Anti-bacterial surfaces: natural agents, mechanisms of action, and plasma surface modification. Rsc Advances, 2015. **5**(60): p. 48739-48759.

20. Bazaka, K., et al., Plasma-assisted surface modification of organic biopolymers to prevent bacterial attachment. Acta biomaterialia, 2011. **7**(5): p. 2015-2028.

21. Ershov, S., et al., Free radical-induced grafting from plasma polymers for the synthesis of thin barrier coatings. RSC Advances, 2015. **5**(19): p. 14256-14265.

22. Gulati, K., et al., Biocompatible polymer coating of titania nanotube arrays for improved drug elution and osteoblast adhesion. Acta biomaterialia, 2012. **8**(1): p. 449-456.

23. Wertheimer, M.R., *Plasma processing and polymers: a personal perspective.* Plasma Chemistry and Plasma Processing, 2014. **34**(3): p. 363-376.

24. Jacobs, T., et al., *Plasma surface modification of biomedical polymers: influence on cell-material interaction.* Plasma Chemistry and Plasma Processing, 2012. **32**(5): p. 1039-1073.

25. Ozaydin-Ince, G., A.M. Coclite, and K.K. Gleason, CVD of polymeric thin films: applications in sensors, biotechnology, microelectronics/organic electronics, microfluidics, MEMS, composites and membranes. Reports on Progress in Physics, 2011. **75**(1): p. 016501.

26. Jacob, M.V., et al., Plasma polymerised thin films for flexible electronic applications. Thin Solid Films, 2013. **546**: p. 167-170.

27. Bazaka, K., et al., Plasma-enhanced synthesis of bioactive polymeric coatings from monoterpene alcohols: a combined experimental and theoretical study. Biomacromolecules, 2010. **11**(8): p. 2016-2026.

28. Calcabrini, A., et al., Terpinen-4-ol, the main component of Melaleuca alternifolia (tea tree) oil inhibits the in vitro growth of human melanoma cells. Journal of Investigative Dermatology, 2004. **122**(2): p. 349-360.

29. Carson, C., K. Hammer, and T. Riley, Melaleuca alternifolia (tea tree) oil: a review of antimicrobial and other medicinal properties. Clinical microbiology reviews, 2006. **19**(1): p. 50-62.

30. Mondello, F., et al., In vivo activity of terpinen-4-ol, the main bioactive component of Melaleuca alternifolia Cheel (tea tree) oil against azole-susceptible and-resistant human pathogenic Candida species. BMC infectious diseases, 2006. **6**(1): p. 1.

31. Jacob, M., et al., *Fabrication of a novel organic polymer thin film.* Thin Solid Films, 2008. **516**(12): p. 3884-3887.

32. Adamson, A.W. and A.P. Gast, *Physical chemistry of surfaces.* 1967.

33. Owens, D.K. and R. Wendt, *Estimation of the surface free energy of polymers.* Journal of applied polymer science, 1969. **13**(8): p. 1741-1747.

34. Konuma, M., *Film deposition by plasma techniques*. Vol. 10. 2012: Springer Science & Business Media.

35. Friedrich, J., Mechanisms of plasma polymerization–reviewed from a chemical point of view. Plasma Processes and Polymers, 2011. **8**(9): p. 783-802.

36. Zanini, S., et al., Pulsed plasma-polymerized 2-isopropenyl-2-oxazoline coatings: Chemical characterization and reactivity studies. Surface and Coatings Technology, 2018. **334**: p. 173-181.

37. Loyer, F.o., et al., Atmospheric Pressure Plasma-Initiated Chemical Vapor Deposition (AP-PiCVD) of Poly (alkyl acrylates): An Experimental Study. Macromolecules, 2017. **50**(11): p. 4351-4362.

38. Coates, J., *Interpretation of infrared spectra, a practical approach.* Encyclopedia of analytical chemistry, 2000.

39. Beamson, G., *High resolution XPS of organic polymers.* the Scienta ESCA 300 database, 1992. **208**: p. 110. 188.

40. Xu, L.-C. and C.A. Siedlecki, Effects of surface wettability and contact time on protein adhesion to biomaterial surfaces. Biomaterials, 2007. **28**(22): p. 3273-3283.

41. Singh, A.V., et al., Quantitative characterization of the influence of the nanoscale morphology of nanostructured surfaces on bacterial adhesion and biofilm formation. PloS one, 2011. **6**(9): p. e25029.

42. Fletcher, M. and D.C. Savage, *Bacterial adhesion: mechanisms and physiological significance*. 2013: Springer Science & Business Media.

43. Bos, R., H.C. Van der Mei, and H.J. Busscher, *Physico-chemistry of initial microbial adhesive interactions–its mechanisms and methods for study.* FEMS microbiology reviews, 1999. **23**(2): p. 179-230.

44. Bruinsma, G.M., et al., Effects of cell surface damage on surface properties and adhesion of Pseudomonas aeruginosa. Journal of Microbiological Methods, 2001. **45**(2): p. 95-101.

45. Poelstra, K., et al., Pooled human immunoglobulins reduce adhesion of Pseudomonas aeruginosa in a parallel plate flow chamber. Journal of biomedical materials research, 2000. **51**(2): p. 224-232.

46. Liu, C., et al., *Reduction of bacterial adhesion on modified DLC coatings.* Colloids and Surfaces B: Biointerfaces, 2008. **61**(2): p. 182-187.

47. Rodrigues, L., et al., Interference in adhesion of bacteria and yeasts isolated from explanted voice prostheses to silicone rubber by rhamnolipid biosurfactants. Journal of applied microbiology, 2006. **100**(3): p. 470-480.

48. Chu, L.Q., Q. Zhang, and R. Förch, Surface Plasmon-Based Techniques for the Analysis of Plasma Deposited Functional Films and Surfaces. Plasma Processes and Polymers, 2015. **12**(9): p. 941-952.

Chapter 6

In-situ Surface modification

In this chapter effect of in-situ surface modification of terpinen-4-ol plasma polymers on antibacterial property is investigated. Changes in thin film property are evaluated with respect to antibacterial performance and UV blocking properties. The result of this section are to be submitted as: *Avishek kumar, Ahmed AL-Jumaili, Kateryna Bazaka, Peter Mulvey, Jeffery Warner, Mohan V. Jacob. Enhanced anti-bacterial and UV absorbing properties in surface modified terpinen-4-ol plasma polymers. Polymers*

Enhanced anti-bacterial and UV absorbing properties in surface modified terpinen-4-ol plasma polymers

Abstract

Surface modification of thin films is often performed to enhance their properties. In this work, *in situ* modification of terpinen-4-ol (T4) plasma polymer is carried out via simultaneous surface functionalization and nanoparticle immobilization. ZnO nanoparticle functionalization was achieved by grafting $Zn(acac)_2$ molecules on the surface of T4 polymer in oxygen plasma environment immediately after polymer deposition. A combination of surface functionalization and ZnO nanoparticle modification led to an enhancement in antibacterial properties. ZnO nanoparticle-modified coatings demonstrated superior antibacterial and UV absorbing characteristics. The ZnO modified coatings were transparent in the visible region of 400 – 700 nm. The finding points towards the potential use of ZnO nanoparticle-modified T4 plasma polymers as optically transparent UV absorbing coatings.

Keywords: In-situ surface modification, ZnO functionalization, Plasma polymers, Antibacterial coatings

As to be submitted :Avishek kumar, Ahmed AL-Jumaili, Kateryna Bazaka, Peter Mulvey, Jeffery Warner, Mohan V. Jacob. Enhanced anti-bacterial and UV absorbing properties in surface modified terpinen-4-ol plasma polymers. Polymers

6.1 Introduction

Bacterial adhesion to material surface is the primary step in biofilm development. Biofilm formation can potentially have severe health and industrial repercussions [1, 2], with examples including implant-associated infections [3, 4] and marine fouling[5]. Planktonic cells of many species have a tendency to form a biofilm matrix on surfaces as a mean of protection against hostile environment and predation. Once the biofilm enters the tertiary phase of development, killing of biofilm-residing cells, and biofilm dissolution and removal become challenging. According to some estimates, hospital acquired infections (HAI) have cost $ 40 billion yearly to US hospitals from 2001-2007 [6].

Surface modification of materials has been frequently used to minimize microbial adhesion [7, 8]. Hydrophilic/hydrophobic modification and immobilization of nanoparticles (Nps), such as Cu, ZnO, and Ag, on the material surface have been used separately as an effective strategy to reduce biofilm formation [9-12]. Surfaces functionalized with enzyme, antibiotics and biocides have also been used as antimicrobial surfaces [13-15]. Surfaces modified to display hydrophilic behavior have shown superior antifouling properties [16-18]. Hydrophilic surfaces form hydrogen bonds with water molecules, leading to the formation of a hydration layer at the water/surface interface. This hydration layer acts as an energetic barrier and prevents the adhesion of fouling molecules. Wu *et al.* used atom transfer radical polymerization to impart hydrophilicity on silicon surfaces using N-vinylpyrrolidone (PVP). The Si-PVP surfaces were characterized by a low water contact angle of 24° and showed that adsorption of human serum albumin, lysosome and fibrinogen were reduced by 93, 81 and 71 %, respectively [19]. Poly (ethylene glycol) (PEG) has been widely used for hydrophilic modification of surfaces for antifouling applications. PEG functionalized surfaces have been widely applied in the fields of central venous catheters [18], hemodialysis membranes [20], and biosensors and biochips [21, 22].

Surface modification techniques such as block co-polymerization [23, 24], covalent grafting of hydrophilic groups to surfaces [25], nanoparticle functionalization [26, 27], atom transfer radical polymerization [28], RF plasma deposition and modifications of surfaces have been used to fabricate surfaces showing antifouling properties. Kim *et al.* modified nanofiltration thin film composite membranes to be more hydrophilic by a treatment with NH_3 plasma. The membranes showed superior antifouling properties on account of their increased hydrophilicity [29] .

Nanoparticles have found wide bio application on account of, among many other attributes, their broad spectrum antibacterial activity [30, 31]. Among a wide range of particles, zinc oxide

nanoparticles have demonstrated enhanced antibacterial and antifouling properties [32, 33]. ZnO nanoparticle incorporation into a polymer matrix such as polyvinylidene fluoride (PVDF) [34], polysulfide (PSF) [35] and polyethersulfone (PES)[36] has enhanced the antifouling activity of these polymer matrices when used as ultrafiltration membranes. Chitosan-ZnO nanocomposites have demonstrated an effective marine antifouling activity against bacteria *Pseudoalteromonas nigrifaciens* and the diatom *Navicula sp*. [37].

Terpinen-4-ol plasma polymers are a recent entry in the range of biodegradable polymer materials that show promising antimicrobial activity and have both biomedical and marine applications [5, 38, 39]. This study investigates the effect of surface modification of terpinen-4-ol plasma polymers via hydrophilic modification by oxygen plasma treatment and ZnO nanoparticle (Np) immobilization on antibacterial activity against E. coli. Plasma enhanced chemical vapor deposition (PECVD) of ZnO films requires high processing temperatures [40]. However, terpinen-4-ol plasma polymers will lose their antimicrobial property if deposited at a high temperature due to excessive loss of original chemical functionality of the monomer. The approach used in this study overcomes this challenge by proposing a method by which the desired antimicrobial property of terpinen-4-ol can be retained and further enhanced by ZnO Np immobilization and surface wettability modification of the polymer.

6.2 Film fabrication and characterization

6.2.1 Materials

Terpinen-4-ol (*$C_{10}H_{18}O$, Mw = 154.24 g/mol, Purity > 99 %) and* Zinc acetylacetonate *($Zn(acac)_2$)* were purchased from Australian Botanical Products and Sigma Aldrich, respectively, and used without any further modification. Microscope cover slips *(Φ = 19 mm, ProSciTech, Australia)* and silicon wafer were used as substrates. The substrates were consecutively ultrasonically cleaned for 30 min each in 5% solution of Decon 90 (*Decon laboratories limited*), followed by double distilled water acetone and propanol. High purity Oxygen and Argon gas (purity > 99.9%) were procured from BOC gas, Australia.

6.2.2 Thin film fabrication

ZnO nanoparticle-functionalized terpinen-4-ol films were fabricated in a custom built capacitively coupled tubular (Quartz, l = 80cm, d = 5cm) RF reactor (13.56 MHz). Electrode separation was maintained at 8 cm for all the depositions. Substrates were placed 1cm away from the leading electrode. Zinc acetyl acetonate [$Zn(C_5H_7O_2)_2 \times H_2O$] was placed in the clean ceramic boat and loaded in the middle of the reactor. External heating was used to vaporize the $Zn(acac)_2$ at a temperature of 140 °C. No external substrate heating was used during the deposition. The temperature of the substrate was found to be 40 °C during ZnO Np functionalization of terpinen-4-ol surfaces. Terpinen-4-ol monomer flow rate was kept constant at 29 cm^3/min. The polymerization of terpinen-4-ol was carried out at 10 W and the process pressure of 5×10^{-2} mbar. Argon and Oxygen were used as a carrier gas with latter providing hydrophilic modification of the surface of the as-deposited terpinen4-ol polymer matrix. Deposition of T4 monomer alone in the oxygen/argon plasma led to the wettability modification. Passing of $Zn(acac)_2$ vapor over the freshly deposited polymer led to *in situ* functionalization of the surface with ZnO nanoparticles. Flow rate of the argon/oxygen carrier gas was kept constant at 6 cm^3/min. The desired thickness of the film was achieved by adjusting the deposition time.

6.2.3 Thin film Characterization

Film thickness was estimated by spectroscopic ellipsometry (VASE J. A. Woollam, M2000 D). The morphology of the films was characterized by field emission scanning electron microscopy at 10 KV (FE-SEM, Hitachi SU 500). The Chemical composition of the films were estimated by FT-IR spectroscopy (Perkin Elmer, Spectrum 100) and x-ray photoelectron spectroscopy (Specs SAGE 150). Hydrophilic/hydrophobic character of the films was determined by static contact angle measurement by means of a goniometer (KSV, CAM 101) using three liquids. Raman spectra of the films were acquired with Confocal Raman microscope (Witec alpha 300 access). Surface roughness parameters were examined using atomic force microscopy in tapping mode (NT-MDT).

6.2.4 Bacterial assay

Antibacterial activity of films was evaluated against *E. coli* (ATCC-924). *E. coli* cells were cultured in Luria-Betani (LB) broth at 37 °C for 24 hr to reach the log phase. The bacterial solution was diluted to 5×10^5 colony forming units (CFU)/ml. The coated and uncoated glass substrates

(control) were sterilized by subsequent washing in ethanol and PBS solution. The sterilized films and controls were placed into 12 well cell culture plates (Falcon, USA). 2 ml of *E. coli* suspension was placed onto samples into each well and incubated at 37 °C for 24 hr. Each sample was washed three times with 10 ml of sterile PBS and placed into 50 ml polyethylene tubes containing 5 ml of sterile PBS solution. Tubes were sonicated for 5 min to detach bacterial cells. 10 µl of bacterial suspension was added to 90 µl of prewarmed LB broth. 100 µl of the diluted bacterial suspension was plated on Agar medium. Agar plates were incubated at 37 °C for 24 hr, and the number of CFU were counted. All tests were carried out with three replicates.

6.3 Results and discussion

6.3.1 Deposition rate

Wettability and ZnO modification of T4 was carried out via plasma enhanced chemical vapor depositions (PECVD). Deposition rates (R_d) of coatings are shown in Figure 6.1. The depostion rate of the T4 alone is also shown for comparison. As seen in Figure 6.1, R_d in oxygen plasma is higher than in the Ar plasma. The higher effective flow rate ($F = F_m + aF_c$) of gases (O_2 + T4 monomer) in oxygen plasma contributes to higher R_d. Formation of oxygen radicals and their reaction with film-forming species enhance the deposition rate. Also, the correction flow factor *a* in the above equation is 0.6 for the oxygen and (0.05-0.1) for argon [41]. The use of argon as a carrier gas has been found to increase the monomer fragmentation [42], however, the deposition mechanism remains unaffected [43].

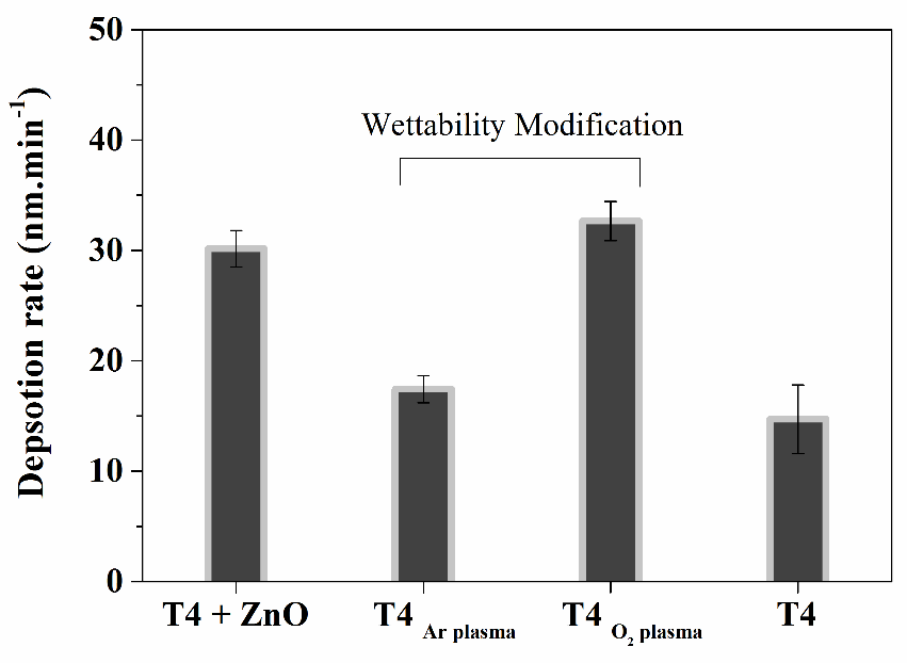

Figure 6. 1 Deposition rate of T4 during wettability and nanoparticle modification. Deposition in Argon/Oxygen plasma led to wettability modification.

6.3.2 Film composition

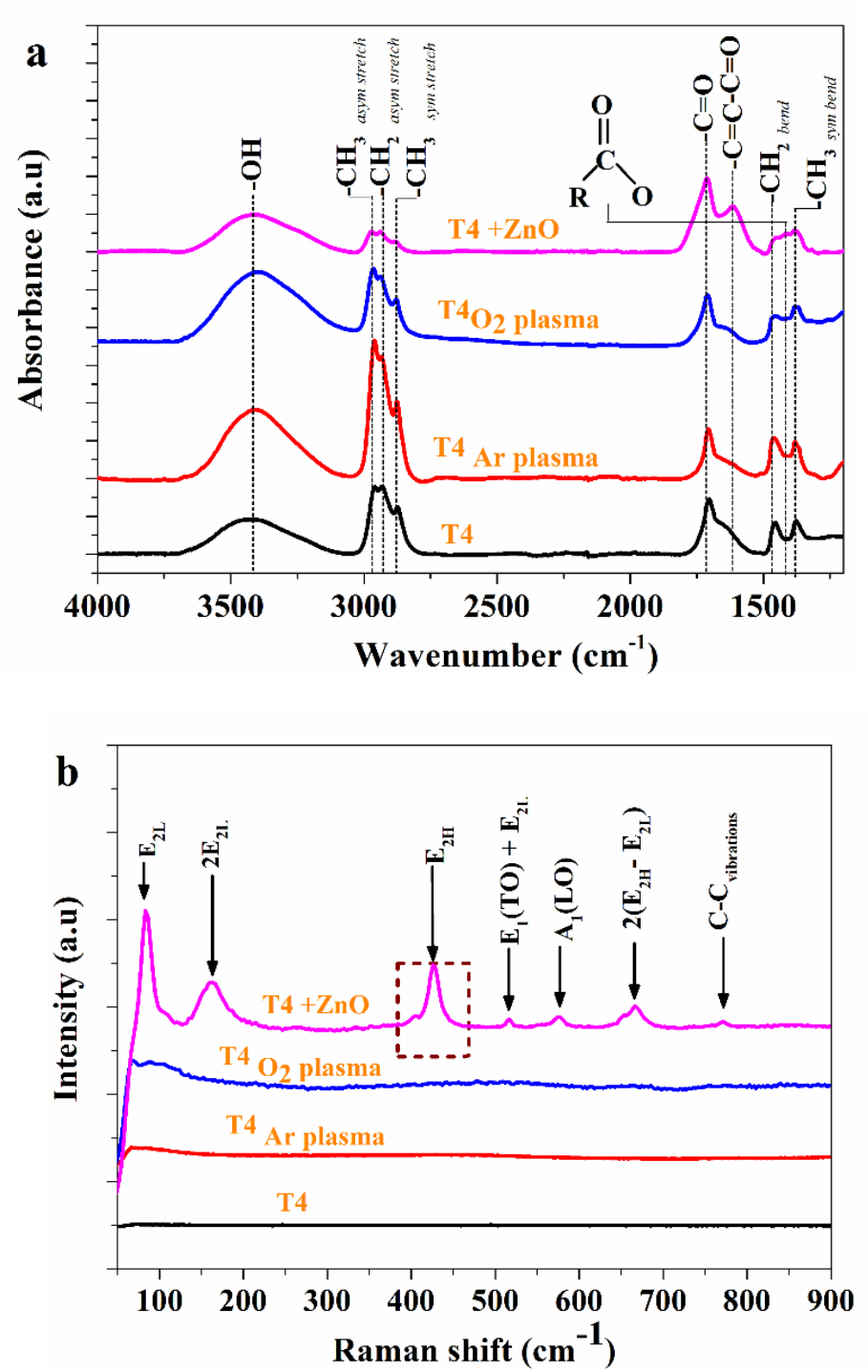

Figure 6. 2 (a) ATR-FTIR spectra of modified T4 surfaces. (b) Raman spectra of modified T4 surfaces.

Figure 6.2 a shows the ATR-FTIR spectra of all modified T4 films. The spectrum of T4-ZnO nanocomposite shows the characteristic peak at 1590, 1521, 1448, 1390 and 1254 cm^{-1}. The peak

occurring at these positions are characteristics of pp-$Zn(acac)_2$ [44]. The appearance of the band at 1710 cm^{-1} in all the deposited films is indicative of the formation of –C=O group during deposition, irrespective of the surface modification. The T4 $_{O2\ plasma}$ and T4 $_{Ar\ plasma}$ films show the characteristic peaks at 2800-3000 cm^{-1} (aliphatic C-H stretching) and 3400 cm^{-1} (O-H stretching vibration). The intensity of the above peaks (2800-3000 cm^{-1}) is greatly reduced in the case of T4-ZnO nanocomposites. It is interesting to note that there is the formation of carboxylate and conjugated ketone functionalities during ZnO modification of T4 in O_2 plasma. Attachment of acetylacetonates groups from $Zn(acac)_2$ on T4 explains their occurrence.

Raman spectroscopy was performed on the samples to get a qualitative estimate of ZnO nanoparticles in the deposited films. Figure 6.2b represents Raman spectra of T4 + ZnO nanocomposite films. Wettability of unmodified T4 is also shown for comparison. Wurtzite ZnO is characterized by a set of eight optical phonons: $\Gamma_{opt} = A_1 + E_1 + 2E_2 + 2B_1$. A_1 and E_1 are polar whereas and E_2 modes are non-polar and Raman active [45, 46]. The E_{2H} vibration mode at 440 cm^{-1} is representative of wurtzite phase of ZnO. The E_{2H} phonon frequency is red shifted by 12 cm^{-1} in the film (T4 + ZnO). Defect formation [47] on nanoparticles and phonon confinement [48] gives rise to this peak shift. The other peaks at about 83, 400 and 574 cm^{-1} are representative of E_{2L} , A_1(TO) and A_1 (LO) fundamental phonon mode of wurtzite ZnO. The other peaks at 514, 666 and 766 cm^{-1} are assigned to E_1(TO) + E_{2L} , 2(E_{2H} – E_{2L}) and A_1(TO) + E_{2L} multiphoton scattering modes. Most of the Raman peaks of deposited films have been found to be red shifted as compared to the well-established ones in the literature [49]. The bonding of organic T4 and acetate molecules on ZnO surface is the possible reason for this lowering of vibrational frequency [50, 51].

6.3.3 Coating wettability

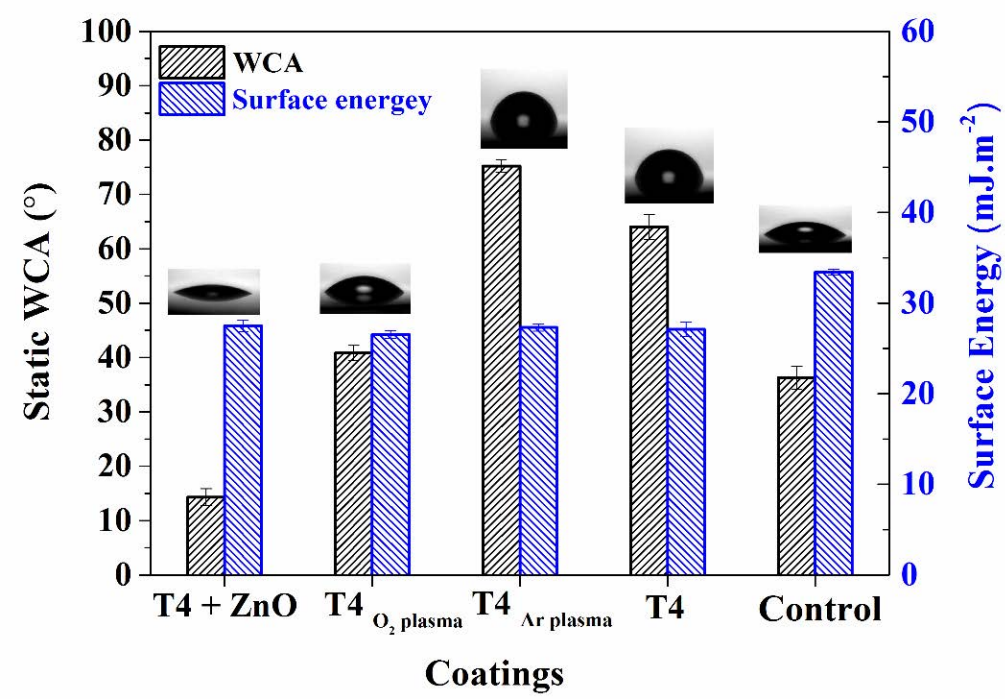

Figure 6. 3 Static water contact angle and surface energy of modified T4 coatings. The inset image shows the contact angle less than 90°.

Table 6. 1 Contact angle of water, ethanediaol and di-iodomethane on modified T4 surfaces

Coatings	Contact angle, °		
	Water	Ethane diol	Di-iodomethane
T4 + ZnO	14.28 ± 0.58	15.96± 1.93	40.75 ± 0.73
T4, O_2	40.83 ± 0.36	16.63 ± 1.11	39.52 ± 0.77
T4, *Ar*	75.19 ± 1.18	18.93 ± 0.57	37.85 ± 0.37
T4	65± 2.58	17.85 ± 3.45	37.83 ± 2.65

Water contact angle (WCA) measurements provide information about the hydrophilic/hydrophobic nature of the films. Figure 6.3 shows the WCA measurements on the modified T4 films along with the surface energy. Table 6.1 lists contact angles for three liquids on the modified surfaces used for free energy calculations. The contact angles on the surfaces of T4 and control samples are also shown for comparison. It can be observed that deposition in oxygen plasma results in the film with hydrophilic attributes. The ZnO-modified T4 shows highly

hydrophilic character (WCA < 15°). Polar character of ZnO and deposition in oxygen plasma render this films highly hydrophilic. T4 films deposited in argon and in oxygen plasmas exhibited contact angles of 75° and 40°, respectively. The high proportion of hydrophobic carbonaceous – CH_x functionalities evident in FTIR spectra explains the increase in the contact angle of T4 deposited in Ar plasma.

6.3.4 Surface morphology

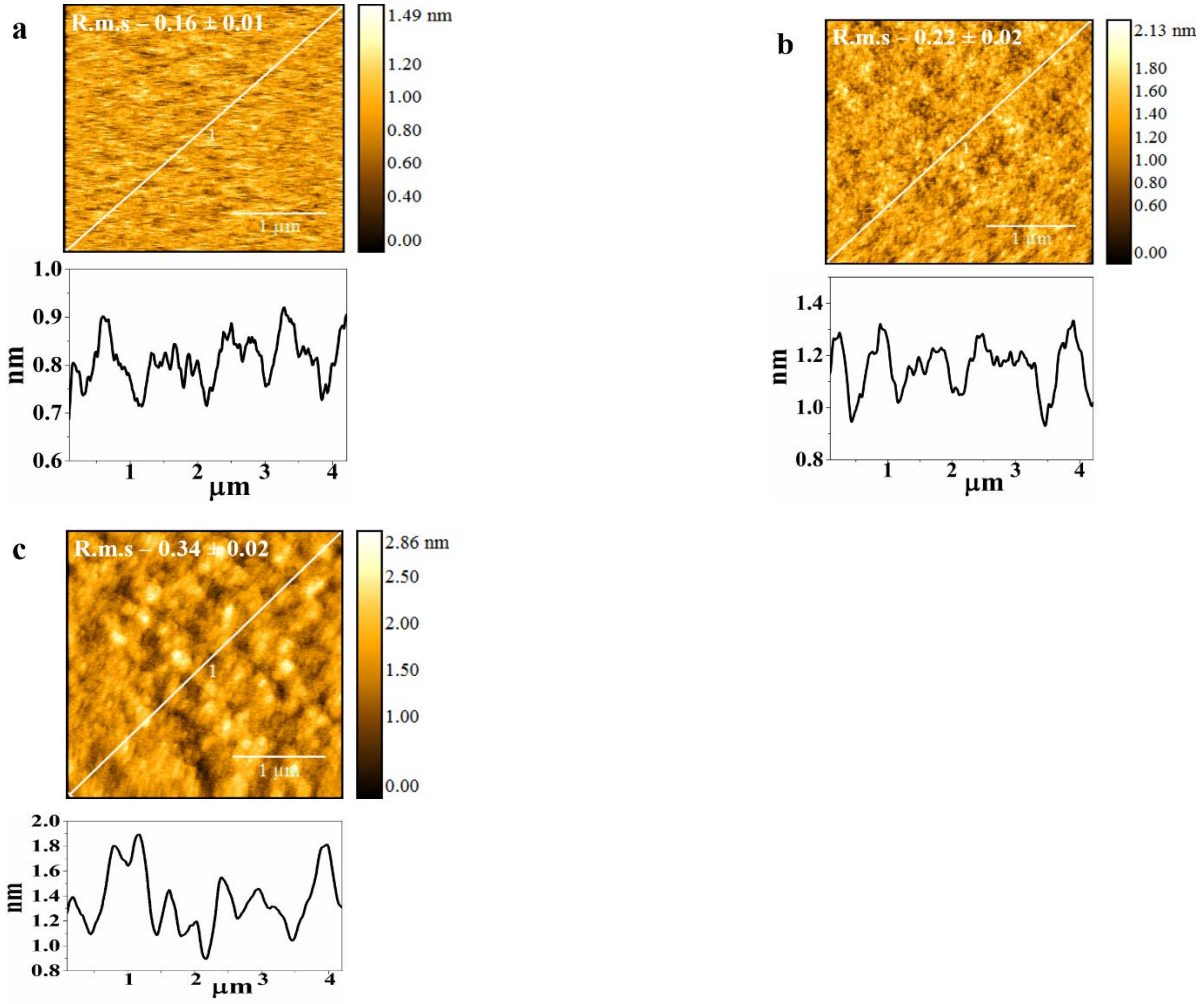

Figure 6. 4. AFM images of (a) T4 $_{O2\ plasma}$, R.m.s = 0.16 ± 0.01 nm, (b) T4 $_{Ar\ plasma}$, R.m.s = 0.16 ± 0.02 nm (c) T4 + ZnO, R.m.s = 0.34 ± 0.02 nm. Scanning area 3 × 3 µm^2. Line profiles of surfaces are also shown.

The effect of wettability and nanoparticle modification on surface roughness is shown in Figure 6.4. The root mean square (R.m.s) roughness of the of oxygen and argon plasma deposited and ZnO modified T4 are 0.16 nm, 0.22 nm and 0.34 nm, respectivley. The roughness reported here shows a nanometer scale. The ZnO-modified and Ar deposited T4 films are found to show a

cauliflower structure. However, this cauliflower morpholgy was not seen in samples deposited under oxygen plasma. The Ar deposited T4 exhibits a slightly increased roughness than that of the oxygen deposited samples.

6.3.5 Light transmission efficiency

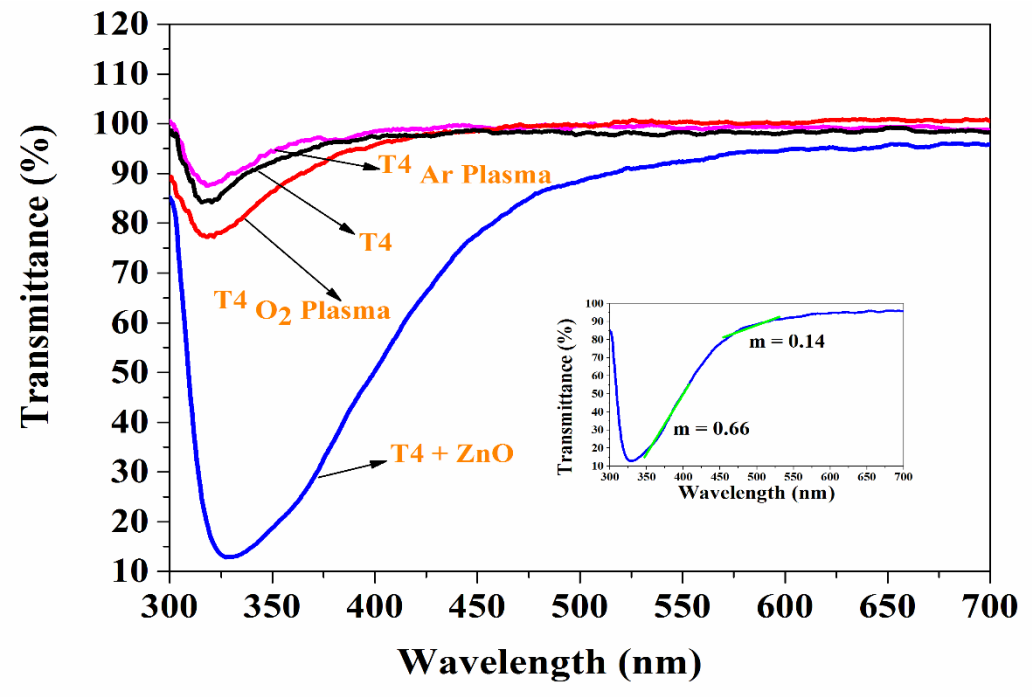

Figure 6. 5. UV-visible spectra of modified T4 films. Inset graph shows the rate of decrease of UV and visible light transmission in two different regions between 300-400 nm and 450-600 nm

Transparency to visible light and UV absorption of modified T4 film were measured within 200-1000 nm range. The transmittance spectra of the modified films are shown in figure 6.5. T4 films functionalized with ZnO nanoparticles showed significant UV-blocking in the 300 – 400 nm region. UV absorption by ZnO nanoparticles seems to be a possible explanation for this phenomena. It is also worthwhile to note that the rate of decrease of UV light transmission is higher than that of visible light. This rate of decrease is shown in the inset graph, where *m* denotes the slope of the graph in the particular region as marked by the green line. Thus, the UV blocking property of this film can be further enhanced by increasing the ZnO concentration on the film surface. Thin films with high UV absorption and visible light transmission property have a

potential application as optically transparent food packaging materials and there are many other applications [52, 53]. Light transmission in the visible range of 400-700 nm is greater than 90 % for T4 films deposited in argon and oxygen plasmas. The oxygen plasma-deposited T4 exhibited some UV blocking property, though it was significantly lower compared to ZnO-functionalized T4 films.

6.3.6 Thermal degradation behaviour

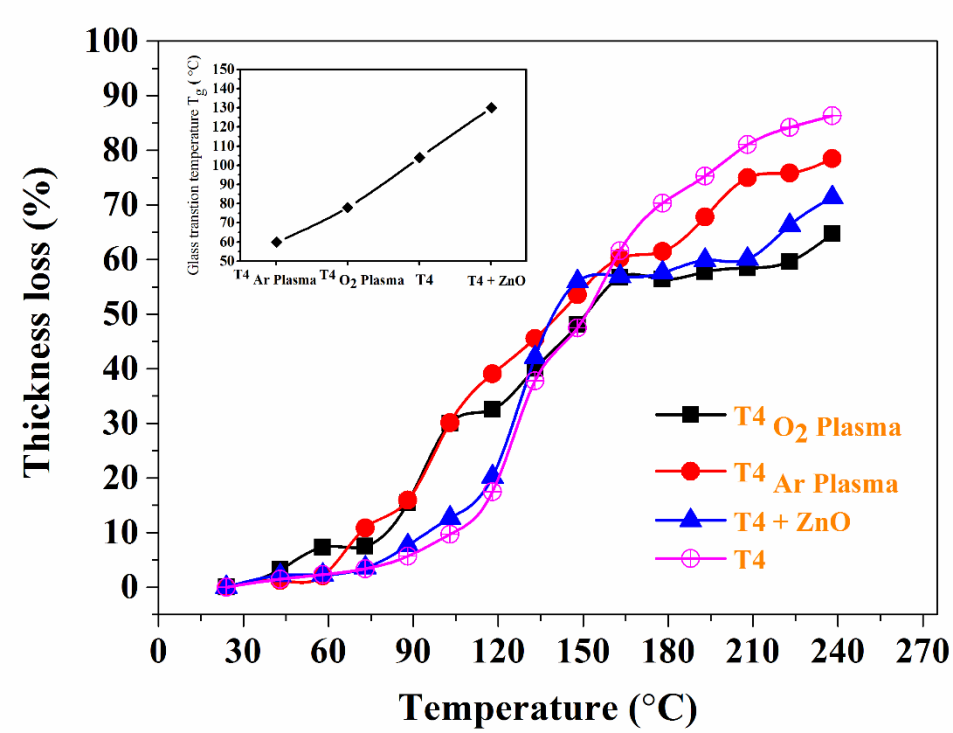

Figure 6. 6 Percentage thickness loss as a function of temperature estimated using ellipsometry data. Inset shows the glass transition temperature T_g of modified T4 plasma polymers

Thermal stability of modified T4 films was studied using in-situ dynamic ellipsometry. A linear fit to acquired data over two temperature ranges was performed using the least square fit method. The glass transition temperature (T_g) was determined by the intersection of two fitted lines. Figure 6.6 shows the percentage thickness loss as a function of temperature. Three kinds of thermal degradation regimes were observed for modified T4 films. Thermal degradation profile of the pristine T4 is also included for comparison. In the temperature regime of 50–90 °C, the rate of thickness loss was well below 20 % for all the deposited films. Loss of trapped moisture and unbound species from the surface may explain this observation. Major thickness loss is observed in the temperature regime of 90-160 °C. This observation can be associated with cleavage of hydroxyl groups, decarboxylation reactions, and breaking of aliphatic carbon chains. The

degradation phenomena above 170 °C can be attributed to breaking of carbon-carbon linkages. The inset in the graph shows the estimated T_g of modified T4 plasma polymers. The T_g of the modified T4 plasma polymer was found to increase in the following order, T4 $_{ar\ plasma}$ < T4 $_{o2\ plasma}$ < T4 < T4 + ZnO. This trend in T_g gives an insight into the chain length in the deposited polymers. The chain length is expected to follow the similar trend as T_g. Higher T4 fragmentation occurs in argon plasma than in the oxygen plasma. Also, less T4 fragmentation is found when depositing without any carrier gases as evident from the above trend.

6.3.7 Anti-bacterial test

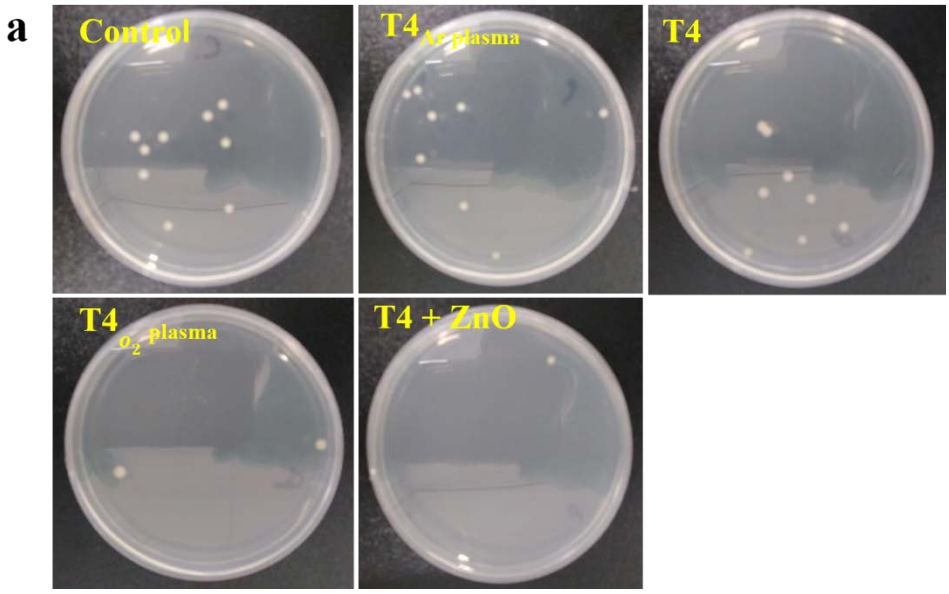

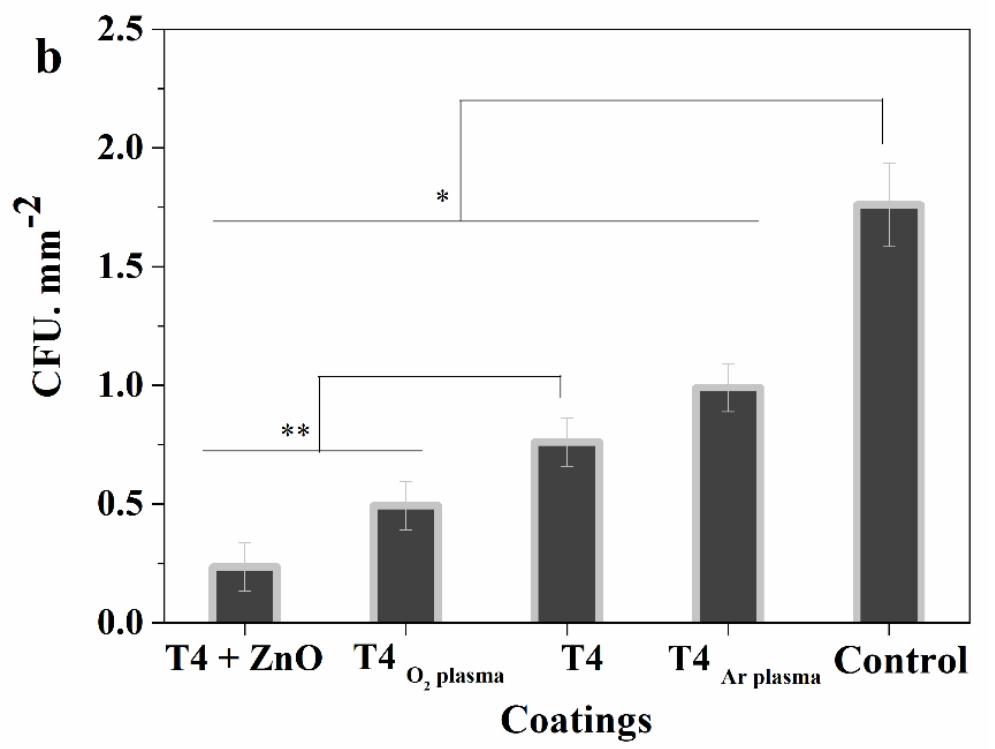

Figure 6. 7 a) Photographs of *E. coli* colonies on agar culture plates after 24 hr incubation on various T4 coatings. b) Colony forming units/mm² on modified T4 surfaces and the control. All T4 surfaces showed a significant reduction in bacterial adhesion w.r.t. control (*$p < 0.05$). T4 + ZnO and $T4_{O2\ plasma}$ demonstrated a significant bacterial adhesion w.r.t. to T4 (**$p < 0.05$).

Antibacterial activity of modified terpinen-4-ol surfaces was tested against *E. coli* cells. Initial adhesion up to 24 hr was examined as it is the preliminary step in biofilm formation. Figure 6.7a shows the bacteria which survived after 24 hr exposure to modified T4 surfaces and control. The small white dots are representative of *E. coli* colonies on agar culture plates. Figure 6.7b shows the colony forming unit (C.F.U.)/mm² for all the modified T4 surfaces. All the modified T4 plasma polymers showed significant reduction in bacterial adhesion w.r.t control ($p < 0.05$). It can be observed that the T4 + ZnO and hydrophilic $T4_{O2\ plasma}$ surface exhibited a significant improvement in antibacterial activity w.r.t. pristine T4 ($p < 0.05$). The ZnO modified T4 demonstrated stronger antibacterial activity than $T4_{O2\ plasma}$, $T4_{Ar\ plasma}$ and T4 films. Also, $T4_{Ar\ plasma}$ which is slightly hydrophobic showed more bacterial adhesion when compared to T4.

The combined effect of the hydrophilic surface along with the antimicrobial properties of T4 and ZnO is the possible reason for enhanced antibacterial performance of the $T4_{O2\ plasma}$ and T4 + ZnO polymers. Microorganism approaching the surface would find difficulties in settling on the surface due to the hydration layer formation between the surface and adjacent water molecules

in the first place. This would be followed by the killing of any attached microorganism by ZnO nanoparticles and T4 molecules. The internalization of ZnO nanoparticles by cells is found to induce oxidative stress, resulting in their death [54, 55]. Also, T4 molecules have the ability to compromise the cell membrane structure inhibiting their growth resulting in the cell death [56, 57].

6.4 Conclusion

Argon and oxygen as carrier gas had a profound influence on the deposition rate and degree of fragmentation of terpinen-4-ol during PECVD. Deposition in argon plasma leads to enhanced monomer fragmentation. This is also evident by the lowest T_g which is observed for $T4_{Ar\ plasma}$. Chemical composition of Terpinen-4-ol films deposited using both argon and oxygen as a carrier gas was found to be similar but in different proportions. The ratio of $–CH_x$/-OH group was greater in T4 films deposited in argon plasma than oxygen plasma. The difference in the proportion of functional group influenced the wettability of T4 films. Films rich in –OH content showed higher hydrophilic character. The oxygen plasma-modified and ZnO-modified T4 plasma polymers demonstrated enhanced antibacterial activity against *E. coli*. ZnO-modified T4 showed the most effective antibacterial activity among all the modified T4 coatings. Highly hydrophilic character combined with the antimicrobial effect of T4 and ZnO seems to be the possible explanation for this observation. Meanwhile ZnO-modified T4 coatings also showed significant UV absorption. However, as compared to unmodified T4 coatings, hydrophilic and ZnO nanoparticle modification played an important role in the enhancement of antimicrobial activity of T4 plasma polymers.

References

1. Bixler, G.D. and B. Bhushan, *Biofouling: lessons from nature.* Phil. Trans. R. Soc. A, 2012. **370**(1967): p. 2381-2417.

2. Leslie, D.C., et al., A bioinspired omniphobic surface coating on medical devices prevents thrombosis and biofouling. Nature biotechnology, 2014. **32**(11): p. 1134.

3. Romanò, C.L., et al., The concept of biofilm-related implant malfunction and "low-grade infection", in A Modern Approach to Biofilm-Related Orthopaedic Implant Infections. 2016, Springer. p. 1-13.

4. Zimmerli, W., Clinical presentation and treatment of orthopaedic implant-associated infection. Journal of internal medicine, 2014. **276**(2): p. 111-119.

5. Kumar, A., et al., Biodegradable optically transparent terpinen-4-ol thin films for marine antifouling applications. Surface and Coatings Technology, 2018.

6. Hassan, M., et al., *Cost of hospital-acquired infection.* Hospital topics, 2010. **88**(3): p. 82-89.

7. Ren, X., et al., Surface modification and endothelialization of biomaterials as potential scaffolds for vascular tissue engineering applications. Chemical Society Reviews, 2015. **44**(15): p. 5680-5742.

8. Bazaka, K., et al., Anti-bacterial surfaces: natural agents, mechanisms of action, and plasma surface modification. Rsc Advances, 2015. **5**(60): p. 48739-48759.

9. Desrousseaux, C., et al., Modification of the surfaces of medical devices to prevent microbial adhesion and biofilm formation. Journal of hospital Infection, 2013. **85**(2): p. 87-93.

10. Gao, G., et al., The biocompatibility and biofilm resistance of implant coatings based on hydrophilic polymer brushes conjugated with antimicrobial peptides. Biomaterials, 2011. **32**(16): p. 3899-3909.

11. Wang, J., et al., Silver-nanoparticles-modified biomaterial surface resistant to staphylococcus: new insight into the antimicrobial action of silver. Scientific reports, 2016. **6**: p. 32699.

12. Liu, C., et al., Mitigation of biofilm development on thin-film composite membranes functionalized with zwitterionic polymers and silver nanoparticles. Environmental science & technology, 2016. **51**(1): p. 182-191.

13. Ivanova, K., et al., Quorum-quenching and matrix-degrading enzymes in multilayer coatings synergistically prevent bacterial biofilm formation on urinary catheters. ACS applied materials & interfaces, 2015. **7**(49): p. 27066-27077.

14. Ashbaugh, A.G., et al., Polymeric nanofiber coating with tunable combinatorial antibiotic delivery prevents biofilm-associated infection in vivo. Proceedings of the National Academy of Sciences, 2016. **113**(45): p. E6919-E6928.

15. Salwiczek, M., et al., *Emerging rules for effective antimicrobial coatings.* Trends in Biotechnology, 2014. **32**(2): p. 82-90.

16. Rahaman, M.S., et al., Control of biofouling on reverse osmosis polyamide membranes modified with biocidal nanoparticles and antifouling polymer brushes. Journal of Materials Chemistry B, 2014. **2**(12): p. 1724-1732.

17. Krishnan, S., C.J. Weinman, and C.K. Ober, *Advances in polymers for anti-biofouling surfaces.* Journal of Materials Chemistry, 2008. **18**(29): p. 3405-3413.

18. Ding, X., et al., Antibacterial and antifouling catheter coatings using surface grafted PEG-b-cationic polycarbonate diblock copolymers. Biomaterials, 2012. **33**(28): p. 6593-6603.

19. Wu, Z., et al., Protein adsorption on poly (N-vinylpyrrolidone)-modified silicon surfaces prepared by surface-initiated atom transfer radical polymerization. Langmuir, 2009. **25**(5): p. 2900-2906.

20. Irfan, M., et al., Surface modification and performance enhancement of nano-hybrid f-MWCNT/PVP90/PES hemodialysis membranes. Journal of Membrane Science, 2014. **467**: p. 73-84.

21. Yu, Q., et al., *Anti-fouling bioactive surfaces.* Acta biomaterialia, 2011. **7**(4): p. 1550-1557.

22. Abraham, S., et al., Molecularly engineered p (HEMA)-based hydrogels for implant biochip biocompatibility. Biomaterials, 2005. **26**(23): p. 4767-4778.

23. Dimitriou, M.D., et al., A general approach to controlling the surface composition of poly (ethylene oxide)-based block copolymers for antifouling coatings. Langmuir, 2011. **27**(22): p. 13762-13772.

24. Gao, Q., et al., Rationally designed dual functional block copolymers for bottlebrush-like coatings: In vitro and in vivo antimicrobial, antibiofilm, and antifouling properties. Acta biomaterialia, 2017. **51**: p. 112-124.

25. Sawada, I., et al., Development of a hydrophilic polymer membrane containing silver nanoparticles with both organic antifouling and antibacterial properties. Journal of membrane science, 2012. **387**: p. 1-6.

26. Schwartz, V.B., et al., Antibacterial surface coatings from zinc oxide nanoparticles embedded in poly (n-isopropylacrylamide) hydrogel surface layers. Advanced Functional Materials, 2012. **22**(11): p. 2376-2386.

27. Lotz, A., et al., Antimicrobial efficacy and optimized cell adhesion from defined plasma polymerised multilayer structures involving zinc acetylacetonate and allylamine. Journal of Materials Chemistry, 2012. **22**(37): p. 19455-19461.

28. Xue, C.-H., et al., Fabrication of robust and antifouling superhydrophobic surfaces via surface-initiated atom transfer radical polymerization. ACS applied materials & interfaces, 2015. **7**(15): p. 8251-8259.

29. Kim, E.-S., Q. Yu, and B. Deng, Plasma surface modification of nanofiltration (NF) thin-film composite (TFC) membranes to improve anti organic fouling. Applied Surface Science, 2011. **257**(23): p. 9863-9871.

30. Wang, L., C. Hu, and L. Shao, *The antimicrobial activity of nanoparticles: present situation and prospects for the future.* International journal of nanomedicine, 2017. **12**: p. 1227.

31. Dizaj, S.M., et al., *Antimicrobial activity of the metals and metal oxide nanoparticles.* Materials Science and Engineering: C, 2014. **44**: p. 278-284.

32. Palza, H., *Antimicrobial polymers with metal nanoparticles.* International journal of molecular sciences, 2015. **16**(1): p. 2099-2116.

33. Jebel, F.S. and H. Almasi, Morphological, physical, antimicrobial and release properties of ZnO nanoparticles-loaded bacterial cellulose films. Carbohydrate polymers, 2016. **149**: p. 8-19.

34. Li, N., et al., Precisely-controlled modification of PVDF membranes with 3D TiO2/ZnO nanolayer: enhanced anti-fouling performance by changing hydrophilicity and photocatalysis under visible light irradiation. Journal of Membrane Science, 2017. **528**: p. 359-368.

35. Chung, Y.T., et al., Development of polysulfone-nanohybrid membranes using ZnO-GO composite for enhanced antifouling and antibacterial control. Desalination, 2017. **402**: p. 123-132.

36. Rajabi, H., et al., Nano-ZnO embedded mixed matrix polyethersulfone (PES) membrane: Influence of nanofiller shape on characterization and fouling resistance. Applied Surface Science, 2015. **349**: p. 66-77.

37. Al-Naamani, L., et al., Chitosan-zinc oxide nanocomposite coatings for the prevention of marine biofouling. Chemosphere, 2017. **168**: p. 408-417.

38. Bazaka, K., et al., Plasma-assisted surface modification of organic biopolymers to prevent bacterial attachment. Acta biomaterialia, 2011. **7**(5): p. 2015-2028.

39. Bazaka, K., M.V. Jacob, and E.P. Ivanova. A study of a retention of antimicrobial activity by plasma polymerized terpinen-4-ol thin films. in Materials Science Forum. 2010. Trans Tech Publ.

40. Panigrahi, J., et al., Radio frequency plasma enhanced chemical vapor based ZnO thin film deposition on glass substrate: A novel approach towards antibacterial agent. Applied Surface Science, 2011. **258**(1): p. 304-311.

41. Hegemann, D., et al., *Macroscopic description of plasma polymerization.* Plasma Processes and Polymers, 2007. **4**(3): p. 229-238.

42. Hubert, J., et al., Chemical and physical effects of the carrier gas on the atmospheric pressure PECVD of fluorinated precursors. Plasma Processes and Polymers, 2015. **12**(10): p. 1174-1185.

43. Hegemann, D. and M.M. Hossain, *Influence of non-polymerizable gases added during plasma polymerization.* Plasma Processes and Polymers, 2005. **2**(7): p. 554-562.

44. Duque, L. and R. Förch, Plasma Polymerization of Zinc Acetyl Acetonate for the Development of a Polymer-based Zinc Release System. Plasma Processes and Polymers, 2011. **8**(5): p. 444-451.

45. Alim, K.A., et al., *Micro-Raman investigation of optical phonons in ZnO nanocrystals.* Journal of Applied Physics, 2005. **97**(12): p. 124313.

46. Golić, D.L., et al., Structural characterization of self-assembled ZnO nanoparticles obtained by the sol–gel method from Zn (CH3COO) 2· 2H2O. Nanotechnology, 2011. **22**(39): p. 395603.

47. Alim, K.A., V.A. Fonoberov, and A.A. Balandin, *Origin of the optical phonon frequency shifts in ZnO quantum dots.* Applied Physics Letters, 2005. **86**(5): p. 053103.

48. Rajalakshmi, M., et al., *Optical phonon confinement in zinc oxide nanoparticles.* Journal of Applied Physics, 2000. **87**(5): p. 2445-2448.

49. Yahia, S.B., et al., *Raman study of oriented ZnO thin films deposited by sol–gel method.* Spectrochimica Acta Part A: Molecular and Biomolecular Spectroscopy, 2008. **71**(4): p. 1234-1238.

50. Gliemann, G., K. Nakamoto: Infrared and Raman Spectra of Inorganic and Coordination Compounds. John Wiley and Sons, New York, Chichester, Brisbane, Toronto 1978. 3. Aufl., XV, 448 Seiten mit 109 Abbildungen und 95 Tabellen. Preis: $31, 15. Berichte der Bunsengesellschaft für physikalische Chemie, 1978. **82**(11): p. 1263-1263.

51. Yang, R.D., et al., Photoluminescence and micro-Raman scattering in ZnO nanoparticles: The influence of acetate adsorption. Chemical physics letters, 2005. **411**(1-3): p. 150-154.

52. Wang, Z., et al., A flexible UV nanosensor based on reduced graphene oxide decorated ZnO nanostructures. Nanoscale, 2012. **4**(8): p. 2678-2684.

53. Lizundia, E., et al., Poly (l-lactide)/zno nanocomposites as efficient UV-shielding coatings for packaging applications. Journal of Applied Polymer Science, 2016. **133**(2).

54. Xie, Y., et al., Antibacterial activity and mechanism of action of zinc oxide nanoparticles against Campylobacter jejuni. Applied and environmental microbiology, 2011. **77**(7): p. 2325-2331.

55. Zhang, L., et al., Mechanistic investigation into antibacterial behaviour of suspensions of ZnO nanoparticles against E. coli. Journal of Nanoparticle Research, 2010. **12**(5): p. 1625-1636.

56. Oussalah, M., et al., Inhibitory effects of selected plant essential oils on the growth of four pathogenic bacteria: E. coli O157: H7, Salmonella typhimurium, Staphylococcus aureus and Listeria monocytogenes. Food control, 2007. **18**(5): p. 414-420.

57. Cox, S., et al., The mode of antimicrobial action of the essential oil of Melaleuca alternifolia (tea tree oil). Journal of applied microbiology, 2000. **88**(1): p. 170-175.

Chapter 7

Conclusion and Recommendation for Future work

7.1 General Conclusion

The objective of the work presented in this thesis was to tailor the material properties of terpinen-4-ol plasma polymers and utilize the material in various applications, especially for biofouling and antibacterial applications.. Terpinen-4-ol polymer thin films were fabricated under some plasma polymerization conditions, however this study expanded the plasma polymerization conditions especially introducing the substrate temperature, high RF power, and pulsed RF signals. In depth physical and chemical characterization has been performed to analyze the variation in the surface and bulk properties of the as deposited film. The antifouling and antibacterial activities of the films were correlated with chemical properties. The thesis was mainly organized as 7 chapters namely,

The important observations have been summarized at the end of each chapter. A summary of the overall outcomes of this thesis work are as follows:

Effect of substrate temperature: In PECVD of terpinen-4-ol, it has been corroborated that substrate temperature plays an important role in determining the deposition rate and mechanism. In a particular deposition power regime (P = 300, 400 W), the deposition rate was found to increase with substrate temperatures (T = 40-180 ˚C). This is indicative of a different deposition mechanism occurring during the deposition. Deposition at various substrate temperatures resulted in a change of chemical composition in as deposited terpinen-4-ol films. In addition to film composition wettability, aqueous stability, surface roughness and light transparency properties were significantly influenced by substrate temperature and deposition power. Films with higher contact angle and cross-linked structure are formed with the increasing substrate temperature.

Effect of Deposition Mode: Terpinen-4-ol plasma polymer deposition by the pulse-PECVD method plays a significant role in terms of antimicrobial properties of the as deposited films. Film

formation via –C-O bond dissociation and radical chain reactions seems to be possible polymerization mechanism at lower duty cycles (DC-10, 20 %). Complete terpinen-4-ol ring fragmentation was observed at higher duty cycle. Films deposited at higher DC 40, 100 % were stable under an aqueous environment. Deposition in pulse mode resulted in films with variable surface wettability. Film deposited at DC-40 exhibited the enhanced antibacterial activity against bacteriaum *P.aeruginosa* w.r.t to other pulse deposited samples and control. Higher retention of monomer molecule structure in the as deposited films explains this phenomena. However, the films deposited at lower DC-10, 20 exhibited unstable underwater behavior.

Surface modification of Terpinen-4-ol plasma polymers: Surface modification of terpinen-4-ol plasma polymers led to improvement in its advantageous properties. Addition of argon and oxygen as a carrier gas influenced the deposition rate of Terpinen-4-ol during PECVD, besides altering the surface wettability of the as deposited thin films. Deposition in argon plasma promotes higher monomer dissociation. Low glass transition temperature of the argon deposited terpinen-4-ol confirms this observation. Terpinen-4-ol plasma polymers deposited utilizing argon/oxygen as a carrier gas was found to have of comparable chemical composition however in varying degrees. A greater proportion of carbonaceous groups impart high contact angle to Terpinen-4-ol films deposited in argon plasma. Films rich in hydrophilic groups such as hydroxyl demonstrated high hydrophilicity. The hydrophilic and ZnO nanoparticle altered films showed improved antibacterial activity against *E.coli*. However, the ZnO incorporated Terpinen-4-ol films demonstrated the most effective antibacterial action among all surface modified films. An exceedingly hydrophilic character combined with the antimicrobial impact of T4 and ZnO is by all accounts the conceivable reason for this observation. Additionally, the ZnO functionalized films exhibited extensive ultra-violet absorption. When contrasted with unmodified coatings, hydrophilic and ZnO nanoparticle change appeared to be essential in the improvement of antimicrobial activity of the as deposited terpinen-4-ol plasma polymers.

Application as marine antifouling coatings: Bilayer terpinen-4-ol films are deposited for application as marine antifouling coatings. Coatings having light transmission of 90– 99% at wavelengths of 400– 1000 nm were fabricated by PECVD. The bioactive films (deposited at 10 W) indicated good stability in artificial sea water for up to one week. The level of fouling was found to be significantly decreased on 10W terpinen-4-ol coatings for the first week compared with the control and other studied surfaces (25 W). The antifouling mechanism of the coating involves both antimicrobial and mechanical action. The coating acted as a biocidal self-polishing coating,

where organisms settling on surface are killed followed by the subsequent dissolution of top most surface along with dead microorganisms. The light transmission effectiveness of the fouled 10W coatings was above 60% for the first seven day of deployment. The work illustrated the utilization of plasma polymerized terpinen-4-ol as an antifouling coatings for marine applications. Essentially, these coatings are biodegradable and do not pose any long term dangers to oceanic biological systems**.**

The important observations pertaining to the structure – property relationship with the deposition conditions are summarized in table 7.1.

Table 7. 1 List showing Influence of physical and chemical features of Terpinen-4-ol plasma polymers on their properties at different deposition conditions.

Parameters studied	Deposition conditions	Key features	Property Enhancement
Substrate temperature	P = 300, 400 W, T : 40 - 180 ^{o}C	High cross-linked structure	High aqueous stability
Pulse plasma deposition	P = 10 W, DC- 40 %	Monomer structure retention	Enhanced antibacterial property
Surface modification	P = 10 W, T = 140 ^{o}C	Hydrophilic and ZnO modification	Enhanced UV absorbing and antifouling properties
Bilayer fabrication	P = 10 ,25, 100 W	Biocidal self-polishing coating	Effective in combating primary marine biofouling

It can be concluded that the enhancement of film properties of Terpinen-4-ol plasma polymer is a function of substrate temperature, deposition mode and surface modification.

7.2 Recommendations for future work

This research has investigated the effect of plasma polymer deposition conditions on structure - property correlation. However many other surface modification techniques which may further enhance the overall properties of deposited thin films. A number of further studies are suggested

- The grafting of plasma polymer with various other nanoparticles such silver, titanium, gold can be carried out. Effect of nanoparticle concentration in polymer on antimicrobial activities can be studied. Also, the fabrication of nanoparticle-plasma polymer composite with controlled nanoparticle release properties can be done.

- Further development of multilayer coating design to act as a self-polishing coating has potential for biofouling reduction. Such coatings may be particularly useful in applications where light transparent antifouling surfaces are required, for example the prevention of fouling on optical sensor heads of aquatic monitoring systems, and currently these require frequent cleaning.

- Co-plasma polymerization with other naturally derived antimicrobial molecules. Thus a new antimicrobial surface can be fabricated with combination of two naturally antimicrobial molecules.